Molecular Dynamics Simulations of Small-Molecule Inhibitors of β-Amyloid Aggregation

Dissertation
zur
Erlangung der naturwissenschaftlichen Doktorwürde
(Dr. sc. nat.)

vorgelegt der
Mathematisch-naturwissenschaftlichen Fakultät
der
Universität Zürich

von
Marino Convertino
aus
Italien

Promotionskomitee

Prof. Dr. Amedeo Caflisch (Vorsitz)
Prof. Dr. Angelo Carotti

Zürich 2011

A coloro che bene o male sono passati in questi anni, a molti va la mia riconoscenza, a pochissimi - per quel che vale - la mia stima.

A mio fratello Piero, che certamente meriterebbe qualcosa di meglio ed anche a me, che male non fa.
Alè.

To all those whom, for better or worse, I've met in these last years, to many of them goes my gratitude, to very few - for what it is worth - my esteem.

To my brother Piero, who surely deserves something better and also to me, that can't hurt anyway.
Alè.

“Sono debitore al mio mestiere anche di ciò che fa maturo l’uomo, il successo e l’insuccesso, riuscire e non riuscire, le due esperienze della vita adulta necessarie per crescere.
Il chimico militante le conosce entrambe: sbagliare e correggersi, incassare colpi e renderli, affrontare un problema e risolverlo oppure uscirne sconfitto e subito ricominciare la battaglia.”
(Echi di una voce perduta. Incontri, interviste e conversazioni con Primo Levi. G. Poli e G. Calcagno, 1992, Ed. Mursia.)

“I also owe my work everything that makes a man mature, succeeding and failing, the two necessary experiences of adult life in order to grow.
The militant chemist is familiar with them both: to make a mistake and to put things right; to take blows and deal with them; to face a problem and solve it or else withdraw defeated and immediately begin the battle again.”
(The black hole of Auschwitz, P. Levi and M. Belpoliti, 2005, Polity Press. This translation first published in 2005 © Polity Press.)

Contents

Contents VII

Summary IX

Zusammenfassung XI

1. Introduction 1
   1.1 Alzheimer's disease 1
   1.2 Amyloid aggregation 3
   1.3 Therapeutic strategies in neurodegenaration induced by amyloid aggregation 5
   1.4 Computational chemistry 8
      1.4.1 Molecular Dynamics 8
      1.4.2 Solvation 11
      1.4.3 Common analysis in Molecular Dynamics 12
      1.4.4 cut-based Free-Energy Profile (cFEP) 14

2. 9,10-Anthraquinone hinders β-aggregation: How does a small molecule interfere with Aβ-peptide amyloid formation? 17
   M. Convertino, R. Pellarin, M. Catto, A. Carotti, A. Caflisch.
   [*Protein Science* 2009, 18:792-800]

3. Complete Phenotypic Recovery of an Alzheimer's Disease Model by a Quinone-Tryptophan Hybrid Aggregation Inhibitor 29
   R. Scherzer-Attali, R. Pellarin, M. Convertino, A. Frydman-Marom, N. Egoz-Matia, S. Peled, M. Levy-Sakin, D. E. Shalev, A. Caflisch, E. Gazit, D. Segal.
   [*PLoS ONE* 2010, 5(6):e11101]

4. $A\beta_{12-28}$ conformational change induced by small molecules 47
   M. Convertino et al. [*manuscript in preparation*]
   4.1 Simulations setup 47
   4.2 Variation of $A\beta_{12-28}$ secondary structure propensity 48
   4.3 Isolation of conformational basins 49

4.3.1 cFEP analysis of the MD trajectory of $A\beta_{12-28}$ 49
4.3.2 cFEP analysis and $A\beta_{12-28}$ in presence of NQTrp or AQ 50
4.4 NQTrp and AQ potential binding mode 52
4.5 Comparison between NMR- and MD-derived NOE 54
4.6 Conclusions 54

5. Appendix to Chapter 4 57

6. Conclusions and outlooks 63

Bibliography 65

Acknowledgements

Curriculum Vitae

Summary

Amyloid aggregation is implicated in various neurodegenerative syndromes including, among others, the well-known Alzheimer's disease, which is the most common form of dementia in elderly people. In this pathology, the β-amyloid peptides (Aβ) are assembled in molecular aggregates evolving from low-oligomers, to protofibrils, fibrils and, ultimately, in structured amyloid plaques representing the characteristic hallmark of Alzheimer's disease. Several low molecular weight compounds interferring with Aβ aggregation are currently known, however a detailed description of their interactions at the molecular level is still missing. In the present study, molecular dynamics (MD) simulations were used in the context of three projects to investigate the ability and mechanism by which low molecular weight compounds interfere with Aβ amyloid aggregation. The first projects, conducted in collaboration with Prof. A. Carotti's research group at the University of Bari (Italy), focused on the effects of 9,10-anthraquinone (AQ) and anthracene (AC) on the aggregation of the $A\beta_{14-20}$ segment, the most aggregation-prone sequence. MD simulations show that AQ interferes with β-sheet formation to a greater extent than does AC; this has been confirmed by *in vitro* Thioflavin T binding assays. A fruitful collaboration with the lab of Prof. E. Gazit at the Tel Aviv University gave life to the second project in which, taking advantage of the role of tryptophan in amyloid recognition and the aggregation inhibitory activity of quinonic moieties, a new hybrid molecule, 1,4-napthoquinon-2-yl-L-tryptophan (NQTrp), was designed and tested as an inhibitor of Aβ aggregation. *In silico*, *in vitro*, *in cell* and *in vivo* models demonstrate NQTrp inhibitory activity toward Aβ oligomerization and fibrillization, as well as NQTrp ability in lowering Aβ cytotoxic effects on neuronal cell lines. In the third (entirely computational) project, the molecular interactions between NQTrp or AQ and the $A\beta_{12-28}$ monomer were investigated through MD simulations. The obtained results suggest a relevant role of these inhibitors in promoting a conformational change in the $A\beta_{12-28}$ monomer, thereby inducing the formation of a collapsed loop conformation that creates a binding pocket in which the inhibitor molecules can bind via hydrogen bond, electrostatic and van der Waals interactions. The atomistic descriptions provided by MD simulations in these three studies can represent a solid basis for the screening and design of small molecule inhibitors of amyloid aggregation having therapeutic potential in Alzheimer's disease.

Zusammenfassung

Amyloid-Aggregation spielt in verschiedenen neurodegenerativen Erkrankungen eine wichtige Rolle, unter anderem bei der bekannten Alzheimer-Krankheit, welche die häufigste Form der Demenz bei älteren Menschen darstellt.
Bei dieser Erkrankung lagern sich β-Amyloidpeptide (Aβ) zu molekularen Aggregaten zusammen, die aus Oligomeren zu Protofibrillen und Fibrillen und schliesslich zu strukturierten Amyloidplaquen evolvieren, die ein Charakteristikum der Alzheimer-Krankheit darstellen.
Einige niedermolekulare Verbindungen, welche die Aβ-Aggregation stören, sind bekannt, aber eine detaillierte Beschreibung ihrer Wechselwirkungen auf molekularer Ebene steht noch aus. In dieser Studie wurden Moleküldynamik-Simulationen (MD) in drei Projekten verwendet um Wirksamkeit und Mechanismus zu untersuchen, mit der diese Moleküle mit geringem Molekulargewicht die Aβ-Amyloid-Aggregation beeinträchtigen können. Der Schwerpunkt der ersten Projekte, die in Kollaboration mit dem Arbeitskreis von Prof. A. Carotti an der Universität Bari (Italien) durchgeführt wurden, lag auf dem Einfluss von 9,10-Anthrachinon (AQ) und Anthrazen (AC) auf die Aggregation des $A\beta_{14-20}$-Segments, der für Aggregation am anfälligsten Sequenz. MD Simulationen zeigen, dass AQ die β-Faltblatt-Bildung stärker beeinträchtigt als AC. Dies wurde durch *in vitro* Thioflavin T Bindungsassays bestätigt.
Eine ergebnisreiche Kollaboration mit der Arbeitsgruppe von Prof. E. Gazit an der Universität Tel Aviv führte zu einem zweiten Projekt, bei dem ein neues Hybridmolekül entworfen und als Inhibitor der Aβ-Aggregation getestet wurde, indem die Rolle des Tryptophans in der Amyloid-Erkennung und die Aggregation inhibierende Wirkung von Chinonstrukturen ausgenutzt wurde.
In silico, *in vitro*, *in cell* und *in vivo* Modelle zeigen NQTrp inhibierende Wirkung auf Aβ-Oligomerisation und Fibrillenbildung sowie eine Herabsetzung der zytotoxischen Effekte von Aβ auf neuronale Zelllinien.
In einem dritten, vollständig computerbasierten Projekt wurden die molekularen Wechselwirkungen zwischen einer Reihe von Aggregationsinhibitoren und des $A\beta_{12-28}$-Monomers mit Hilfe von MD Simulationen untersucht. Die Resultate lassen auf eine relevante Rolle der Inhibitoren bei der Promotion von Konformationsänderungen in $A\beta_{12-28}$ schliessen, wodurch die Bildung einer 'collapsed loop' Konformation induziert wird, die zur Formation einer Bindungstasche führt, in der die

Inhibitoren via Wasserstoffbrückenbindungen, elektrostatischen und Van der Waals Wechselwirkungen binden können.
Die in diesen drei Projekten durch MD Simulationen erhaltenen atomaren Beschreibungen können eine solide Grundlage für das Screenen und Design von niedermolekularen Inhibitoren der Amyloid-Aggregation mit therapeutischem Potenzial gegen die Alzheimer-Krankheit darstellen.

Chapter 1

Introduction

"Ich habe mich verloren."
A. Deter

The 25th of November 1901, Auguste Deter was hospitalized at the Frankfurt Mental Institution in Germany; Dr. Alois Alzheimer and his assistant, Dr. Gaetano Perusini, examined and asked her many questions, which they again later asked to check her memory. When instructed to write her name, she tried to but could not and repeated "Ich habe mich verloren." ("I have lost myself.")[1]. A few years later, Dr. Alzheimer gave a lecture at a congress in the German town of Tübingen, describing typical clinical characteristics with memory disturbances and showing neuropathological pictures with miliary bodies (plaques) and dense fibrils bundles (tangles); his colleague, Dr. Emil Kräpelin, named the pathology of this case the Alzheimer's Disease[2].

1.1 Alzheimer's disease

"I am I plus circumstances."
J. Ortega y Gasset

Alzheimer's disease (AD) is the most common form of dementia accounting for 50-60% of all cases. The prevalence of dementia is lower than 1% in individuals aged 60-64 years, but it shows an exponential increase with age, such that in people aged 85 years and older, the prevalence is around 28%. In 2006, there were 26.6 million known sufferers worldwide and AD is predicted to affect about 80 million people in 2040 due to the increases in life expectancy[3, 4].
AD is a progressive neurodegenerative disorder for which there is currently no cure or effective treatment. Symptoms include confusion, impaired judgments, memory loss, personality changes, disorentation and loss of language abilities[3, 4].

Neuropathological changes in AD patients' brains include neuronal death in the regions related to memory and cognition, as well as the abnormal presence of intra- and extra-cellular protein aggregates[5, 6] known as neurofibrillary tangles and amyloid plaques. The precise relationship between protein aggregates in the brains of AD-affected individuals and their neurodegeneration symptoms has not yet been determined[7, 8]. The hypothesis that protein aggregation plays crucial role in neurodegeneration is based on the discovery that a gene linked to autosomal dominant familial AD encodes a precursor protein (amyloid precursor protein, APP) of the β-amyloid peptide (Aβ)[9].

In various organelles and on cell surfaces, the full-length APP is sequentially processed by at least three proteinases termed α-, β- and γ-secretases (Figure 1). APP cleavage by α- or β-secretase within the luminal/extracellular domain results in the shedding of nearly the entire ectodomain, yielding large soluble APP derivatives (called APPsα and APPsβ, respectively) and generating membrane-tethered α- or β-carboxyl-terminal fragments (CTFs). Following these extracellular cleavages, γ-secretase processes APP derivatives at the carboxyl-terminus of Aβ aminoacidic sequence, producing either a 3 kDa product (p3 in combination with α-secretase) or Aβ peptide (in concert with β-secretase cleavage), respectively, and the APP intracellular domain (AICD)[10].

Aβ is an intrinsically disordered 39-, 40- 42-residue peptide of ~ 4 kDa (D_1AEFRHDSGY$_{10}$EVHHQKLVFF$_{20}$AEDVGSNKGA$_{30}$IIGLMVGGV$_{39}$VI A_{42}) known as $A\beta_{39}$, $A\beta_{40}$ and $A\beta_{42}$, respectively. $A\beta_{39}$ is not toxic, while $A\beta_{40}$ and $A\beta_{42}$, the most common Aβ isoforms, are fibrillar components of AD amyloid plaques[11].

During the last fifteen years, a working hypothesis has been developed implicating protein aggregation as the trigger of the cascade of events resulting in neurodegeneration and disease[12].

This model, known as the 'amyloid hypothesis', has been upheld (and generalized to other neurodegenerative diseases characterized by protein aggregates, albeit of varying composition, such as Parkinson's and Huntington diseases) with the general understanding of the protein aggregation process, mainly thanks to neuropathology, genetics and experimental and computational biophysics[8].

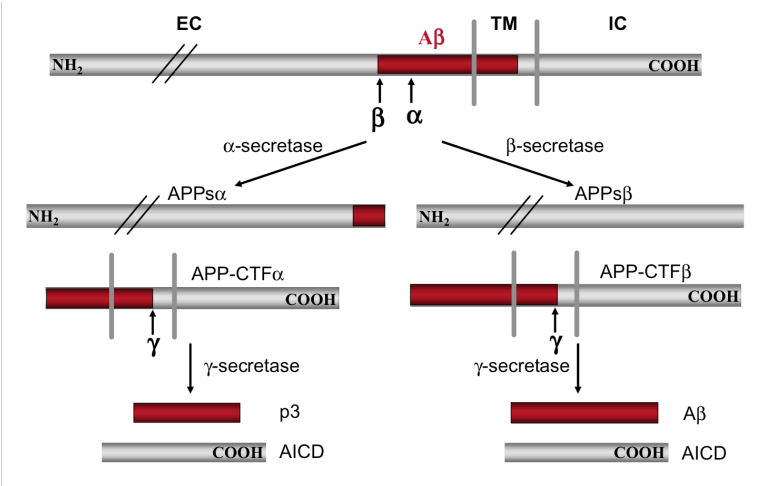

Figure 1. Schematic diagram of APP sequential processing (not drawn to scale). EC: extracellular; TM: transmembrane; IC: intracellular. The Aβ domain is highlighted in red. For simplicity, only one cleavage site is shown for each enzyme. This figure was taken from Zhen H. and Koo E. *Molecular Neurodegeneration* 2006, *1*:5.

1.2 Amyloid aggregation

"Everything should be made as simple as it is, but not simpler."
A. Einstein

Amyloid aggregates are fibrillar protein assemblies composed of polypeptide chains arranged in β-conformation, with their backbone perpendicular to the fibril axis[13, 14].
They are the final results of a complex series of oligomerization and polymerization events[15]. Amyloid fibril formation is characterized by a nucleation growth mechanism (see Figure 2), which is strongly influenced by either peptide sequence or external conditions such as pH, temperature and denaturing alcohol concentration[15-22]. The time course of peptide/protein conversion to its fibrillar form (measured by Thioflavin T fluorescence, light scattering or other techniques) typically includes a lag phase followed by a rapid exponential growth phase[23-25]. The lag phase is assumed to be the time required for "nuclei" to form.
Once a nucleus is formed, fibril growth proceeds rapidly by further association of either monomers or oligomers with the nucleus. The addition of preformed fibrillar species ("seeding") causes the lag phase to be shortened or totally abolished as the aggregation rate is no longer limited by nucleation[23, 25].

As regards Aβ aggregation, Atomic Force Microscopy (AFM) and Transmission Electron Microscopy (TEM) have revealed that *in vitro* Aβ fibrils are straight, unbranched and often twisted with diameters ranging from 1 to 10 nm. Morover, AFM and TEM have revealed the formation of a series of metastabile, non-fibrillar species. Some are in the form of spherical beads having a diameter of 2-5 nm, others are beaded-chains (composed of individual beads of 2-5 nm diameter) having a linear curly form, yet others appear as annular structures formed by circularization of beaded chains[26-29]. All of these aggregates evolve to protofilaments that are the constituent units of mature fibrils. Protofibrils can bind Congo Red (CR) and Thioflavin T (ThT), and they contain an extensive β-sheet structure[29].

During prefibrillar aggregate assembly, oligomeric species precede protofibril formation[30, 31]. Both $A\beta_{40}$ and $A\beta_{42}$ have been shown to exist as soluble oligomers in rapid equilibrium with the corresponding monomeric forms. Oligomers are composed of 2-4 and 5-6 molecules for $A\beta_{40}$ and $A\beta_{42}$, respectively, and Circular Dichroism (CD) measurements have revelead the disorganization of their molecular structures[31].

Aβ oligomers have also been detected in the brains of AD patients[32], as well as in the lysates and conditioned growth media of cultured cells expressing APP[33, 34].

The traditional formulation of the amyloid hypothesis pointed to the cytotoxicity of mature amyloid aggregates. Amyloid fibrils were believed to be toxic species, responsible for disrupting cell homeostasis and, thus, inducing apoptosis[35].

This idea was supported by a correlation between higher levels of *in vitro* faster-fibril-forming Aβ mutants and an earlier disease onset, as well as greater cognitive impairment in mouse models[36].

On the other hand, a more recent and broadly supported variation of the amyloid hypothesis identifies the oligomers as the cytotoxic species that might induce apoptosis by physically disrupting (i.e. piercing) cell membranes[37].

Because of its complexity, a complete elucidation of amyloid aggregation mechanism is still missing; nevertheless, even our present knowledge is leading to more reliable and rational therapeutic strategies. Experimental and computational evidence suggest that the central hydrophobic region of $A\beta_{14\text{-}21}$ is the trigger of the aggregation process[38] and that the central phenylalanines (Phe19 and Phe20)[39] play a relevant role in the cascade of events leading to the formation of Aβ fibrils.

For these reasons, all of the computational studies presented herein focus on the central segment of Aβ, considered as the segment most prone to aggregation.

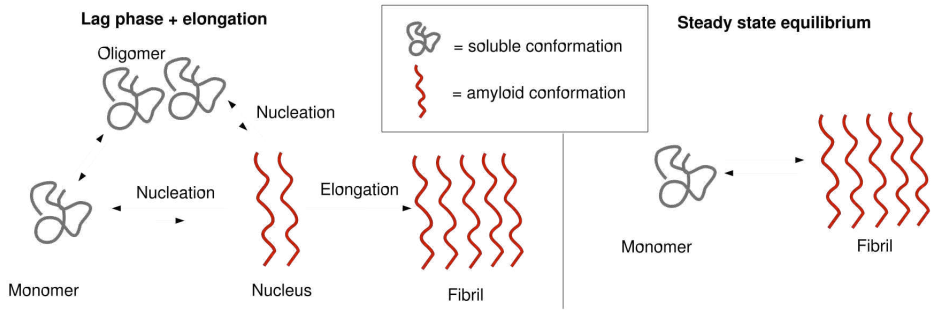

Figure 2. Amyloid formation displays the typical kinetics of a nucleated polymerization where the rate limiting step for fibril formation is the creation of a nucleus. In this figure, the kinetic phases of fibril formation are shown. **Left:** nucleation (or lag phase) and elongation. In the lag phase soluble monomeric and/or oligomeric species are in pre-equilibrium with the nuclei, which are unstable species that can either progress to form fibrils or regress to soluble species. **Right:** steady state equilibrium between isolated monomers and fibrils at the end of fibrillization. Credits are due to Dr. R. Pellarin, whose PhD thesis this figure was taken from.

1.3 Therapeutic strategies in neurodegeneration induced by amyloid aggregation

"Corpora non agunt nisi fixata."
P. Erlich

The aim of drug discovery is to use the biochemical knowledge of disease processes to define relevant targets for therapy. In neurodegenerative diseases induced by amyloid aggregation, the focus is on protein aggregation pathways. Neglecting β- and γ-secretase inhibitors and focusing on the protein aggregation event, at least four different strategies have been proposed:

i) decreasing expression of aggregation prone proteins;
ii) stabilizing native protein conformations;
iii) inhibiting protein conformational changes and aggregation;
iv) increasing clearance of aggregates.

Selected modern techniques of gene therapy could be envisioned as means to lower or prevent the expression of proteins involved in aggregation;

while antisense oligonucleotide, stem cells and genetically engineered ribozyme are promising options[40-44], their effective application is still under development. Furthermore, until the biological function of normal proteins is established, lowering protein production may produce undesirable side effects.

Stabilization of the native protein fold has been attempted in several protein aggregation diseases[45]. The rationale behind this approach is that if the native fold is stabilized, the propensity to undergo misfolding and aggregation is diminished. In AD, nicotine and cotinine have been shown to inhibit Aβ amyloid formation by specifically binding to the peptide and stabilizing its α-helix structure[46, 47]. 1,4-naphtoquinon-2-yl-L-triptophan (NQTrp)[48] and 9,10-anthraquinone (AQ)[49]) have been found to stabilize a collapsed loop conformation (see Chapter 3).

Protein engineering has been proposed as an approach to create sequence-modified proteins with higher stability, a lower tendency to aggregate and the ability to suppress wild-type protein aggregation[50]. Perhaps the most promising strategy to increase the clearance of misfolded proteins is the immunization approach, which has already been tested for AD[51-53]. The rationale is that vaccination with protein components of the aggregates can result in the production of antibodies and a cellular response able to remove the aggregation-prone proteins.

Immunization can reduce amyloid load, cerebral damage and behavioral impairments in transgenic AD animal models[51, 54-58], however a clinical trial to evaluate the efficacy of the immunization strategy in AD patients had to be stopped due to several cases of meningoencephalitis[59].

Among the different strategies proposed against protein aggregation, the inhibition of structural changes involved in the formation of aggregates is the most attempted one, the reason being that the formation of misfolded monomers and oligomers is the first pathological event in the cascade leading to disease. There are, essentially, two classes of molecules under development: peptides and small chemical compounds. A successful strategy in identifying potential inhibitors has been the rational development of short peptides targeting the protein sequence involved in protein-protein interaction. The self-recognition domain is typically the region of the protein implicated in early misfolding and conformational changes.

Different disrupting elements have been used: (1) amino-termini modified peptides with bulky groups sterically inhibiting protein aggregation[60], (2) non-natural aminoacids including α-aminoisobutyric acid[61], (3) N-methylated peptides[62-64] and (4) β-sheet breakers[65, 66] alone or in combination with charged residues to reduce hydrophobic interactions

triggering the protein aggregation[67]. A great advantage of peptidic inhibitors is their high inhibition potency and specificity and low toxicity; however, their aminoacidic nature imposes serious problems for administration and delivery[68]. By contrast, small chemical entities present the advantage of their drug-like properties (pharmacokinetics, bioavailability, brain uptake); they do, however, commonly have specificity and toxicity issues. Several low-molecular-weight compounds have been observed to inhibit fibril formation and toxicity[39,69-71] and, in particular, aromatic and heteroaromatic rings have been identified as potent inhibitors of amyloid aggregation[39]. As an example, indole derivatives, nordihydroguaiaretic acid, curcumin, rosmarinic acid and poliphenols such as epigallocathechin-3-gallate (EGCG) have been shown to inhibit the Aβ fibril formation[71-74] (Figure 3 reports relevant chemical structures).
Despite the relatively high number of low-molecular-weight compounds able to impair the Aβ aggregation process, a detailed description of their interactions with Aβ monomers and oligomers has hitherto been missed. The main goal of the present thesis has been the investigation, at the molecular level, of small molecule interactions with different Aβ segments by means of the computational tools described in the next section.

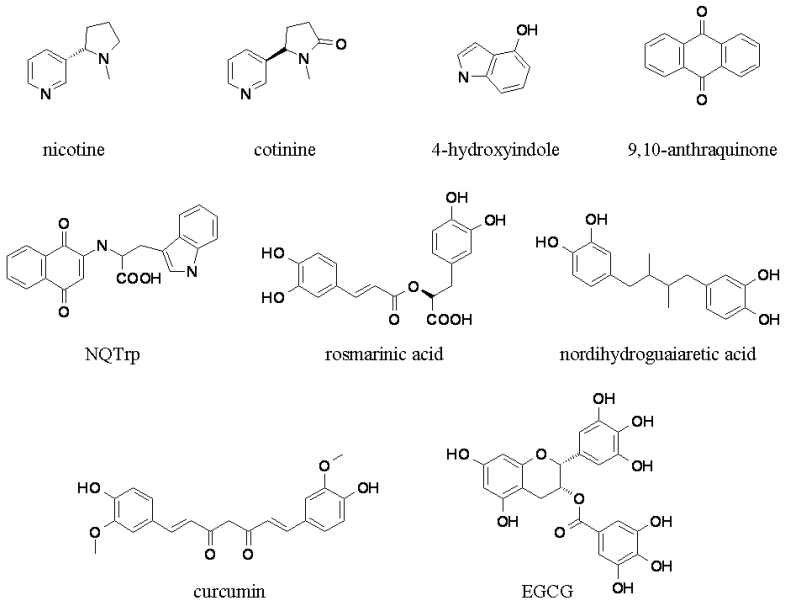

Figure 3. Chemical structures of small molecules active in preventing amyloid aggregation [71-74].

1.3 Computational chemistry

"In theory there is not any difference between practice and theory, in practice there is."
Anonymous

Computational chemistry and the concept of *in silico* experiments are, nowadays, an established branch of research whose contribution is determinant for the comprehension of many biomolecular processes. In an *in silico* experiment, a model of a real experiment is built, and observables are measured and compared with experimental measurements. If the model results agree with experiment, it can be used to make predictions. In particular, computational chemistry is useful to describe the following:

i) structure and stability of molecular systems;
ii) free-energy of different molecular system states;
iii) kinetics of different molecular systems;
iv) reaction processes within a molecular system.

Molecular Dynamics (MD) is among the privileged computational techniques; it permits the study at atomic level of detail of complex dynamic processes that occur in biological systems, such as protein stability, conformational changes, protein folding and aggregation.

1.4.1 Molecular Dynamics

"Everything that living things do can be understood in terms of the jiggling and wigglings of atoms."
R. Feynman

Molecular Dynamics (MD) is a computational technique for the simulation of the temporal evolution of the degrees of freedom of a molecular system. Since the publication of the first MD simulation of the bovine pancreatic trypsin inhibitor 33 years ago[75], MD has become one of the most important tools for understanding the basis of the relationship between structure and function of biological macromolecules. MD simulations can provide molecular detail concerning individual particle motions as a function of time and, thus, can be used to address specific questions about the properties of a model system. Of course, experimental validation plays

an essential role: comparison of simulation and experimental data serves to test the accuracy of calculated results and to provide a basis for improving the methodology. This is particularly important as theoretical estimates of the simulation systematic errors of a simulation by use of empirical potentials (force field, see later) are difficult to quantify[76].

Generally, molecular simulations can be roughly classified in *ab initio* methods, which apply the principles of quantum physics, and molecular mechanics, which is based on classical mechanics[77]. The latter uses an empirical energy potential, called force field, and is the main equation defining a structure-energy relationship in molecular systems. Different force fields for protein and nucleic acids are currently in use, including CHARMM[78-81], AMBER[82], GROMOS[83] and OPLS[84]. The typical equation of the potential energy is a pairwise, conservative function:

$$E = E_{cov}(r) + E_{noncov}(r)$$

where E_{cov} and E_{noncov} are the covalent and non-covalent energy terms, respectively and r is the $N \times 3$-dimensional array of atoms coordinates. The covalent term is the sum of bonds b, covalent angles θ, dihedral angles ϕ and improper dihedral angles ω:

$$\begin{aligned} E_{cov}(r) &= E_b + E_\theta + E_\phi + E_\omega = \\ &= \sum_b \frac{1}{2} k_b (b - b_0)^2 + \sum_\theta \frac{1}{2} k_\theta (\theta - \theta_0)^2 + \\ &\sum_\phi \frac{1}{2} k_\phi [1 + cos(n\phi + \psi)] + \sum_\omega \frac{1}{2} k_\omega (\omega - \omega_0)^2 \end{aligned}$$

where k_b, k_θ, k_ϕ and k_ω are the force constants. Note that the bond, angle and improper potentials are modelled as harmonic potentials that assume a minimum value at r_{b_0}, θ_0, ω_0. The torsional potential is a sum of periodic functions, whose indices are n and phases are ψ.

The non-covalent term is the sum of Lennard-Jones and Coulombic potentials:

$$E_{noncov}(r_{ij}) = E_{LJ}(r_{ij}) + E_C(r_{ij}) = \sum_{i<j} \varepsilon_{ij} \left[\left(\frac{r_{ij}^{min}}{r_{ij}} \right)^{12} - 2 \left(\frac{r_{ij}^{min}}{r_{ij}} \right)^{6} \right] + \sum_{i<j} \frac{q_i q_j}{4\pi\varepsilon_0 r_{ij}}$$

where q_i is the partial charge of atom i, ε_0 is the vacuum permittivity, r_{ij}^{min} is the equilibrium separation distance of the Lennard-Jones potential and ε_{ij} is the energy well depth, i.e., $E_{LJ}(r_{ij}^{min}) = -\varepsilon_{ij}$.

The Lennard-Jones potential E_{LJ} is an effective pairwise function that mimics the van der Waals interactions, while the Coulombic potential E_C is the energy term that accounts for electrostatic attractions and repulsions between charges.
The trajectories of atoms belonging to the molecular system are calculated by iterative numerical integration of Newton's equation of motion:

$$m_i \frac{d^2}{dt^2} r_i = m_i \frac{d}{dt} v_i = m_i a_i = F_i(r_i) = -\nabla_i E(r_i)$$

that express the relationship between the force field potential $E(r)$ and the kinematic quantities, i.e. force F_i, acceleration a_i, velocity v_i and coordinates r_i of the atom i.
Note that in MD, observables are calculated as time averages, whereas experimental observables are assumed to be ensemble averages.
This difference is only apparent as the ergodic hypothesis states that the time average equals the ensemble average.

$$\langle A \rangle_{ensemble} = \langle A \rangle_{time}$$

The basic idea is that if a molecular system is allowed to evolve indefinitely over time, it will eventually pass through all possible states. Therefore, it is of utmost importance, particularly in MD simulations of proteins/peptides aggregation events, to generate enough representative conformations of the analyzed system (sampling), such that the ergodic hypothesis is satisfied. Only in this case, experimentally relevant information concerning structural, kinetic and thermodynamic properties may be calculated.

1.4.2 Solvation

"Not to be confused with Salvation."
Wikipedia

Water is the main component of the biological environment in which many macromolecules operate. It is a complex medium whose modeling is particularly difficult. A common approach in MD is to employ explicit solvent, which consists in including, in the simulation, water molecules that are parametrized at the atomistic level[85]. This has the major disadvantage of being extremely time demanding and, thus, inefficient in the sampling of slow molecular events such as protein aggregation. A very good solution is the use of an implicit solvent (i.e. a mean field approximation of the solvent medium), which improves the calculation efficiency.
In implict solvent models, the degrees of freedom of the water molecules are not considered in the force field; they are replaced by a potential depending only on the degrees of freedom of the solute[86]. Moreover, the lack of viscosity effects, arising from the absence of water molecules, reduces the overall frustration of the system and, thus, improves the sampling of the observed phenomenon. Several implicit solvent models have been adopted to approximate either the non-polar or polar contributions of solvation. Continuum electrostatics approaches based on the numerical solution of the Poisson equation reliably reproduces polar contributions and have been implemented in force fields[87], though they remain inefficient in terms of sampling. A convenient alternative is to use an analytical treatment of continuum electrostatics, as the Generalized Born (GB) approximation[88], which simplifies the electrostatic solvation energy to a pairwise potential. In some of the *in silico* experiments developed in the present thesis, the FACTS implicit solvent model[89] has been adopted in conjunction with the CHARMM force field[78, 79]. FACTS is based on the fully analytical evaluation of the volume and spatial symmetry of the solvent that is displaced from around a solute atom by its neighboring atoms. The two measures of solvent displacement are combined in an empirical equation to approximate the atom electrostatic solvation energy and the solvent accessibile surface area.

$$\Delta G^{FACTS} = \Delta G^{el,FACTS} + \gamma \sum_{I}^{N} S_i^{FACTS}$$

While the first term yields the effective Born radius (used in the GB formula to calculate the solvent-screened electrostatic interaction energy), the

second is used to approximate the non-polar contribution to solvation (for further details refer to [89]).
However, the most efficient implicit solvent models are those based on solvent accessibile surface area (SASA)[90-92]. These models are based on the idea that solvation energies are mostly defined by the first solvation shell and can be decomposed into atomic contributions, which are determined by the local solute geometry:

$$G_{solv} = \sum_i \sigma_i S_i$$

where i is the solute atom index, σ_i is the surface tension coefficient and S_i is the atomic solvent accessibile area. The solute surface (a measure of the water accessibility in the first hydration shell) is responsible for the main contributions to the solvation energies. In many of the *in silico* experiments developed in the present thesis, the SASA implicit solvent model[89] has been adopted.

1.4.3 Common analysis in Molecular Dynamics

"Prediction is very difficult, expecially about the future."
N. Bohr

From the trajectory of a molecular dynamics simulation, several properties can be easily calculated.

RMSD
The Root Mean Square Distance (RMSD) between two (or a series of) structures, such as the protein X-ray structure and a simulation frame or two frames of the same time series, is defined as:

$$RMSD = \sqrt{\frac{1}{N}\sum_{i=1}^{N}\left[\left(x_i - x_r\right)^2 + \left(y_i - y_r\right)^2 + \left(z_i - z_r\right)^2\right]}$$

where N is the number of atoms, x_i, y_i, z_i, are the coordinates of atom i after optimal superposition on a reference structure, x_r, y_r, z_r, are the coordinates of atom i in the reference structure. RMSD expresses how different an object is with respect to another after the optimal superposition of the two.

Radius of Gyration

The Radius of Gyration, or gyradius (RGYR) describes the dimension of a molecular system in space and is defined as:

$$RGYR = \sqrt{\frac{1}{N}\sum_{i=1}^{N}\left[\left(x_i - \bar{x}\right)^2 + \left(y_i - \bar{y}\right)^2 + \left(z_i - \bar{z}\right)^2\right]}$$

where N is the number of atoms, x_i, y_i, z_i, are the coordinates of atom i, $\bar{x}$, $\bar{y}$, $\bar{z}$, are the coordinates of the center of mass of the considered system.

Secondary structure analysis

It is useful, particularly for peptides, to analyze the regular secondary structures, which consist of polipeptide segments in α-helical or β-sheet arrangment. Given the atomic-resolution coordinates of a protein, one of the standard methods for assigning secondary structure to its amino acids is to use the DSSP (Define Secondary Structure of Proteins[93]) algorithm.

DSSP begins by identifying the hydrogen bonds of the protein structure using a purely electrostatic definition. The energy is assumed to be:

$$E = q_1 q_2 \left(\frac{1}{r_{ON}} + \frac{1}{r_{CH}} - \frac{1}{r_{OH}} - \frac{1}{r_{CN}}\right) \cdot 332 kcal / mol$$

where q_1 = (±) 0.42e and q_2 = (±) 0.20e (based on the assignment of partial charges of -0.42e and +0.20e to the carbonyl oxygens and amide hydrogens, and the opposite charges to the carbonyl carbons and amide nitrogens) and r_{ON}, r_{CH}, r_{OH}, r_{CN}, are the distances between carbonyl oxygens and amide nitrogens, carbonyl carbons and amide hydrogens, carbonyl oxygens and amide hydrogens, carbonyl carbons and amide hydrogens, respectively.

The DSSP algorithm identifies a hydrogen bond if the energy E is lower than -0.5 kcal/mol; it then recognizes eight types of secondary structure (each identified by its own symbol, i.e., G, H, I, T, B, E, S, L) depending on the pattern of hydrogen bonds.

Those secondary structure types are then usually grouped into three larger classes: helix (G, H, I and T), strand (B, E and S) and loop (L).

P_2 parameter

The nematic order parameter P_2 is widely used for studying the properties of anisotropic fluids such as liquid crystals[38, 94-97]. It is defined as:

$$\overline{P_2} = \frac{1}{N}\sum_{i=1}^{N}\frac{3}{2}\left(\hat{z}_i \cdot \hat{d}\right)^2 - \frac{1}{2}$$

where $\hat{d}$ (the director) is a unit vector defining the preferred direction of alignment and is defined as the eigenvector of the ordering matrix[97] that corresponds to the largest positive eigenvalue, $\hat{z}_i$ is a suitably defined molecular vector, and N is the number of molecules in the simulation box. In the present thesis, the molecular vector $\hat{z}_i$ has been defined as a unit vector linking the peptide's Cα and Cα+2.

The nematic order parameter P_2 describes the orientational order of the system and discriminates between ordered and disordered conformations. Its minimal value depends on the number of peptides according the following relation $\sqrt{81/40\pi \cdot N}$ [97], while its maximal value can reach the theoretical value of one (in a situation of perfect order). P_2 can be used to estimate and compare the amyloidogenic propensity of different peptide sequences.

In the present studies, the value of P_2, as adopted by Cecchini et al.[39, 97], is used to determine the β-aggregation stability of different Aβ segments in the presence and absence of a potential aggregation inhibitor.

1.4.4 cut-based Free-Energy Profile (cFEP)

"The miracle of the appropriateness of the language of mathematics for the formulation of the laws of physics is a wonderful gift which we neither understand nor deserve."
E. P. Wigner

Protein and peptide folding, starting from a very broad set of denatured conformations to a well-defined conformational state, is a very complex reaction governed by the free-energy surface[98].

The simplest way to study the free-energy surface (and in particular the free energy barriers between different states) is to project it as a function of one or two order parameters, such as RMSD, RGYR or number of native contacts[99].

The main disadvantage of these projections is that the essential information

about the free-energy surface and its barriers is lost because of the high number of degrees of freedom of the investigated system.

In recent years, new approaches based on complex networks have emerged for studying the free-energy landscape of peptide (and protein) folding[100-102]. Krivov and Karplus have introduced the minimum-cut procedure for the free-energy profile determination (cFEP) along a progress coordinate that preserves barriers[101].

The input for the cFEP calculation is the network of conformational transitions, which is derived from the direct transitions between clusterized snapshots (nodes of the network) sampled at a given time interval along the MD simulations. The cFEP procedure uses a partition function of the coordinates defined by a method based on the folding probability (pfold) or by the mean first passage time (mfpt) to a selected node[103].

Briefly, given a network, the partition function of a node, i, is given by $Z_i=\sum_j c_{ij}$, where c_{ij} is the edge capacity from node j to i, which is proportional to the number of direct transitions from j to i.

When the nodes are partitioned into two groups, A and B, according to the minimum-cut procedure[101], then $Z_A=\sum_{i\in A} Z_i$, $Z_B=\sum_{i\in B} Z_i$ and $Z_{AB}=\sum_{i\in A,\ j\in B} c_{ij}$, where Z_A is the partition function of the region A, Z_B is the partition function of the region B and Z_{AB} is the partition function of the cutting surface (i.e., of the barrier) that divides the network nodes into A and B. Thus the free-energy of the barrier can be written as $\Delta G=-kTln(Z_{AB})$.

It is possible to isolate all of the basins and barriers by iterative determinations of the minimum cuts between all pairs of nodes.

In practice, to calculate the cFEP using the mfpt as progress coordinate, the nodes are sorted according to their value of mfpt with respect to a target node. For each value of mfpt ($mfpt_{cut}$) between zero and $mfpt_{MAX}$, a point ($-kTln(Z_{AB}/Z)$, being Z the total number of nodes) on the cFEP can be calculated, where A is the set of all nodes with mfpt < $mfpt_{cut}$ and B is the set of nodes with mfpt > $mfpt_{cut}$ (see Figure 4). The cFEP method was previously used to accurately describe the free-energy surface of the folding of a β-hairpin[101], of a three-stranded β-sheet peptide[103] and of a cross-linked peptide[104], as well as to identifying pathways and intermediates of amyloid fibril formation[105, 106].

In the present thesis, cFEP has been used to characterize the Aβ monomer conformational variations in absence and presence of aggregation inhibitors as well as to identify their potential binding modes.

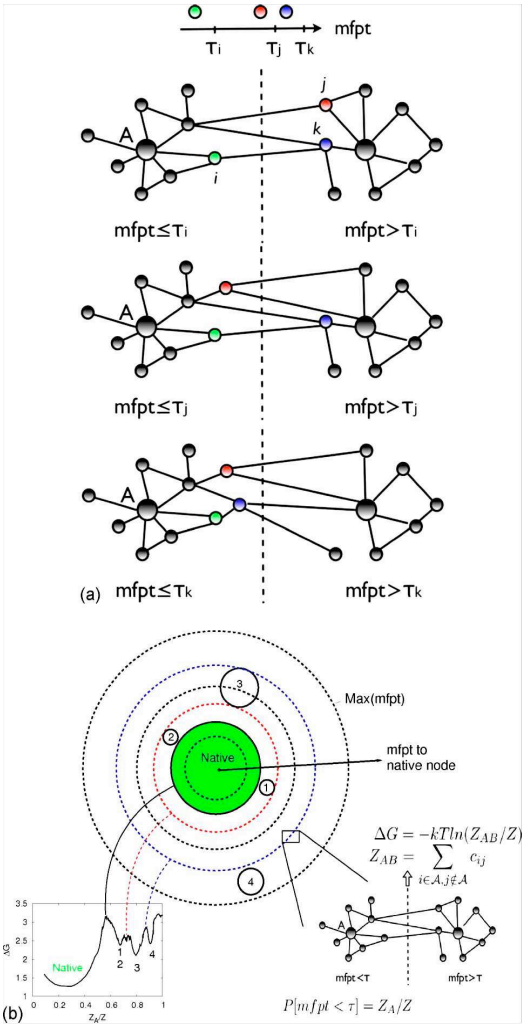

Figure 4. Schematic illustration of the cFEP procedure. **a)** Network nodes are first sorted according to increasing mfpt. For each $mfpt_{cut}$ value, in the range from zero (node A) to $mfpt_{MAX}$, a cut value Z_{AB} is computed. The set A of nodes on the left of the cut contains node A and all nodes with mfpt ≤ $mfpt_{cut}$, and Z_A/Z is its relative partition function. The green, red and blue nodes have increasing values of mfpt in this simplified illustration. **b)** Relationship between free-energy basins and the cFEP. Solid circles represent basins, while concentric dashed circle represent values of mfpt. To plot the cFEP, $\Delta G=-kTln(Z_{AB}/Z)$ is calculated as a function of Z_A/Z. Basins 1 and 2 overlap on the one-dimensional cFEP because they have the same mfpt distance from the native state and are therefore not seperated; they are both located in the first minimum of the profile after the first, (i.e. unfolding) barrier. This figure was taken from Muff S. and Caflisch A. *J Chem Phys* **2008**, *130*:125104-1-11.

Chapter 2

9,10-Anthraquinone hinders β-aggregation: How does a small molecule interfere with Aβ-peptide amyloid formation?

M. Convertino, R. Pellarin, M. Catto, A. Carotti, A. Caflisch.

Protein Science **2009**, *18*:792-800.

9,10-Anthraquinone hinders β-aggregation: How does a small molecule interfere with Aβ-peptide amyloid fibrillation?

Marino Convertino,[1,2] Riccardo Pellarin,[1]* Marco Catto,[2] Angelo Carotti,[2] and Amedeo Caflisch[1]*

[1]Department of Biochemistry, University of Zurich, CH-8057 Zurich, Switzerland
[2]Dipartimento Farmaco-Chimico, Università degli Studi di Bari, I-70125 Bari, Italy

Received 19 November 2008; Revised 22 January 2009; Accepted 26 January 2009
DOI: 10.1002/pro.87
Published online 10 February 2009 proteinscience.org

Abstract: Amyloid aggregation is linked to a number of neurodegenerative syndromes, the most prevalent one being Alzheimer's disease. In this pathology, the β-amyloid peptides (Aβ) aggregate into oligomers, protofibrils, and fibrils and eventually into plaques, which constitute the characteristic hallmark of Alzheimer's disease. Several low-molecular-weight compounds able to impair the Aβ aggregation process have been recently discovered; yet, a detailed description of their interactions with oligomers and fibrils is hitherto missing. Here, molecular dynamics simulations are used to investigate the influence of two relatively similar tricyclic, planar compounds, that is, 9, 10-anthraquinone (AQ) and anthracene (AC), on the early phase of the aggregation of the Aβ heptapeptide segment $H_{14}QKLVFF_{20}$, the hydrophobic stretch that promotes the Aβ self-assembly. The simulations show that AQ interferes with β-sheet formation more than AC. In particular, AQ intercalates into the β-sheet because polar interactions between the compound and the peptide backbone destabilize the interstrand hydrogen bonds, thereby favoring disorder. The thioflavin T-binding assay indicates that AQ, but not AC, sensibly reduces the amount of aggregated $Aβ_{1–40}$ peptide. Taken together, the *in silico* and *in vitro* results provide evidence that structural perturbations by AQ can remarkably affect ordered oligomerization. Moreover, the simulations shed light at the atomic level on the interactions between AQ and Aβ oligomers, providing useful insights for the design of small-molecule inhibitors of aggregation with therapeutic potential in Alzheimer's disease.

Keywords: molecular dynamics; implicit solvent; Alzheimer's disease; 9,10-anthraquinone; amyloid; aggregation inhibition

Introduction

Fibrillar aggregation and plaques deposition of the β-amyloid peptide (Aβ) in the brain are common hallmarks of Alzheimer's disease. The Aβ peptide is a 39- to 43-residue segment generated by proteolysis of the amyloid precursor protein. Although little is known on the link between the aggregation mechanism and neurotoxicity,[1] experimental evidence indicates that soluble oligomers and fibrillar precursors of Aβ may be the neurotoxic species.[2]

Abbreviations: Aβ, β-amyloid peptide; AC, anthracene; AQ, 9,10-anthraquinone; MD, molecular dynamics; ThT, thioflavin T.

Grant sponsor: Ministry of University and Scientific Research, Rome, Italy (FIRB project); Grant number: RBAU01LSCE; Grant sponsor: Swiss National Competence Center in Neural Plasticity and Repair.

*Correspondence to: Riccardo Pellarin, or Amedeo Caflisch Department of Biochemistry, University of Zurich, Winterthurerstrasse 190, CH-8057 Zurich, Switzerland. E-mail: pellarin@bioc.uzh.ch or caflisch@bioc.uzh.ch

Several therapeutic strategies have been suggested for blocking different key-steps in the amyloid aggregation process, including the direct inhibition of the aggregation by using either peptides or small molecules.[3,4] N-methylated peptides[5,6] and L/D-polypeptides[7] were shown to block Aβ aggregation. Several nonpeptidic low-molecular-weight molecules were observed to reduce Aβ fibril formation and cytotoxicity,[8–10] in particular, scaffolds with aromatic or heteroaromatic rings have been identified as potent inhibitors of amyloid aggregation.[11] As an example, indole derivatives inhibited fibril formation of Aβ peptide[12] and lysozyme.[13] Rifampicin and *p*-benzoquinone reduced the toxicity of islet amyloid peptide aggregates[14] as well as inhibited amyloid fibril formation of hen egg-white lysozymes.[15] Anthraquinones were shown to be effective inhibitors of tau protein aggregation.[16] Notably, some small molecules active *in vitro* also showed beneficial activity against Alzheimer's disease in a mouse model.[17]

Molecular dynamics (MD) simulations have shed light on the very early events of amyloid aggregation.[18–28] These studies have focused on the driving forces governing the β assembly, emphasizing the role of aromatic packing,[19] hydrophobic forces[20,21,23,27] and electrostatic interactions.[20] The arrangement of peptides within oligomers and the process of reorganization have also been investigated by MD studies.[18,19,22,24,26] Moreover, the crucial role of amino acid sequence in determining the propensity to form aggregates has been studied in detail.[23,29] Recently, based on simulations of the inhibition of $A\beta_{16-22}$ fibrillation by a N-methylated peptide, it has been postulated that the inhibitor can bind to different sites of a preformed fibril, and thereby perturb it via different mechanisms.[30] Because of both poor oral absorption and low penetration through the blood-brain barrier, peptidic inhibitors have much smaller potential as drugs than small nonpeptidic compounds, although important exceptions based on nonnatural aminoacids exist.[31] The mechanism of inhibition of fibril formation by small compounds is however still obscure.

Here, we analyze the influence of two planar and tricyclic compounds on the early phase of ordered aggregation of a segment of the Aβ peptide that promotes oligomerization. Implicit solvent MD simulations are used to investigate the aggregation of three $A\beta_{14-20}$ (Ac-H_{14}QKLVFF$_{20}$-NHMe) terminally blocked heptapeptides in the presence and absence of AQ or AC. The $A\beta_{14-20}$ segment is chosen because it has a high β-aggregation propensity according to biophysical experiments,[32,33] as well as atomistic simulations[29,34] and a phenomenological equation based on physicochemical properties of the primary structure.[35] Notably, the MD simulations show that a small substitution in molecular structure (two carbonyl groups replacing two aromatic CH) results in significant differences in the ability to influence early aggregation. The simulation results are validated by the thioflavin T (ThT)-binding fluorimetric assay.

Results and Discussion

Properties of $A\beta_{14-20}$ aggregates with and without tricyclic compounds

During the simulation the three-peptide system explores many different configurations, including aggregated, disaggregated, β structures with a variety of registers, and other spatial arrangements. The P_2 order parameter (described in the Methods section) has been adopted to monitor the degree of orientational order within the oligomers: a value close to one corresponds to an ordered trimer, with either parallel or antiparallel β-sheet, while a value close to zero reflects a fully disordered system [Fig. 1(A)]. The frequency histograms of P_2 for the unperturbed and perturbed systems [Fig. 1(B)] display a prominent peak at $P_2 = 0.8$, and a shoulder for P_2 values lower than 0.5, which includes disordered aggregates and isolated peptides. The P_2 value for which the three distributions cross each other ($P_2^* = 0.665$) is chosen as the crossover value between ordered and disordered states. With this definition, the values of order-disorder ratio r can be calculated (Table I). AQ perturbs the oligomer order more than AC, suggesting that the quinonic moiety significantly contributes to the process of disorganization.

The frequency distribution of interpeptide interaction energies [Fig. 1(C)] shows two peaks. By visual inspection, and by comparing the energies with the average P_2 [circles in Fig. 1(C)], we could assign the oligomer structures relative to the different regions in the energy [see insets in Fig. 1(C)]. The peak at −80 kcal/mol and the peak at −40 kcal/mol correspond to a peptide placed in the centre and at the edge of an ordered trimer, respectively. From the plot it is evident that the simulations with AQ have more events with interaction energy close to zero, originating from unstructured peptides bound to the oligomeric or isolated monomers. This indicates that the system's order is perturbed by AQ, which is able to intercalate into the oligomer and influence its structure.

Binding mechanism

The interactions at the basis of the activity of AQ are the hydrogen bonds, the aromatic contacts and, moreover, the ability to establish a favorable interaction between the central electron-poor quinonic ring and the electron-rich peptidic carbonyls, which here is called as $\pi^+\delta^-$ interaction (see Figs. 2 and 3). A typical series of events leading to β structure disruption by AQ is described in Figure 2. Once approached the oligomer, AQ separates the ordered peptides by interacting with amide hydrogens (blue dashed lines). It then penetrates into the oligomer, interfacing the

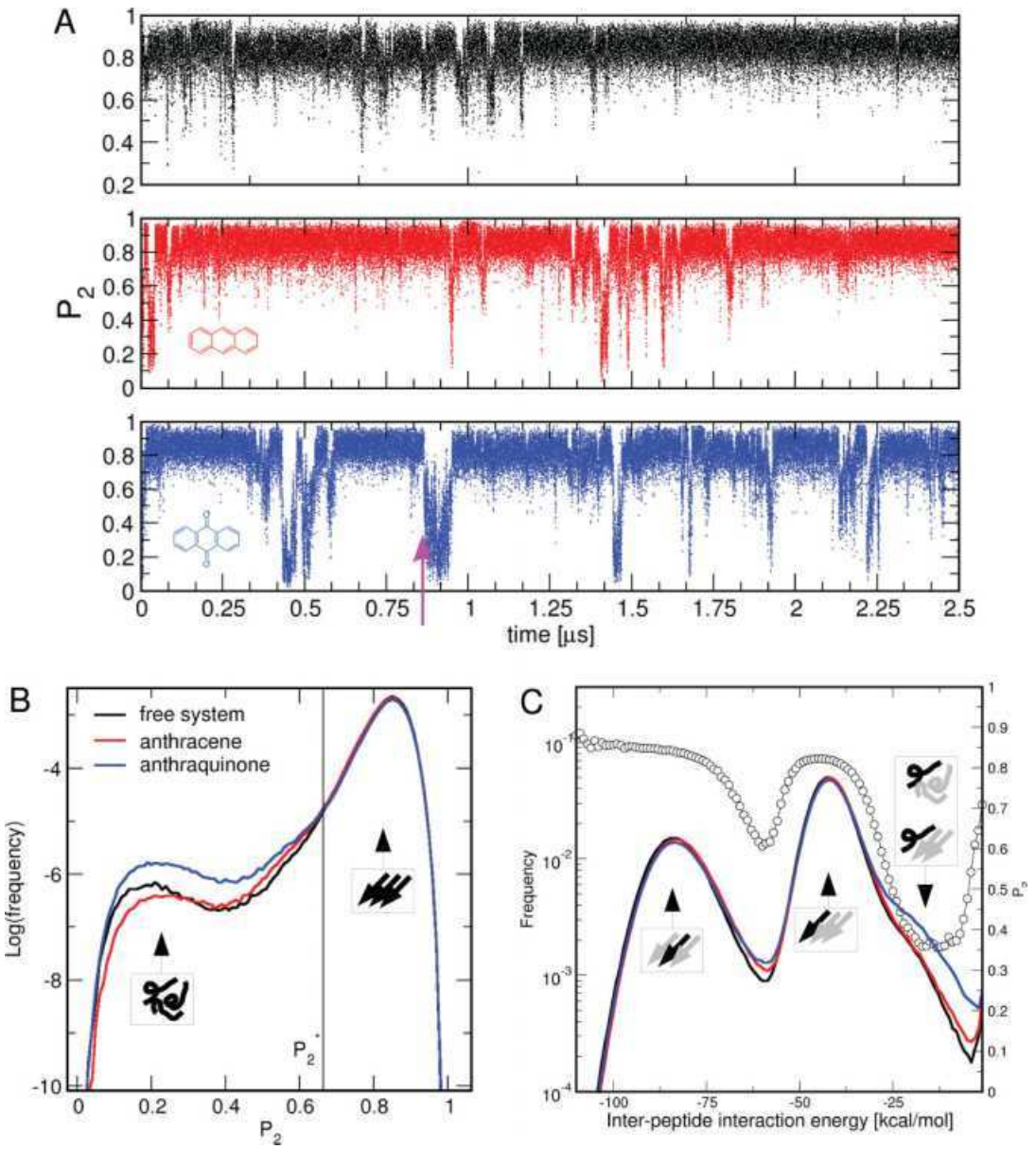

Figure 1. AQ hinders β-sheet formation more than AC. (A) Time series of the nematic order parameter P_2 for the free system (black), and in presence of AC (red) or AQ (blue). A similar behavior was observed in the other nine runs for each system. The magenta arrow indicates the temporal location of the snapshots shown in Figure 2. Molecular structures of AC and AQ are represented in the insets. (B) Distribution of the nematic order parameter P_2. Values of P_2 close to 0.2 and 0.8 correspond to disordered conformations and β-sheet structures, respectively. The three distributions cross each other at $P_2^* = 0.665$ (vertical solid line), which is the threshold value that separates the ordered from the disordered phase. (C) Interpeptide interaction energy distributions (solid lines, left *y*-axis; see Methods section) and average P_2 as a function of interaction energy (black circles, right *y*-axis). The two peaks of the energy distributions correspond to a peptide in the centre of an ordered oligomer (about −80 kcal/mol) and a peptide at the edge of an ordered oligomer (about −40 kcal/mol). The shoulder of the energy distribution at values of about −20 kcal/mol contains events with disordered or partially ordered oligomers. The P_2 values higher than 0.5 for interaction energy close to zero is due to the propensity of the isolated peptide for an extended conformation. The insets in (B) and (C) are schematic pictures of the oligomer conformations. [Color figure can be viewed in the online issue, which is available at www.interscience.wiley.com.]

carbonyl oxygens (red dashed lines). The β-sheet disruption is very rapid (less than 1 ns), which is in part a consequence of the low friction constant.

The distribution of backbone oxygens (see Fig. 3, top) shows the enrichment of coordinated carbonyl oxygens around the quinonic moieties of AQ with respect to the condensed aromatic rings of AC. Being able to coordinate two amide hydrogens, and two backbone carbonyl oxygens at the same time, the quinonic moiety plays a major role in the intercalation into the oligomer. In this way, AQ is able to sequestrate not only donors, but also acceptors of interchain

Table I. *Order-Disorder Ratio (r), Inhibition of Fibril Formation, and Number of Aromatic Contacts Between the Compounds and the Phenyl Rings of Phenylalanine*

System	r[a]	Activity[b] (%)	Aromatic contacts[c] (no. contacts per frame)
Unperturbed	10.2		
with AC	9.9	11	0.262
with AQ	6.7	33	0.242

[a] Ratio between order and disorder events sampled in the trajectories and estimated by Eq. (1).
[b] Inhibition of fibril formation measured by ThT fluorescence at a concentration of 30 μM $A\beta_{1-40}$ and 100 μM AC or AQ.
[c] Average number of aromatic contacts between the compounds and the phenyl ring of phenylalanine normalized by the total number of frames of simulations.

hydrogen bonds, which has three main consequences: (1) the disruption of the local intermolecular hydrogen bond geometry, (2) destabilization of the β-sheet structure, and (3) global disorganization of the oligomer, that is, reduction of the total order. On the other hand, AC is not able to interact with the peptides by hydrogen-bonds, or $\pi^+\delta^-$ interactions. Hydrophobic interactions alone are apparently not sufficient to perturb the ordered β architecture, as indicated by the similar values of r of the unperturbed and AC systems.

The number of aromatic contacts between the compounds and the phenyl rings of phenylalanine is reported in Table I. This interaction is slightly less frequent for AQ. This is due to the fact that, if compared with AC, AQ has also the ability to interact with peptide polar moieties, which are competitive with the hydrophobic ones. These results suggest that the aromatic interactions alone are not sufficient to drive the perturbation of $A\beta_{14-20}$ ordered oligomers, although they may favor the encounter of the tricyclic molecule with the peptides.

Experimental results on $A\beta_{1-40}$

The anti-aggregating activity of AC and AQ was determined in co-incubation experiments with $A\beta_{1-40}$ by monitoring maximal ThT emission intensity over the course of 21 days (see Methods section). As shown in Figure 4, the amyloid aggregation obeys the characteristic nucleation-dependent pattern, with three distinct phases: initial nucleation (lag phase), elongation, and

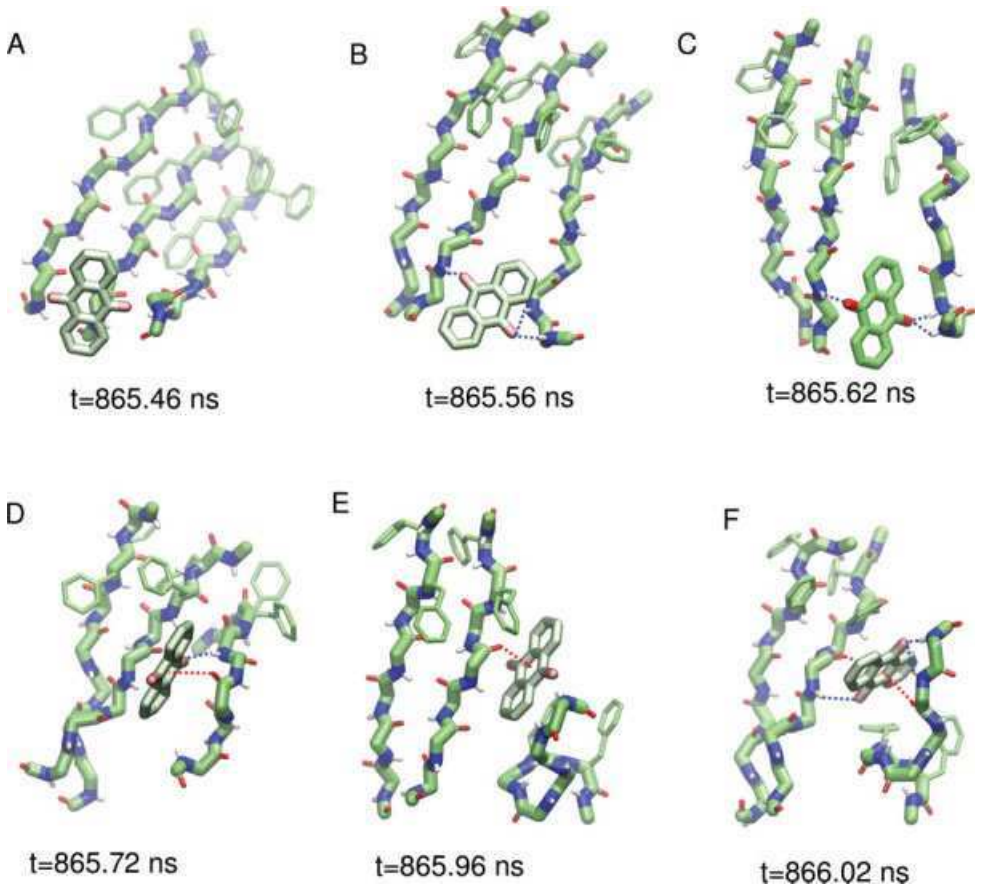

Figure 2. Atomistic details of β-sheet disruption by AQ. The times of the snapshots correspond to the time interval emphasized by an arrow in Figure 1(A). The quinonic moiety interacts with the peptide oligomer in a kind of "butter-knife" mechanism. AQ approaches the ordered oligomer (A) and starts to interact via hydrogen bond interactions (B and C, blue dashed lines). It subsequently intercalates into the ordered structure via hydrogen bonds and $\pi^+\delta^-$ interactions (D–F, red dashed line) and causes the disruption of the oligomer (F). [Color figure can be viewed in the online issue, which is available at www.interscience.wiley.com.]

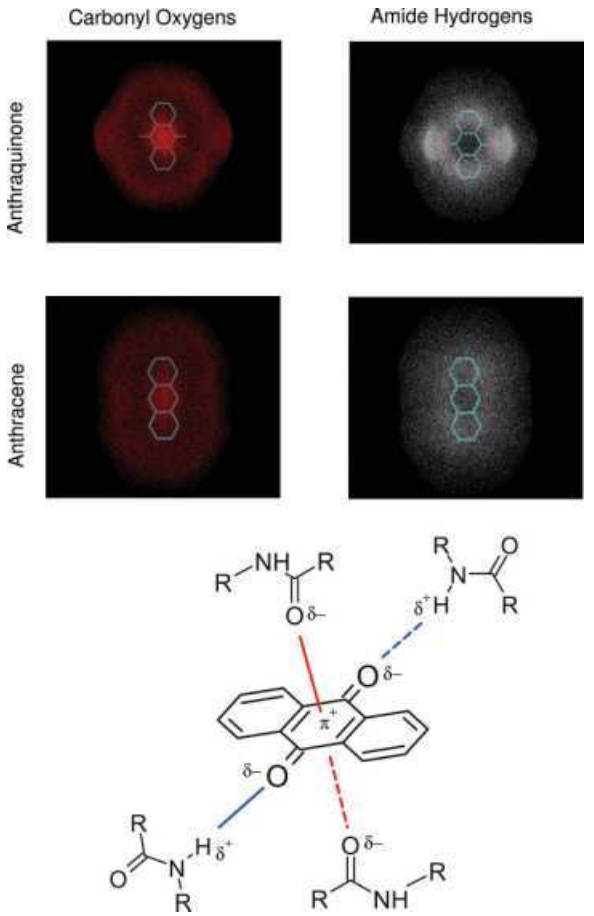

Figure 3. Interactions between backbone polar groups and AQ or AC. (Top) Positions of backbone carbonyl oxygens and amide hydrogens that are within 5 Å from any atom in AQ or AC are shown by dots to display the corresponding coordination. Denser clouds indicate a volume with higher coordination. (Bottom) $\pi^{+}\delta^{-}$ interaction scheme. Two electron-rich (δ^{-}) peptidic carbonyl oxygens interact with both faces of the electron-poor (π^{+}) AQ central ring.

equilibration. Under the present experimental conditions, the system reached its final equilibration phase after about 20 days. The shape of the curves presented in Figure 4 indicates that the final plateau is influenced by the presence of AQ and much less by AC. The ThT fluorescence emission intensity in the co-incubation with AQ (blue symbols) was nearly 33% lower than with the control peptide alone (black symbols). A significantly lower inhibitory effect, 11% decrease of ThT fluorescence emission intensity at the final plateau, was observed for AC (red symbols). The different inhibitory effects of AC and AQ are consistent with the MD simulation results (Table I). A quantitative agreement is not expected because of differences in the sequence (full-length Aβ in ThT assay versus seven-residue segment in MD), in relative mass concentrations, and temperature values (see Methods section).

The elongation rate marginally decreases in the presence of AQ, while the lag phase is not influenced at all by AQ or AC. Yamada and coworkers showed that nordihydroguaiaretic acid, curcumin, and rosmarinic acid, though reducing the amount of fibril at the equilibrium, did not extend the length of the lag phase in the formation of fibrillar Aβ, nor the time to proceed to equilibrium.[36] Recently, to explain the variable influence of compounds on $A\beta_{42}$ aggregation kinetics, a new mechanism of inhibition was suggested.[37] Compounds able to influence the elongation and the steady-state, but not the lag-phase, can prevent the self-assembly by blocking only the interstrand hydrogen-bond formation, in agreement with the AQ-binding mechanism discussed earlier, and not by stabilizing the nonamyloidogenic conformations of the polypeptide.

ThT measurements alone cannot unambiguously distinguish between inhibition of amyloid aggregation and competition of compounds with ThT binding. Meng *et al.*[38] showed that it is possible to determine whether an inhibitor is a false positive by adding the compound to a preincubated fibril sample and measuring ThT fluorescence thereafter. A fast decay (within few minutes) of the signal indicates that the compound is indeed competing with ThT. We measured the ThT fluorescence just after adding AQ and AC to two preincubated Aβ samples. Within few hours, we couldn't observe any signal decrease (data not shown), allowing us to exclude any direct competition between AC/AQ and ThT at the ThT-binding site.

Methods

Simulation protocol and analysis

The MD simulations were performed with the CHARMM program.[39] The peptide and compounds were modeled using the united atoms CHARMM

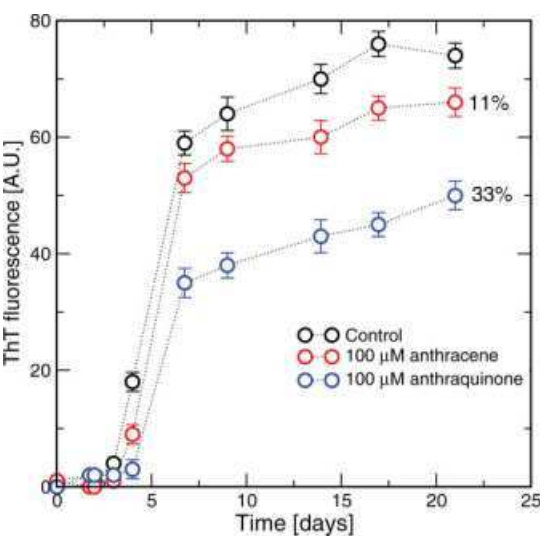

Figure 4. Time-dependent aggregation of $A\beta_{1-40}$ 30 μM, incubated in PBS (phosphate 10 mM, NaCl 100 mM, pH 7.4) at 25°C and monitored by ThT fluorescence. Error bars are standard deviations calculated from triplicate measures.

PARAM19 force field with its default truncation scheme for nonbonding interactions (cutoff of 7.5 Å). Hydration effects were accounted for by using SASA, a solvent-accessible surface based implicit model.[40] Partial charges for AQ were computed with the modified partial equalization of orbital electronegativity (MPEOE) algorithm.[41,42] To be consistent with the united atom model, charge summation of carbon atoms and their directly connected hydrogens was performed. The results were in agreement with the original CHARMM PARAM19 partial charges for phenylalanine, tryptophan and peptidic carbonyl. The difference in electronegativity between the oxygen atom in the peptidic moiety (partial charge: −0.55) and in the quinonic central ring (partial charge: −0.51) is due to the fact that the peptidic carbonyl is directly linked to a nitrogen, more electron-withdrawing with respect to the carbon atoms in the quinonic ring. There is a favorable interaction energy of −3.6 kcal/mol between *N*-methylacetamide and *p*-benzoquinone, computed at low dielectric conditions (i.e., distance depending dielectric function, without the SASA solvation contribution). This value is in agreement with the −3.9 kcal/mol value obtained by *ab initio* QM calculations.[43] To validate the parameterization of the bonding energy terms, two short MD simulations were performed for AQ and AC, using the SASA solvation model. Both molecules are stable, and the average bond distances and bond angles are comparable with the crystallographic data.[44]

The simulation box was prepared by introducing three monodispersed replicas of the same heptapeptide, with or without the presence of a single small molecule (AQ or AC). The concentration ratio peptide:compound of 3:1 is the minimal choice to have inhibitory effects and complex oligomeric structures. Note that the mass ratio peptide:compound is about 16 for the simulation and seven for the experiments (see ThT-Binding Assay section). To have the same mass ratio, one would have either to halve the compound concentration in the ThT assay, or to double the number of compounds in the simulation. In the first case the inhibition effect of AC would be undetectable. In the second case the compound-compound interactions would generate undesirable spurious effects, which is a disadvantage if one is interested in the oligomer–compound interaction mechanism. Simulations were carried out with periodic boundary conditions at fixed peptide concentration of 4.88 mM (the simulation box side was set to 98 Å), using Langevin integrator at low friction constant (0.1 ps^{-1}) and at the temperature of 330 K, which yields reversible aggregation within a reasonable computational time. Ten, 2.5 μs long, independent simulations were run for each system. A 2.5-μs run takes 3 weeks on a single AMD Opteron 252 CPU at 2.6 GHz.

Order parameters are useful quantities to monitor the structural transition within peptide oligomers.[25,29] In particular, the nematic order parameter P_2 allows to measure the amount of ordered β-structure in the system:

$$P_2 = \frac{1}{N}\sum_{i=1}^{N}\frac{3}{2}\left(\hat{\mathbf{z}}_i\cdot\hat{\mathbf{d}}\right)^2 - \frac{1}{2}$$

The unit vector $\hat{\mathbf{d}}$ that defines a preferential direction is the eigenvector of the order matrix that corresponds to the largest positive eigenvalue. The N molecular unit vectors $\hat{\mathbf{z}}_i$ are built joining the Cα atom of residue i to the Cα atom of residue $i + 2$ ($N = 3 \times 7$). The values of P_2 ranges from 0 to 1, which correspond to complete disorder and complete order, respectively. The complete order is achieved when all the unit vectors are parallel or antiparallel, while the disorder is obtained when none of unit vectors is parallel to any of the others.

P_2^* is a value of the order parameter chosen such that it separates the ordered from the disordered phase. Thus, the order-disorder ratio r is defined by the number of events where the system has a nematic order parameter lower than P_2^* (disorder) and greater that P_2^* (order):

$$r = \frac{n(P_2 > P_2^*)}{n(P_2 < P_2^*)} \quad (1)$$

Furthermore, the activity of the compounds is measured by calculating the interpeptide interaction energy, which is the CHARMM nonbond energy (van der Waals plus electrostatics) of a single peptide with the other two, without considering the compound molecule.

Aromatic contacts between the tricyclic compounds and the phenyl ring of Phe are calculated as follows. Given a trajectory frame, the centroids of the three rings of AC or AQ are calculated, together with the centroids of the six phenyl rings of Phe belonging to the three peptides. If any compound centroid is within 4 Å from any Phe centroid, then an aromatic contact is accounted. Note that more than one aromatic contact can be present at the same time, because the compounds have two sides available for the interfacing. The AC/AQ ratio of aromatic contacts is robust with respect to the choice of the cutoff up to 5 Å.

ThT-binding assay

The traditional spectrofluorimetric assay with ThT was chosen to assess the influence of the two tricyclic molecules, AQ and AC, on the kinetic of aggregation of $A\beta_{1-40}$. This technique easily enables to monitor the formation of β-sheet structures of aggregating peptides with ThT that leads to a marked increase of the fluorescence of ThT at defined wavelengths. Nevertheless, the β-sheet/ThT interaction is unselective and does not discriminate among oligomers, protofibrils, and

other transient species formed across the aggregation pathway.

The spectrofluorimetric assay was performed through the classical method of LeVine.[45] Briefly, ThT solution for fluorescence experiments was 25 μM in 25 mM phosphate buffer (pH 6.0). Quartz cuvette for aggregation tests contained $A\beta_{1-40}$ 30 μM control peptide (from AnaSpec, San José, CA) alone, or added either with AC or AQ 100 μM, in phosphate buffered saline (phosphate 10 mM, NaCl 100 mM, pH 7.4) containing 20% dimethyl sulphoxide to solubilize the test compounds. The concentration of compounds was chosen to have the highest yield of inhibition without precipitation effects. Samples were incubated at 25°C for 3 weeks. During this period, spectrofluorimetric readings were made in triplicate by dilution of 30 μL of sample in 470 μL of ThT solution at 25°C. Analyses were performed with a Perkin-Elmer LS 55 fluorimeter, in a 700-μL quartz cuvette, using FLWinLab software. Parameters were fixed as follows: excitation wavelength at 440 nm with 5-nm slit; emission at 485 nm with 10-nm slit; integration time 2 s. Plots of fluorescence emission intensity versus time (see Fig. 4) showed the typical sigmoidal curve of aggregation kinetics. Activities were calculated as percent of inhibition of free peptide aggregation after 3 weeks.

Conclusions

In previous works, the $A\beta_{14-20}$ heptapeptide was shown to have high aggregation propensity by biophysical experiments[32,33] and computational approaches,[34,35] suggesting a key role in the self-assembly of the full-length Aβ peptide. We have therefore hypothesized that the perturbation of the aggregation propensity of $A\beta_{14-20}$ can influence the assembly properties of the full-length Aβ sequence. Here, implicit solvent MD simulations have been used to investigate the effect of AQ and AC on the β-aggregation of three replicas of $A\beta_{14-20}$. The nematic order parameter P_2 was used to monitor the perturbation extent of β-aggregation.[34] Compared with AC, which is almost inert, AQ destabilizes the interstrand hydrogen bonds through favorable polar interactions with the backbone of the peptide. The quinonic moiety is able to tightly bind peptide backbone carbonyl oxygens and amide hydrogens through $\pi^+\delta^-$ interactions and hydrogen bonds, respectively, facilitating the intercalation of the molecule into the oligomer. The stability of the $\pi^+\delta^-$ interaction[46] has been previously documented in *ab initio* QM calculations,[43] the crystal packing of isocyanurate derivatives resolved by X-ray diffractometry,[47] and coordination of anions with electron-poor rings.[48,49]

Aromatic interactions have been shown to be determinant in the inhibition of fibril formation as well as the reduction of amyloid toxicity.[11] Our simulations reveal that such interactions favor the formation of the compound–oligomer complex, but are not sufficiently strong to significantly perturb the β-sheet formation of $A\beta_{14-20}$, as observed by comparing AC with AQ.

Perturbation of multimeric assembly is the basis for the activity of small compounds able to inhibit amyloid fibril formation. AQ only marginally affects the equilibrium properties of the unperturbed oligomeric system, that is, it slightly increases the disorderer events. Coarse grained simulations[50] have shown that even a small perturbation of the polypeptide free energy landscape, for example, a fraction of kcal/mol, dramatically influences the kinetics and the thermodynamics of the aggregation process. These simulation results could explain why a small perturbation produces the macroscopic decrease of amyloid aggregation observed *in vitro* in presence of inhibiting compounds. On the other hand, the slowing down or the inhibition of the ordered aggregation process, can multiply the alternative pathways for the aggregation,[51] increasing the chance to create other toxic species. For this reason, blocking the formation of oligomeric soluble species at their very early stages (note that the smallest oligomer, the Aβ dimer, has been recently reported to be synaptotoxic[52]) should be a viable strategy, providing that the accumulation of the Aβ monomer would not trigger any significant toxic effect.[53]

One of the main goals of the present work is the understanding of the interactions between tricyclic compounds and ordered oligomers. Knowledge of such interactions may suggest modifications of AQ for improving its antiaggregation activity. New functional groups potentially able to establish additional strong interactions with Aβ could be added to the quinonic scaffold to improve the strength of binding. Among them, positively charged aminic groups, such as those present in anthracyclinic and xantronic antitumor drugs, might be selected to engage in strong ionic interactions and hydrogen bonds with polar groups of Aβ. Indeed, some anthracyclines have shown excellent antifibrillogenic activity.[54] Moreover, pixantrone, an antitumor drug in phase III clinical trials for the treatment of relapsed or refractory indolent non-Hodgkin's lymphoma, showed activity and proved to selectively target soluble low oligomers of Aβ protein.[55] Another suggestion, inspired by the present simulation results, would be to link AQ to one or both termini of a recently discovered dipeptide inhibitor of Aβ oligomerization.[31] These experimental findings, together with the results obtained in the present study, provide useful insights for the design of new molecular entities targeting the early steps of formation of low oligomeric, toxic species.

Acknowledgments

The authors are grateful to F. Marchand and Dr. O. Nicolotti for interesting discussions and precious suggestions, Dr. R. Friedman for comments to the manuscript, and A. Widmer for providing the WitnotP program used

for visual analysis of the trajectories. The simulations were performed on the Matterhorn cluster of the University of Zurich and the support of C. Bolliger and A. Godknecht is gratefully acknowledged.

References

1. Lansbury PT, Lashuel HA (2006) A century-old debate on protein aggregation and neurodegeneration enters the clinic. Nature 443:774–779.
2. Haass C, Selkoe DJ (2007) Soluble protein oligomers in neurodegeneration: lessons from the Alzheimer's amyloid β-peptide. Nat Rev Mol Cell Biol 8:101–112.
3. Cohen FE, Kelly JW (2003) Therapeutic approaches to protein-misfolding diseases. Nature 426:905–909.
4. Necula M, Kayed R, Milton S, Glabe CG (2007) Small molecule inhibitors of aggregation indicate that amyloid β oligomerization and fibrillization pathways are independent and distinct. J Biol Chem 282:10311–10324.
5. Kokkoni N, Stott K, Amijee H, Mason JM, Doig AJ (2006) N-methylated peptide inhibitors of β-amyloid aggregation and toxicity. optimization of the inhibitor structure. Biochemistry 45:9906–9918.
6. Yan L-M, Velkova A, Tatarek-Nossol M, Andreetto E, Kapurniotu A (2007) IAPP mimic blocks Aβ cytotoxic self-assembly: cross-suppression of amyloid toxicity of Aβ and IAPP suggests a molecular link between Alzheimer's disease and type II diabetes. Angew Chem Int Ed Engl 46:1246–1252.
7. Ban T, Hoshino M, Takahashi S, Hamada D, Hasegawa K, Naiki H, Goto Y (2004) Direct observation of Aβ amyloid fibril growth and inhibition. J Mol Biol 344: 757–767.
8. Kanapathipillai M, Lentzen G, Sierks M, Park CB (2005) Ectoine and hydroxyectoine inhibit aggregation and neurotoxicity of Alzheimer's β-amyloid. FEBS Lett 579: 4775–4780.
9. Gervais F, Paquette J, Morissette C, Krzywkowski P, Yu M, Azzi M, Lacombe D, Kong X, Aman A, Laurin J, Szarek WA, Tremblay P (2007) Targeting soluble Aβ peptide with tramiprosate for the treatment of brain amyloidosis. Neurobiol Aging 28:537–547.
10. Mishra R, Bulic B, Sellin D, Jha S, Waldmann H, Winter R (2008) Small-molecule inhibitors of islet amyloid polypeptide fibril formation. Angew Chem Int Ed Engl 47: 4679–4682.
11. Porat Y, Mazor Y, Efrat S, Gazit E (2004) Inhibition of islet amyloid polypeptide fibril formation: a potential role for heteroaromatic interactions. Biochemistry 43: 14454–14462.
12. Cohen T, Frydman-Marom A, Rechter M, Gazit E (2006) Inhibition of amyloid fibril formation and cytotoxicity by hydroxyindole derivatives. Biochemistry 45:4727–4735.
13. Morshedi D, Rezaei-Ghaleh N, Ebrahim-Habibi A, Ahmadian S Nemat-Gorgani M (2007) Inhibition of amyloid fibrillation of lysozyme by indole derivatives-possible mechanism of action. FEBS J 274:6415–6425.
14. Tomiyama T, Kaneko H, Kataoka K, Asano S, Endo N (1997) Rifampicin inhibits the toxicity of pre-aggregated amyloid peptides by binding to peptide fibrils and preventing amyloid-cell interaction. Biochem J 322 (Part 3): 859–865.
15. Lieu VH, Wu JW, Wang SS-S, Wu C-H (2007) Inhibition of amyloid fibrillization of hen egg-white lysozymes by rifampicin and *p*-benzoquinone. Biotechnol Prog 23: 698–706.
16. Pickhardt M, Gazova Z, von Bergen M, Khlistunova I, Wang Y, Hascher A, Mandelkow E-M, Biernat J, Mandelkow E (2005) Anthraquinones inhibit tau aggregation and dissolve Alzheimer's paired helical filaments in vitro and in cells. J Biol Chem 280:3628–3635.
17. McLaurin J, Kierstead ME, Brown ME, Hawkes CA, Lambermon MHL, Phinney AL, Darabie AA, Cousins JE, French JE, Lan MF, Chen F, Wong SSN, Mount HTJ, Fraser PE, Westaway D, George-Hyslop PS (2006) Cyclohexanehexol inhibitors of Aβ aggregation prevent and reverse Alzheimer phenotype in a mouse model. Nat Med 12:801–808.
18. Ma B, Nussinov R (2002) Stabilities and conformations of Alzheimer's β-amyloid peptide oligomers (Aβ 16–22, Aβ 16–35, and Aβ 10–35): sequence effects. Proc Natl Acad Sci USA 99:14126–14131.
19. Gsponer J, Haberthür U, Caflisch A (2003) The role of side-chain interactions in the early steps of aggregation: Molecular dynamics simulations of an amyloid-forming peptide from the yeast prion Sup35. Proc Natl Acad Sci USA 100:5154–5159.
20. Klimov DK, Thirumalai D (2003) Dissecting the assembly of Aβ16–22 amyloid peptides into antiparallel β sheets. Structure 11:295–307.
21. Hwang W, Zhang S, Kamm RD, Karplus M (2004) Kinetic control of dimer structure formation in amyloid fibrillogenesis. Proc Natl Acad Sci USA 101:12916–12921.
22. Buchete N-V, Tycko R, Hummer G (2005) Molecular dynamics simulations of Alzheimer's β-amyloid protofilaments. J Mol Biol 353:804–821.
23. de la Paz ML, de Mori GMS, Serrano L, Colombo G (2005) Sequence dependence of amyloid fibril formation: insights from molecular dynamics simulations. J Mol Biol 349:583–596.
24. Melquiond A, Mousseau N, Derreumaux P (2006) Structures of soluble amyloid oligomers from computer simulations. Proteins 65:180–191.
25. Cecchini M, Rao F, Seeber M, Caflisch A (2004) Replica exchange molecular dynamics simulations of amyloid peptide aggregation. J Chem Phys 121:10748–10756.
26. Cheon M, Chang I, Mohanty S, Luheshi LM, Dobson CM, Vendruscolo M, Favrin G (2007) Structural reorganisation and potential toxicity of oligomeric species formed during the assembly of amyloid fibrils. PLoS Comput Biol 3:1727–1738.
27. Hills RD, Brooks CL (2007) Hydrophobic cooperativity as a mechanism for amyloid nucleation. J Mol Biol 368: 894–901.
28. Simone AD, Esposito L, Pedone C, Vitagliano L (2008) Insights into stability and toxicity of amyloid-like oligomers by replica exchange molecular dynamics analyses. Biophys J 95:1965–1973.
29. Cecchini M, Curcio R, Pappalardo M, Melki R, Caflisch A (2006) A molecular dynamics approach to the structural characterization of amyloid aggregation. J Mol Biol 357: 1306–1321.
30. Soto P, Griffin MA, Shea J-E (2007) New insights into the mechanism of Alzheimer amyloid-beta fibrillogenesis inhibition by N-methylated peptides. Biophys J 93: 3015–3025.
31. Frydman-Marom A, Rechter M, Bram Y, Shalev DE, Gazit E (2009) Cognitive performance recovery of Alzheimer's disease model mice by modulating early soluble amyloidal assemblies. Angew Chem Int Ed Engl 48:1981–1986.
32. Tjernberg LO, Näslund J, Lindqvist F, Johansson J, Karlström AR, Thyberg J, Terenius L, Nordstedt C (1996) Arrest of β-amyloid fibril formation by a pentapeptide ligand. J Biol Chem 271:8545–8548.
33. Williams AD, Portelius E, Kheterpal I, Tao Guo J, Cook KD, Xu Y, Wetzel R (2004) Mapping Aβ amyloid fibril secondary structure using scanning proline mutagenesis. J Mol Biol 335:833–842.

34. Caflisch A (2006) Computational models for the prediction of polypeptide aggregation propensity. Curr Opin Chem Biol 10:437–444.
35. Tartaglia GG, Cavalli A, Pellarin R, Caflisch A (2005) Prediction of aggregation rate and aggregation-prone segments in polypeptide sequences. Protein Sci 14:2723–2734.
36. Ono K, Hasegawa K, Naiki H, Yamada M (2004) Curcumin has potent anti-amyloidogenic affects for Alzheimer's β-amyloid fibrils in vitro. J Neurosci Res 75:742–750.
37. Bartolini M, Bertucci C, Bolognesi ML, Cavalli A, Melchiorre C, Andrisano V (2007) Insight into the kinetic of Amyloid β (1–42) peptide self-aggregation: elucidation of inhibitors' mechanism of action. Chem Biol Chem 8: 2152–2161.
38. Meng F, Marek P, Potter KJ, Verchere CB, Raleigh DP (2008) Rifampicin does not prevent amyloid fibril formation by human islet amyloid polypeptide but does inhibit fibril Thioflavin-T interactions: implications for mechanistic studies of β-cell death. Biochemistry 47:6016–6024.
39. Brooks BR, Bruccoleri RE, Olafson BD, States DJ, Swaminathan S, Karplus M (1983) CHARMM: A program for macromolecular energy, minimization, and dynamics calculations. J Comput Chem 4:187–217.
40. Ferrara P, Apostolakis J, Caflisch A (2002) Evaluation of a fast implicit solvent model for molecular dynamics simulations. Proteins: Struct Funct Bioinformat 46:24–33.
41. No K, Grant J, Scheraga H (1990) Determination of net atomic charges using a modified partial equalization of orbital electronegativity method. 1. Application to neutral molecules as models for polypeptides. J Phys Chem 94: 4732–4739.
42. No K, Grant J, Jhon M, Scheraga H (1990) Determination of net atomic charges using a modified partial equalization of orbital electronegativity method. 2. Application to ionic and aromatic molecules as models for polypeptides. J Phys Chem 94:4740–4746.
43. Li Y, Snyder L, Langley DR (2003) Electrostatic interaction of π-acidic amides with hydrogen-bond acceptors. Bioorganic & Medicinal Chemistry Letters 13:3261–3266.
44. Fu Y, Brock CP (1998) Temperature dependence of the rigid-body motion of Anthraquinone. Acta Cryst B 54: 308–315.
45. LeVine H, III. 1993. Thioflavine T interaction with synthetic Alzheimer's disease β-amyloid peptides: detection of amyloid aggregation in solution. Protein 2:404–410.
46. Meyer EA, Castellano RK, Diederich F (2003) Interactions with aromatic rings in chemical and biological recognition. Angew Chem Int Ed Engl 42:1210–1250.
47. Thalladi VR, Katz AK, Carrell HL, Nangia A, Desiraju GR (1998) Trimethyl isocyanurate and triethyl isocyanurate. Acta Crystallogr C 54 (Part 1):86–89.
48. Frontera A, Saczewski F, Gdaniec M, Dziemidowicz-Borys E, Kurland A, Deyà PM, Quiñonero D, Garau C (2005) Anion-π interactions in cyanuric acids: a combined crystallographic and computational study. Chemistry 11: 6560–6567.
49. Garau C, Frontera A, Quinonero D, Ballester P, Costa A, Deyà PM. (2004) Cation-π versus anion-π interactions: a comparative *ab initio* study based on energetic, electron charge density and aromatic features. Chem Phys Lett 392:85–89.
50. Pellarin R, Caflisch A (2006) Interpreting the aggregation kinetics of amyloid peptides. J Mol Biol 360:882–892.
51. Pellarin R, Guarnera E, Caflisch A (2007) Pathways and intermediates of amyloid fibril formation. J Mol Biol 374: 917–924.
52. Shankar GM, Li S, Mehta TH, Garcia-Munoz A, Shepardson NE, Smith I, Brett FM, Farrell MA, Rowan MJ, Lemere CA, Regan CM, Walsh DM, Sabatini BL, Selkoe DJ (2008) Amyloid-β protein dimers isolated directly from Alzheimer's brains impair synaptic plasticity and memory. Nat Med 14:837–842.
53. Brody DL, Magnoni S, Schwetye KE, Spinner ML, Esparza TJ, Stocchetti N, Zipfel GJ, Holtzman DM (2008) Amyloid-β dynamics correlate with neurological status in the injured human brain. Science 321: 1221–1224.
54. Bandiera T, Lansen J, Post C, Varasi M (1997) Inhibitors of Aβ peptide aggregation as potential anti-Alzheimer agents. Curr Med Chem 4:159–170.
55. Colombo R, Carotti A, Catto M, Racchi M, Lanni C, Verga L, Gabriele C, De Lorenzi E (in press) Capillary electrophoresis can identify small molecules that selectively target soluble oligomers of Aβ protein and display antifibrillogenic activity. Electrophoresis.

Chapter 3

Complete Phenotypic Recovery of an Alzheimer's Disease Model by a Quinone-Tryptophan Hybrid Aggregation Inhibitor

R. Scherzer-Attali, R. Pellarin, M. Convertino, A. Frydman-Marom, N. Egoz-Matia, S. Peled, M. Levy-Sakin, D. E. Shalev, A. Caflisch, E. Gazit, D. Segal.

PLoS ONE **2010**, *5(6)*:e11101.

Supporting informations available at the following web-page:
http://www.plosone.org/article/info%3Adoi%2F10.1371%2Fjournal.pone.0011101#s5

OPEN ACCESS Freely available online

PLoS one

Complete Phenotypic Recovery of an Alzheimer's Disease Model by a Quinone-Tryptophan Hybrid Aggregation Inhibitor

Roni Scherzer-Attali[1], Riccardo Pellarin[2], Marino Convertino[2], Anat Frydman-Marom[1], Nirit Egoz-Matia[1], Sivan Peled[1], Michal Levy-Sakin[1], Deborah E. Shalev[3], Amedeo Caflisch[2], Ehud Gazit[1]*, Daniel Segal[1]*

1 Department of Molecular Microbiology and Biotechnology, Tel-Aviv University, Tel-Aviv, Israel, **2** Department of Biochemistry, University of Zurich, Zurich, Switzerland, **3** Wolfson Centre for Applied Structural Biology, Hebrew University of Jerusalem, Jerusalem, Israel

Abstract

The rational design of amyloid oligomer inhibitors is yet an unmet drug development need. Previous studies have identified the role of tryptophan in amyloid recognition, association and inhibition. Furthermore, tryptophan was ranked as the residue with highest amyloidogenic propensity. Other studies have demonstrated that quinones, specifically anthraquinones, can serve as aggregation inhibitors probably due to the dipole interaction of the quinonic ring with aromatic recognition sites within the amyloidogenic proteins. Here, using *in vitro*, *in vivo* and *in silico* tools we describe the synthesis and functional characterization of a rationally designed inhibitor of the Alzheimer's disease-associated β-amyloid. This compound, 1,4-naphthoquinon-2-yl-L-tryptophan (NQTrp), combines the recognition capacities of both quinone and tryptophan moieties and completely inhibited Aβ oligomerization and fibrillization, as well as the cytotoxic effect of Aβ oligomers towards cultured neuronal cell line. Furthermore, when fed to transgenic Alzheimer's disease Drosophila model it prolonged their life span and completely abolished their defective locomotion. Analysis of the brains of these flies showed a significant reduction in oligomeric species of Aβ while immuno-staining of the 3rd instar larval brains showed a significant reduction in Aβ accumulation. Computational studies, as well as NMR and CD spectroscopy provide mechanistic insight into the activity of the compound which is most likely mediated by clamping of the aromatic recognition interface in the central segment of Aβ. Our results demonstrate that interfering with the aromatic core of amyloidogenic peptides is a promising approach for inhibiting various pathogenic species associated with amyloidogenic diseases. The compound NQTrp can serve as a lead for developing a new class of disease modifying drugs for Alzheimer's disease.

Citation: Scherzer-Attali R, Pellarin R, Convertino M, Frydman-Marom A, Egoz-Matia N, et al. (2010) Complete Phenotypic Recovery of an Alzheimer's Disease Model by a Quinone-Tryptophan Hybrid Aggregation Inhibitor. PLoS ONE 5(6): e11101. doi:10.1371/journal.pone.0011101

Editor: Juliet Ann Gerrard, University of Canterbury, New Zealand

Received March 22, 2010; **Accepted** May 20, 2010; **Published** June 14, 2010

Funding: The authors acknowledge the funding by the German-Israeli Project Cooperation (DIP) to UG and the Swiss National Competence Center in Research (NCCR) on Neural Plasticity and Repair and the Swiss National Science Foundation, to AC. The funders had no role in study design, data collection and analysis, decision to publish, or preparation of the manuscript.

Competing Interests: The authors have declared that no competing interests exist.

* E-mail: vpr@tauex.tau.ac.il (EG); dsegal@post.tau.ac.il (DS)

Introduction

Alzheimer's disease (AD), a progressive neurodegenerative disorder for which there is no cure or effective treatment, is the leading cause of dementia in aged humans. Symptoms include memory loss, confusion, impaired judgment, personality changes, disorientation and loss of language skills [1,2]. The major neuropathological changes in the brains of AD patients include neuronal death, particularly in regions related to memory and cognition and the presence of intra- and extra-cellular abnormal protein aggregates [3,4] known as neurofibrillary tangles and amyloid plaques, respectively. In the past several years a large body of evidence has established a pathological role for β-amyloid polypeptide (Aβ) in AD [5–10]. Accumulating evidence indicate a fundamental role of the early soluble oligomeric species of Aβ, rather than the mature fibrillar species, in the pathogenesis of AD [11–15]. Yet, the molecular mechanism underlying the assembly of the different Aβ species is not fully understood. However, since these structures self-assemble, from monomers to higher oligomeric or fibrillar structures in a highly ordered and efficient manner, it is likely that specific recognition elements mediate the process.

We and others have identified a central role of aromatic residues in formation and stabilization of amyloid structures [16–19]. This notion has gained direct evidence by high-resolution structural studies [20,21], theoretical analysis and molecular dynamics simulations [22–25]. Among the aromatic moieties, tryptophan was ranked as the residue with highest amyloidogenic potential by Dobson and co-workers [26] and an un-biased analysis, using peptide array technology, has clearly indicated a significantly higher affinity of tryptophan-modified recognition module in the molecular association of the islet amyloid polypeptide [27]. Indeed, as expected from these findings, several small aromatic molecules such as polyphenols [28–30] and small aromatic peptides [31] were shown to inhibit the aggregation of several amyloidogenic peptides. Furthermore, we have shown significant inhibition *in vitro* of the Aβ polypeptide by indole derivatives [32]. Moreover, we have recently demonstrated efficient inhibition of Aβ oligomerization by a short D-tryptophan-Aib dipeptide both *in vitro* and *in vivo* [31], further underscoring the important role of

tryptophan in the binding and inhibition of Aβ. These findings have led to the suggestion that targeting of aromatic recognition interfaces by tryptophan could be a useful strategy for anti-amyloid formation.

Quinones have long been known to act as inhibitors of various metabolic pathways in the cell, to have anti-bacterial, anti-viral, and also anti-cancer activities [33,34]. Several quinones have been shown to be effective inhibitors of the aggregation of several amyloidogenic proteins. For example, *p*-benzoquinone was reported to reduce the toxicity of islet amyloid peptide aggregates [35] and inhibit amyloid fibril formation by hen egg-white lysozymes [36]. Likewise, anthraquinones were demonstrated to be effective inhibitors of Tau protein aggregation [37]. Recently, 1,2-naphthoquinone was shown to effectively inhibit $A\beta_{42}$ oligomerization *in vitro* [38]. It appears that the asymmetric dipole of the quinonic ring plays a central role in the interaction between the molecule and the amyloidogenic peptides. The interactions at the basis of the anti-amyloid activity of anthraquinone (a tri-cyclic quinone) were recently shown to be the hydrogen bonds, the aromatic contacts and, moreover, the ability to establish a favorable interaction between the central electron-poor quinonic ring and the electron-rich peptidic carbonyls [39].

Here we sought to combine the strong interaction and recognition between tryptophan and the Aβ peptide with the documented inhibitory capability of quinones towards Aβ assembly. To that end we examined the effect of 12 different hybrid molecules, consisting of a naphthoquinone and different linked residues, towards Aβ oligomerization and fibrillization. Among the compounds tested the hybrid 1,4-naphthoquinon-2-yl-L-tryptophan (termed hereafter NQTrp) [40] was found to be the most effective.

We hypothesize that intermolecular alignment of the phenyl-alanine (at position 19 or 20 of the Aβ sequence) intercalated between the flat electron-deficient naphthoquinone moiety and the high electron-dense indole ring of the tryptophan, would lead to formation of a near face-to-face stable complex. Due to near face-to-face and edge-to-face geometry accompanied by sterical hindrance, the intermolecular complex of the aromatic elements effectively prevents Aβ assembly. Structural analysis supports this proposed mode of action of NQTrp. *In vivo* assays demonstrate that Aβ inhibition is accompanied by significant amelioration of AD-engendered symptoms.

Results

Twelve naphthoquinone hybrid molecules were screened for their ability to inhibit formation of Aβ oligomers and fibrils *in vitro* [Figure S1, Table S1]. All twelve molecules included a 1,4-naphthoquinone, but with different residues linked to it, some aromatic and some not. All hybrid molecules were analyzed both in the oligomer inhibition assay and ThT fibril inhibition assay described below for NQTrp, followed by TEM analysis (not shown). Results of all hybrids are summed up in Table S1. They show that NQTrp had strongest inhibition activity, towards the formation of both Aβ oligomers and fibrils. It is also apparent that both the D isomer of NQTrp (compound IID in Table S2) and the indole derivative (compound III) are good inhibitors. These results strongly suggest that the linking between 1,4-naphthoquinone and a molecule containing an indole ring is crucial for optimal inhibition.

Inhibition of toxic Aβ oligomer species

The effect of NQTrp on the ability of early non-toxic intermediate Aβ oligomers (~18 kDa) to further grow into the toxic dodecameric oligomer assemblies (~56 kDa) was analyzed using the protocol established by Hillen and coworkers [15]. This protocol results in the formation of SDS-stable oligomers that display toxic effects on the long-term potentiation of cultured neural cells [15]. For example, to evaluate the effect of NQTrp (Figure 1A) on the transformation of the Aβ into the toxic assemblies, the inhibitor was incubated with $A\beta_{1-42}$ at increasing molar ratios, and the reaction mixtures were resolved on SDS-PAGE (Figure 1B). The results reveal dose-dependent inhibition, by NQTrp, of the ability of Aβ to assemble into toxic oligomers (~56 kDa), inhibition was apparent at a low 5:1 ($A\beta_{1-42}$:NQTrp);

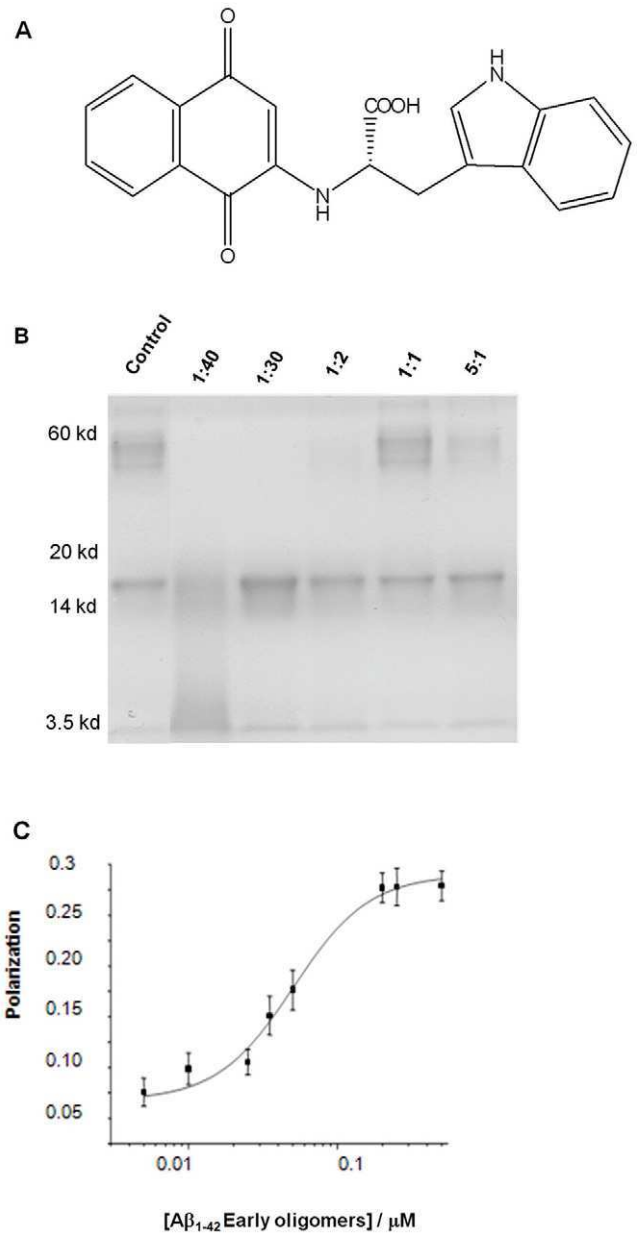

Figure 1. Inhibition of Aβ oligomer formation *in vitro*. A. Structure of 1,4-naphthoquinon-2-yl-L-tryptophan (NQTrp). **B**. Determination of the dose-dependent effect of NQTrp on soluble oligomer formation. Soluble oligomers were prepared according to the method of Barghorn *et al.* [15] with and without increasing concentration of NQTrp. Aβ concentration was set at 133 μM. Molar ratios of Aβ:NQTrp are indicated. The control is Aβ only. **C**. The affinity of NQTrp towards early oligomers was determined using fluorescence anisotropy.
doi:10.1371/journal.pone.0011101.g001

however the inhibition profile is non linear. The decreased inhibition effect at mid-range molar rations such as at a 1:1 ratio may be due to a competing homomolecular noncovalent interaction as observed for various other small molecular inhibitors such as indole moieties and small peptides. The inhibitor appears to stabilize the non-toxic early oligomers and inhibit their further growth into toxic species. Complete inhibition was seen only at molar excess of NQTrp.

Characterization of the interaction between NQTrp and Aβ

The affinity of NQTrp towards the early $A\beta_{1-42}$ assemblies was demonstrated using fluorescence anisotropy assay, taking advantage of the intrinsic fluorescence of the Trp-substituted quinone and its relatively small size as compared to the Aβ oligomers. Increasing amounts of early assemblies of Aβ were titrated into a solution of NQTrp and anisotropy was determined (Figure 1C). The affinity constant of NQTrp was estimated to be 90 nM.

Inhibition of amyloid fibril formation by NQTrp

The relative contribution of Aβ fibrils versus oligomers to the pathogenesis of AD has not been completely resolved [41]. We therefore wanted to discern whether or not NQTrp also inhibits the formation of mature β-amyloid fibrils. To that end we used the Thioflavin-T (ThT) binding assay, which provides a quantitative measure of amyloid fibril formation. $A\beta_{1-40}$ was allowed to form amyloid fibrils either in the absence or in the presence of increasing concentrations of NQTrp (Figure 2A). The process of fibrillization was followed for several days until a plateau was reached and its kinetics was measured. The formation of Aβ fibrils was significantly reduced in the presence of the inhibitor, even at low molar ratios of 4:1 ($A\beta_{1-40}$:NQTrp). This is especially evident after 270 hours (Figure 2B). A similar experiment using $A\beta_{1-42}$ resulted in IC_{50} of 50 nM (Figure 2E). These results clearly indicate that the NQTrp is an effective inhibitor of Aβ fibril formation.

The morphology of the Aβ fibrils formed during the course of fibrillization was compared, in the presence and in the absence of NQTrp, using transmission electron microscopy (TEM). Samples were taken from the amyloid fibril formation experiment after 7 days of incubation. The fibrils formed by Aβ alone were large, broad and ribbon-like (Figure 2C). The samples containing Aβ and NQTrp showed drastic reduction of fibrils. The few fibrils that formed in the presence of the inhibitor were much thinner and

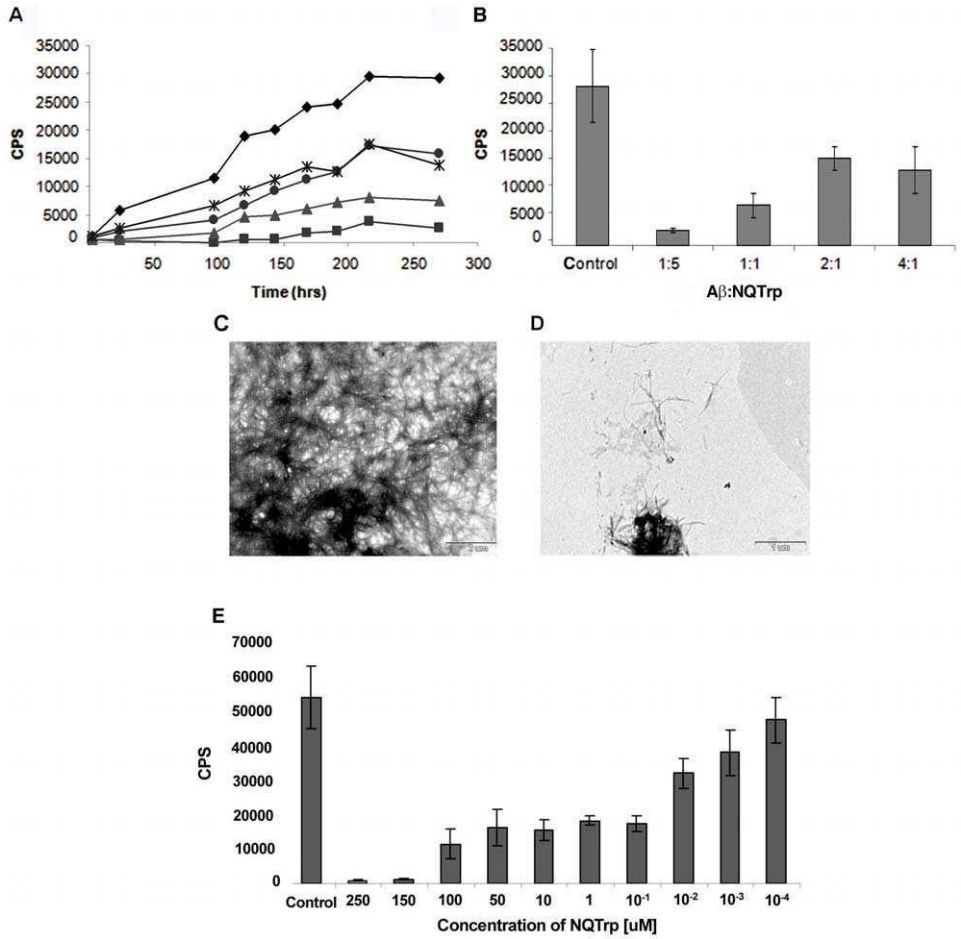

Figure 2. Inhibition of Aβ fibril formation *in vitro*. A. Dose dependent kinetic analysis of the inhibition of NQTrp towards fibril formation of $A\beta_{1-42}$ over the course of 270 hours. Aβ concentration was set to 5μM. Concentrations are expressed as Aβ:quinone molar ratio: Control - $A\beta_{1-42}$ only (♦), 1:5 (■), 1:1 (▲), 2:1 (●), 4:1 (*). (CPS = Counts Per Second) **B**. Endpoint of ThT analysis after 270 hours. **C–D**. Transmission Electron Microscope images taken from ThT analysis after 270 hours. $A\beta_{1-42}$ alone (**C**), $A\beta_{1-42}$ with NQTrp (1:5) (**D**). E. Dose dependent inhibition by NQTrp of the fibrillization of $A\beta_{1-42}$ (ThT assay). Concentration of $A\beta_{1-42}$ was set to 5uM. Control - $A\beta_{1-42}$ alone. An IC_{50} of 50nM was calculated.
doi:10.1371/journal.pone.0011101.g002

shorter (Figure 2D). This strongly correlated with the values observed in the amyloid fibril formation experiment.

NMR analysis of the interaction of NQTrp with Aβ

To characterize the precise interaction between NQTrp and Aβ, NMR analysis was conducted. NQTrp was incubated with a truncated fragment of Aβ, $Aβ_{12–28}$, which is a less-aggregative fragment, commonly used to avoid complications of oligomerization and fibrillization during the NMR process. Aβ residues 16–22 have been shown to participate in the transition into the β-sheet secondary structure and are independently capable of forming amyloid fibrils [42–44]. Furthermore, this short fragment of Aβ contains the central aromatic recognition motif of the polypeptide [44].

NQTrp was titrated into $Aβ_{12–28}$ sample in 10 µL aliquots, in the same solvent batch as the peptide samples, to achieve increments of 0.11 mM of NQTrp per aliquot. After each addition, the ^{1}H-NMR spectrum was taken. The addition of NQTrp to $Aβ_{12–28}$ in solution affected the backbone amide chemical shifts of the peptide (Figure 3A). Changes in chemical shift at a 2:1 molar ratio ($Aβ_{12–28}$:NQTrp) were compared to the average change in chemical shift of 0.1 Hz when a 0.1 mM aliquot of NQTrp was added as a control. These were most evident in residues Phe20, Ala21 and Glu22, which showed changes of 8, 5 and 3 Hz, respectively. Both Val18 and Val24, also showed a lesser change in chemical shift of 2 Hz. Non-terminal residues that were unaffected by the addition of NQTrp showed mostly chemical shift deviations of less than 1 Hz. The NMR

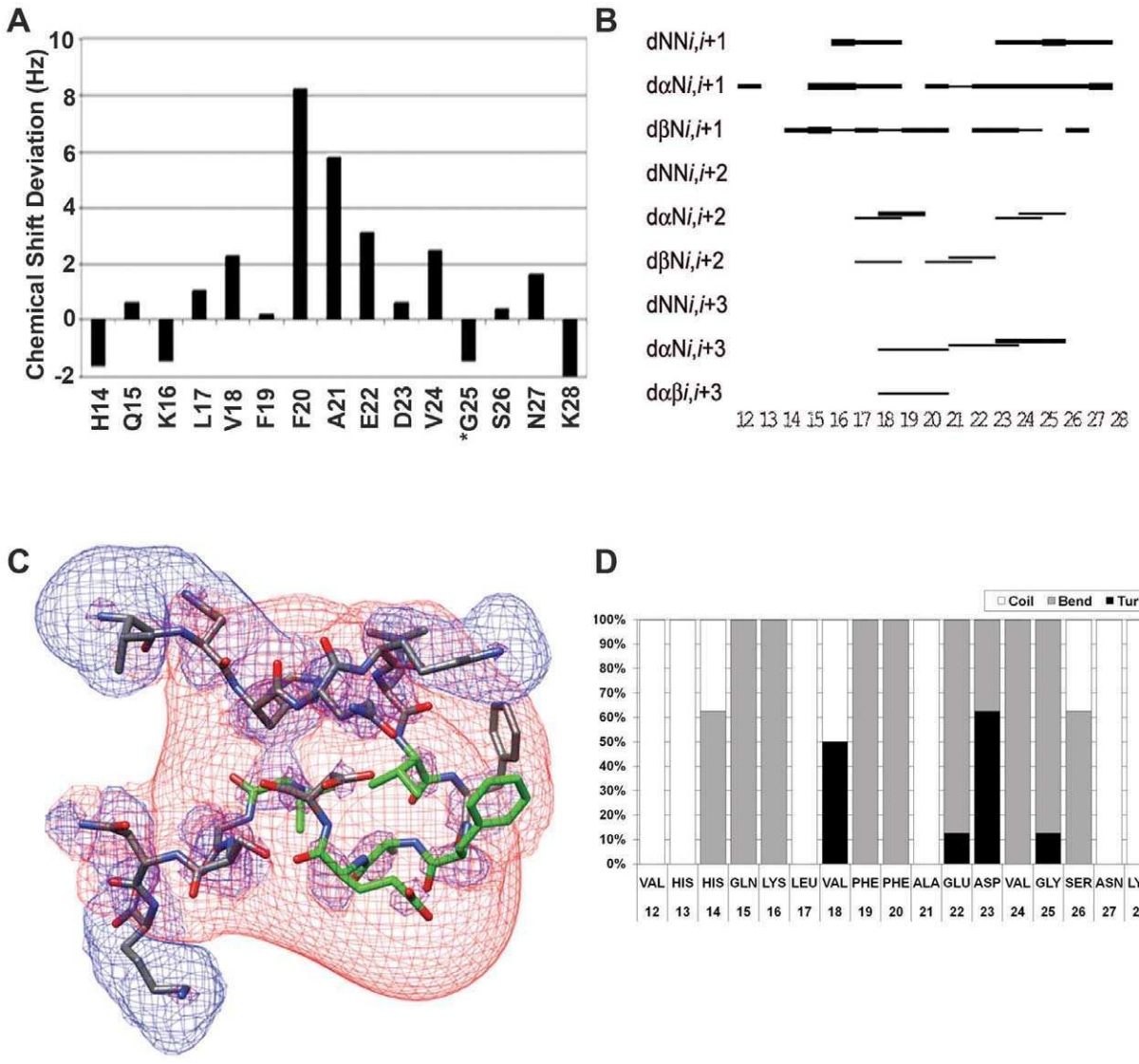

Figure 3. NMR analysis of Aβ with NQTrp. A. Amide proton chemical shifts deviations of $Aβ_{12–28}$ residues upon interacting with NQTrp at molar ratio between 1:0.1 and 1:0.5 ($Aβ_{12–28}$:NQTrp). *Residues Lys16 and Gly25 were unresolved. **B**. NOE connectivity plot: NOE interactions are proportional to the thickness of the interconnecting lines. **C**. Lowest energy structure generated for $Aβ_{12–28}$ with NQTrp (at 4:1 molar ratio). Ensemble of 28 from 50 starting structures had a RMSD of 2.28 Å overall and 0.71 Å and 0.74 Å in regions 16–20 and 22–26. Residues that showed significant deviations upon binding NQTrp are colored in green. The positive (blue) and negative (red) electrostatic potential distribution for ±2 kT/e is mapped onto the structure. **D**. Secondary structure statistics: percentage of low energy structures in turn (black), bend (grey) or coil (white), secondary structures.

doi:10.1371/journal.pone.0011101.g003

Table 1. ^{1}H chemical shift assignment of $A\beta_{12\text{-}28}$.

HN	Hα	Hβ	Others	
V12		3.72	2.10	CH_3 γ 0.89
H13	8.89	4.66	3.15	Hδ2 7.24, Hε1 8.55
H14	8.73	4.66	3.18, 3.06	Hδ1 8.49, Hδ2 7.26, Hε1 8.56
Q15	8.59	4.28	2.02, 1.94	CH_2 γ 2.32, Hε 7.6, 6.95
K16	8.48	4.24	1.76, 1.71	CH_2 γ 1.41, 1.34, CH_2 δ 1.64, CH_2 ε 2.93
L17	8.32	4.31	1.56, 1.42	CH γ 1.56, CH_3 δ 0.89, 0.82
V18	7.96	4.01	1.88	CH_3 γ 0.79, 0.72
F19	8.21	4.54	2.96, 2.85	CH_2 δ 7.30, Hε7.28, Hζ7.14
F20	8.14	4.54	3.09, 2.93	CH_2 δ 7.33, Hε7.31, Hζ7.22
A21	8.26	4.19	1.33	
E22	8.28	4.24	2.04, 1.91	CH_2 γ 2.35
D23	8.39	4.65	2.78, 2.67	
V24	8.07	4.11	2.14	CH_3 γ 0.92, 0.91
G25	8.50	3.94		
S26	8.13	4.42	3.84	
N27	8.45	4.70	2.80, 2.73	CH_2 δ 7.61
K28	7.87	4.13	1.80, 1.67	CH_2 γ 1.35, CH_2 δ 1.62, CH_2 ε 2.96, Hζ2 7.54
NQTrp	7.04	4.23	3.51, 3.26	CH_2 δ 7.26, Hε1 10.18, Hε3 7.63, Hη1 7.13,

doi:10.1371/journal.pone.0011101.t001

experiments of NQTrp-$A\beta_{12-28}$ binding thus showed the most prominent interactions in the region of Phe20 to Glu22. The changes in chemical shift indicate altered chemical environment either due to a direct interaction with NQTrp itself or due to a structural change that occurs upon binding.

The structure of $A\beta_{12-28}$ was solved in the presence of 0.25 molar ratio of NQTrp to Aβ (Table 1 and Figure 3B). The spectrum was resolved and showed numerous interactions (Table 2, Table S2, Figure S2 and S3). Of the 50 calculated structures (RMSD 2.37 Å on the backbone), 28 had no violations and a RMSD value of 2.28 Å and 9 low-energy structures were chosen for structural analysis. (Figure S3, backbone (bb) RMSD 1.12 Å). These had three regions of stability (Figure 3D): Residues 14–16 (bb RMSD 0.71 Å) showed a number of NOE interactions between the region of His13 and His14 and Leu17; residues18–20 showed a turn including phenylalanines 19 and 20 (bb RMSD 0.12 Å). The general structure of the ensemble showed a loose β-hairpin with a turn at residues18–20 including phenylalanines 19 and 20 (bb RMSD 0.12 Å). Additional regions of stability (Figure 3D) included residues 14–16 (bb RMSD 0.71 Å) that showed a number of NOE interactions between the region of His13 and His14 and Leu17; and a turn at residues 22–26 (bb RMSD 0.0.67 Å) that were stabilized by hydrogen bonding between the amide proton of Ser26 and the backbone oxygen of Asp23 in the majority of the conformations. This turn was unexpected and may either be an artifact of working with a truncated peptide, or part of the mechanism by which NQTrp disrupts plaque accumulation.

Table 2. NOE interaction statistics.

Total number of restraints 177
Intra-residual restraints 52
i+1 restraints 74
i+2 restraints 25
i+3 restraints 18
Long range restraints 8

doi:10.1371/journal.pone.0011101.t002

Figure 3C shows the lowest calculated energy conformation with residues Val18, Phe20, Ala21, Glu22 and Val24, colored in green to indicate residues whose chemical shift changed upon interacting with NQTrp. The positive (blue) and negative (red) electrostatic potential distribution for ±2 kT/e is mapped onto the structure; showing the positively charged N-terminus and Lys28, and the negative potential in the central region of the Aβ12–28 peptide.

CD characterization of the interaction of NQTrp with Aβ

Samples containing $A\beta_{1-42}$ and NQTrp were subsequently analyzed by Circular Dichroism (CD) to gain information on the secondary structural changes that the early Aβ species undergo when incubated with NQTrp. Native $A\beta_{1-42}$ oligomers exhibit a strong positive band around 195 nm and a negative band at 217 nm, indicating a β-sheet conformation. A dose dependent decrease in both of these bands and a small shift in the spectrum were evident with increasing concentrations of NQTrp, yet the typical β-sheet spectrum is still apparent (Figure 4). This implies that, when incubated with NQTrp, Aβ retains its β-sheet conformation, yet this conformation is gradually lost with increasing concentrations of the naphthoquinone.

Simulation of Aβ assembly with and without NQTrp

Computer simulations were carried out to further investigate the interactions between NQTrp and Aβ. We examined the influence of NQTrp on the early phase of ordered aggregation of the central region of the Aβ peptide, focusing on the segment 14–24, centered on Phe 19 and Phe 20. A divide-and-conquer approach [46] has

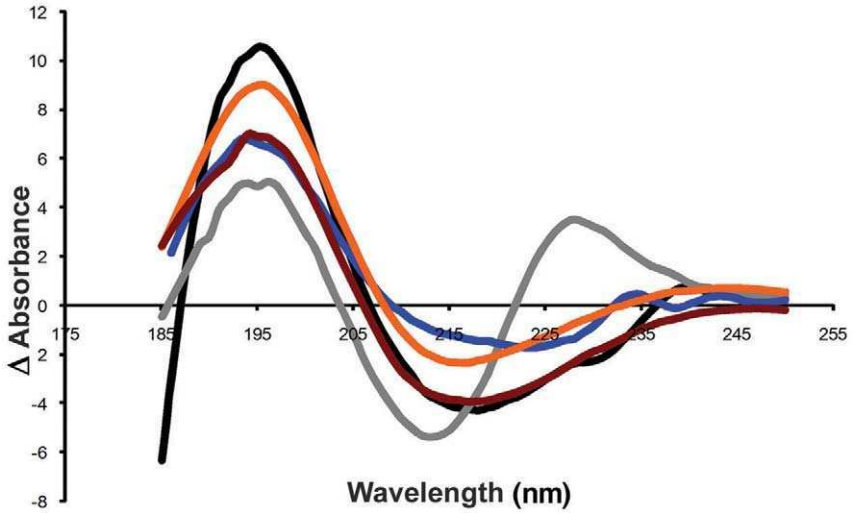

Figure 4. CD studies of Aβ with NQTrp. CD spectrum of $A\beta_{1-42}$. Concentration indicated as Aβ:NQTrp molar ratio. Control - $A\beta_{1-42}$ only (black), 1:60 (grey), 1:30 (blue), 1:1 (orange), 5:1 (red).
doi:10.1371/journal.pone.0011101.g004

been adopted to efficiently sample the conformational transitions of the system. Therefore, the segment was decomposed into three overlapping heptapeptides: $A\beta_{14-20}$, $A\beta_{16-22}$, and $A\beta_{18-24}$ (see sequences in Table S3). Implicit solvent molecular dynamics (MD) simulations were used to simulate the aggregation of three replicas of the considered peptides in presence and absence of NQTrp.

During the simulations the three-peptide system explores several configurations. The P_2 order parameter (described in Materials and Methods) has been adopted to monitor the degree of orientational order within the oligomers: a value close to one corresponds to an ordered trimer, with either parallel or antiparallel β-sheet, while a value close to zero reflects a fully disordered system. The frequency histograms of P_2 for the unperturbed and perturbed systems (Figure 5) display a prominent peak at $P_2 = 0.8$, and a shoulder for P_2 values lower than 0.5, which includes disordered aggregates and isolated peptides. The

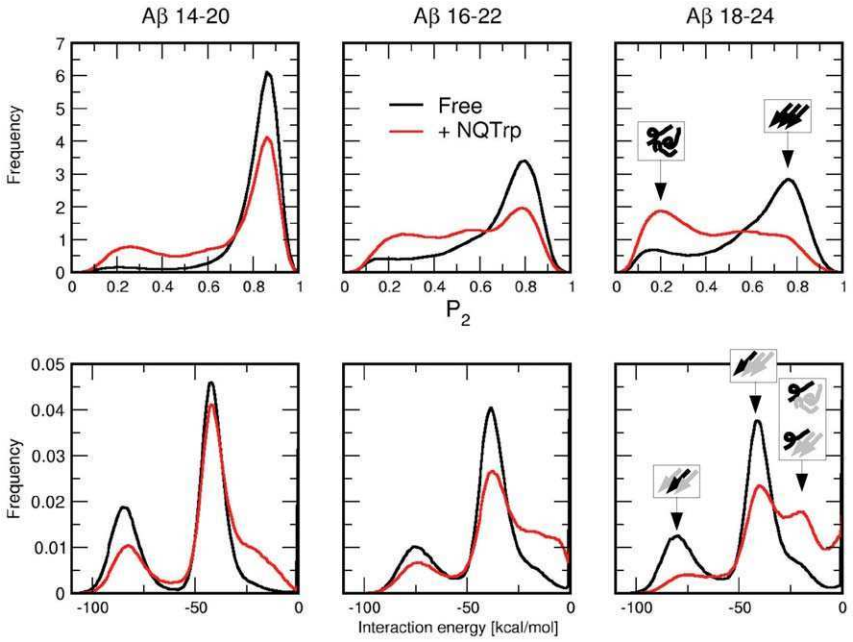

Figure 5. NQTrp hinders β-sheet formation. Red lines and black lines correspond to simulations with and without NQTrp, respectively. (Top) Frequency histograms of the nematic order parameter P2 for the three Aβ segments. Values of P2 close to 0.2 and 0.8 correspond to disordered conformations and β-sheet structures, respectively (see the insets in the top right plot). The presence of NQTrp sensibly increases the amount of disordered structures for all peptides. (Bottom) Inter-peptide interaction energy distributions. The two peaks of the distributions correspond to a peptide in the center of an ordered oligomer (about −80 kcal/mol) and a peptide at the edge of an ordered oligomer (about −40 kcal/mol). The shoulder of the energy distribution at values of about −20 kcal/mol contains events with disordered or partially ordered oligomers (see insets in the bottom right plot). NQTrp markedly increases the amount of structures with unfavorable inter-peptide interaction energy.
doi:10.1371/journal.pone.0011101.g005

threshold value $P_2^* = 0.665$ is chosen as the crossover between ordered and disordered states (see Materials and Methods) [39]. The ratio between order and disorder clearly shows that NQTrp perturbs the order of the aggregate (Table S3) by increasing the population of disordered conformations for all three peptides. The frequency distribution of inter-peptide interaction energies (Figure 5) shows two peaks. The peak at −80 kcal/mol and the peak at −40 kcal/mol correspond to a peptide interacting with the center and at the edge of an ordered trimer, respectively. From the plots it is evident that the presence of NQTrp increases the number of events with interaction energy close to zero, originating from unstructured peptides bound to the oligomeric or isolated Aβ species. The presence of NQTrp alters the number of backbone hydrogen bonds by increasing the intra-chain and decreasing the inter-chain interactions (Table S3). The simulation results indicate that the trimer structure is perturbed by NQTrp, which is able to intercalate into the oligomer and influence its structure, supporting the evidence attained above by NMR and CD spectroscopy.

Binding mechanism of NQTrp to Aβ by computational analysis

Further computational analysis was conducted in order to determine the binding mechanism of NQTrp to Aβ. Hereafter, the hydrogen bonds between NQTrp and the Aβ peptide backbone will be identified using the labels of polar groups of NQTrp (see inset of Figure 6 for the labels), e.g., NH1-CO is the hydrogen bond between NH1 group and any carbonyl group of the backbone. Furthermore the interaction with a certain residue will be specified with the amino acid name, e.g., NH1-Phe20 is the hydrogen bond between NH1 group and backbone carbonyl of Phe20, and CO1-Phe20 is the hydrogen bond between CO1 group and Phe20 backbone amide. Due to the symmetry of the carboxyl oxygens of NQTrp, the hydrogen bond that can be formed with one of the two CO moieties will be referred as to CO3-NH. The frequency of hydrogen bond formation between the carbonyl groups of NQTrp and the amide backbone is shown in Figure 6. The agreement with the NMR amide proton chemical shift deviations is remarkable. The backbone amides that interact most with NQTrp through hydrogen bonds belong to Phe20, Ala21, and Glu22. It is worth noting that, although the van der Waals interaction energies between NQTrp and Phe19 or Phe20 are very similar, there is a much higher propensity for NQTrp to form a hydrogen bond with Phe20. The most frequent hydrogen bonds involving the peptide backbone are NH1-CO, CO1-NH and CO3-NH (Figure S4, Table S4). Interestingly, the hydrogen bond pairs NH1-CO, with CO1-NH or CO3-NH occur simultaneously at high probability (about 10% of the trajectory), and very frequently the three hydrogen bonds are formed at the same time (5% of the trajectory) (Table S5). These hydrogen bonds occur either within the same residue (Phe20 or Ala21), or within two amino acids that are separated by a single residue (Val18, Phe20, or Phe20, Glu22) (Table S5).

Notably, the MD simulations show that NQTrp strongly perturbs the ordered aggregation of the Aβ peptides by binding with specific hydrogen bonds and aromatic interactions. The snapshots shown in Figure 7 were extracted from the trajectories according to the most frequent hydrogen bond pairs (See Methods). In the most frequent binding patterns, NQTrp has a closed conformation in which the indole and the naphthoquinone "clamp" the phenyl rings of Phe19 or Phe20 (Figures 7A–C). In addition, there are stable hydrogen bonds: CO1-Ala21, and NH1-Ala21 (Figures 7A and B), or CO1-Phe20,

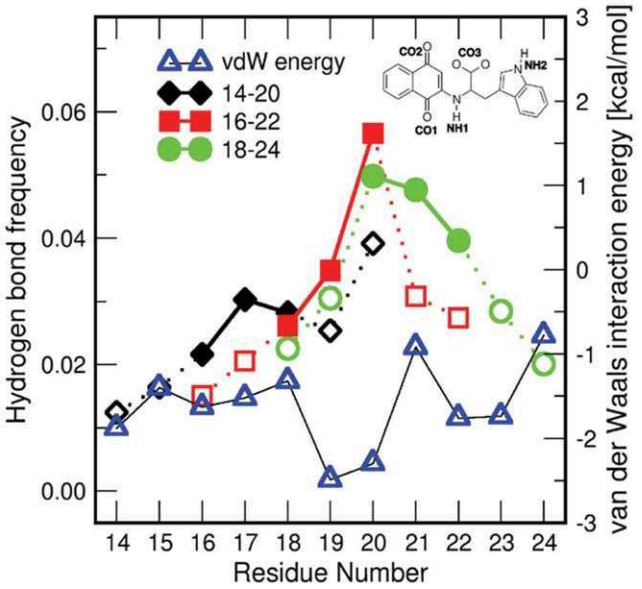

Figure 6. Computer analysis of the interactions between NQTrp and Aβ. Frequency of interactions between all NQTrp CO groups and peptide backbone NHs (left y-axis). Open symbols correspond to residues proximal to the N-terminal or C-terminal of the peptide (positions 1, 2, 6, and 7 in each heptapeptide). Closed symbols correspond to the central residues (positions 3, 4, and 5). Average van der Waals interaction energy between the residues and NQTrp are shown by blue triangles (right y-axis). Lower values correspond to more favorable interaction energy.
doi:10.1371/journal.pone.0011101.g006

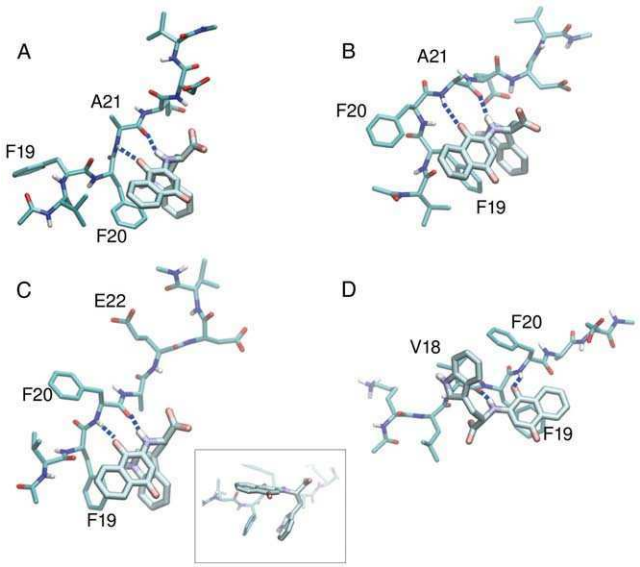

Figure 7. Modeling of representative snapshots of the binding modes of NQTrp to the Aβ_peptide. (**A,B**) The two most frequent conformations (12% and 9%) when NQTrp is bound to Aβ18–24 through CO1-NH and NH1-CO interactions with Ala21. The main difference between the two structures is the swap of Phe20 and Phe19 as a counterpart for aromatic interactions with NQTrp. **C** The most frequent conformation (17%) obtained when NQTrp is bound to Aβ18–24 and is involved in CO1-NH and NH1-CO interactions with Phe20. To emphasize the aromatic interactions of the naphthoquinone and the indole moieties of NQTrp with the phenyl ring of Phe19, a lateral view of the conformation **c**. is shown in the inset. **D** The most frequent conformation (11%) when NQTrp is bound to Aβ16–22 through CO1-NH with Phe20 and NH1-CO with Val18. Here the indole of NQTrp interacts with Val18, and naphthoquinone with Phe19. See inset of Fig. 5 for the labeling of the polar groups.
doi:10.1371/journal.pone.0011101.g007

NH1-Phe20 and CO3-Glu22 (Figure 7C). In this case Phe19 interacts with both aromatic groups of NQTrp as well. Conversely, in the presence of the NH1-Val18 and CO1-Phe20 hydrogen bonds, the indole and naphthoquinone moieties do not act as "clamp" but rather interact with the Val18 and Phe19 side chains, respectively (Figure 7D). Note that in all cases aromatic stacking and hydrogen bonds with polar groups of the backbone are present.

NQTrp inhibits the cytotoxic effect of Aβ towards cultured cell line

To further substantiate the inhibition by NQTrp we tested whether it affects the cytotoxicity of $A\beta_{1-42}$ oligomers towards the rat PC12 neuronal cell line. Toxic Aβ oligomers were incubated with increasing concentrations of NQTrp and cell viability was measured using the MTT assay. While showing no toxic effect of its own towards cultured cells (Figure S5), NQTrp significantly inhibited the cytotoxic effect of the Aβ oligomers and caused a significant dose dependent increase in the viability of the cells (Figure 8A). This effect was most apparent at molar excess of NQTrp which correlates with results attained from the inhibition of toxic Aβ oligomers analysis.

The effect of NQTrp in an *in vivo* transgenic fly system

In order to assess the effect of NQTrp on Aβ in the living organism, we used a Drosophila model of AD. Transgenic flies expressing the human $A\beta_{1-42}$ protein in their nervous system, via the Gal4-UAS system, display various symptoms reminiscent of AD including defective locomotion, and memory, which deteriorate with age, as well as markedly reduced longevity. Their brains display characteristic amyloid plaques and pathology [47].

Crossing male flies carrying the pan-neuronal elav-Gal4 driver (on their X chromosome) with females homozygous for the autosomal UAS-regulated $A\beta_{1-42}$ transgene, resulted in female offspring expressing $A\beta_{1-42}$ in their nervous system. The male offspring carried the $A\beta_{1-42}$ transgene but did not express it because they lacked the Gal4 driver and served as control. This cross was performed either on regular Drosophila medium or on medium supplemented with 0.75 mg/mL NQTrp. The animals fed on the appropriate medium from the beginning of the larval stage onwards. Each class of adult offspring was monitored daily for survival and locomotion (climbing).

Flies expressing the $A\beta_{1-42}$ transgene grown on regular medium exhibited a significantly shorter life span than the control (male) classes, as reported [47]. By day 16, only 50% of the flies expressing the $A\beta_{1-42}$ transgene, were viable, while in the control class viability was reduced to 50% only after 26 days. The life span of $A\beta_{1-42}$-expressing flies reared on medium containing NQTrp (Figure 8B) was much longer and was nearly identical to that of control flies grown on regular medium (50% viability observed only at day 26). The compound had no significant effect on longevity of the control flies. Statistical analysis was performed using the SPSS 15 Kaplan-Meier software package. Results show a significant difference between flies (females) expressing the $A\beta_{1-42}$ transgene grown on regular medium versus medium supplemented with NQTrp ($P<0.0005$). In contrast, no significant difference was observed between $A\beta_{1-42}$-expressing flies supplemented NQTrp and the control class grown on the same medium ($P>0.8$). No significant difference was seen either between the control class (males) grown on regular medium versus medium supplemented NQTrp ($P>0.5$) (data not shown).

$A\beta_{1-42}$-expressing flies behaved normally at eclosion from the pupal case and subsequently developed locomotion deficits as reported [47–49]. At four days after eclosion these flies exhibited a marked decrease (60%) in their climbing ability becoming almost immobile by day 15, while the control classes were very active at this time (Figure 8C). In contrast, $A\beta_{1-42}$-expressing flies reared on

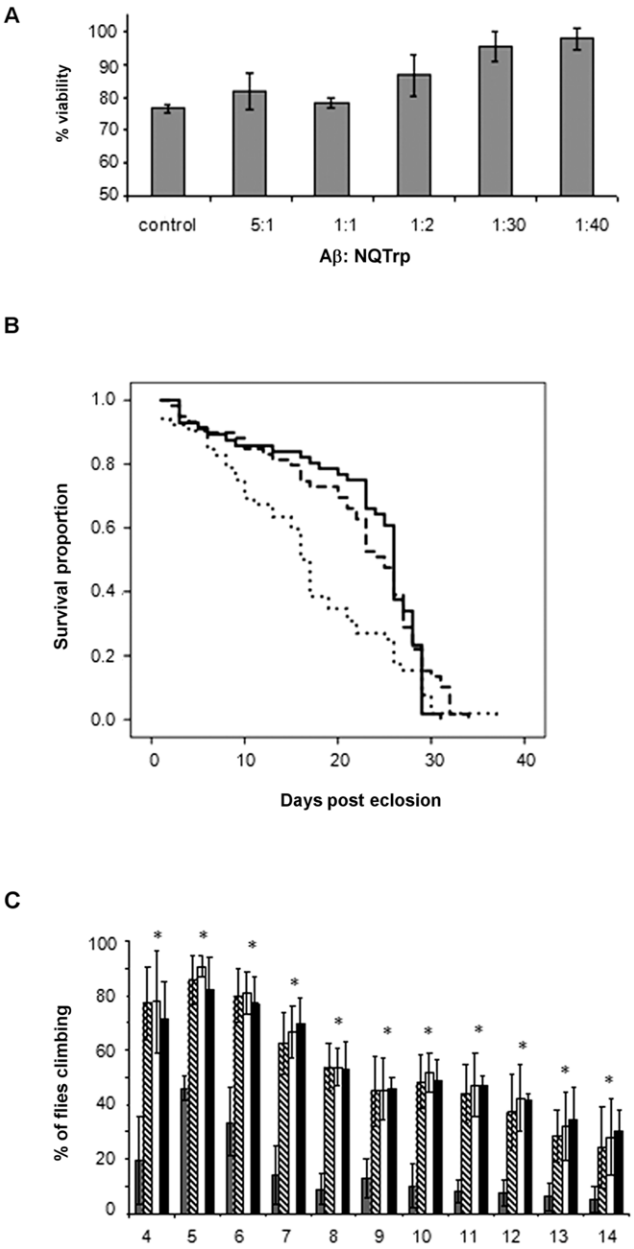

Figure 8. NQTrp alleviates toxic effects of Aβ – cell and fly assays. A. The effect of NQTrp on cytotoxicity of soluble Aβ oligmers. Soluble oligomers were prepared with and without increasing concentrations of NQTrp. The cytotoxic effect of the preparations towards cultured PC12 cells was determined using the MTT assay. Concentration are indicated as Aβ:NQTrp molar ratio. **B**. The effect of NQTrp on longevity of $A\beta_{1-42}$-expressing flies. The life span of four classes of flies was evaluated $n=60$. Females expressing $A\beta_{1-42}$ grown on regular medium (dotted line), females expressing $A\beta_{1-42}$ grown on medium containing NQTrp (dashed line), males (control, carrying the $A\beta_{1-42}$ transgene but not expressing it) grown on medium containing NQTrp males (control, carrying the $A\beta_{1-42}$ transgene but not expressing it) grown on regular medium(not shown). **C**. The effect of NQTrp on climbing behavior of $A\beta_{1-42}$-expressing flies.. Four classes, each containing six vials with 10 flies in each: femalesexpressing $A\beta_{1-42}$ grown on regular medium (grey), females expressing $A\beta_{1-42}$ grown on medium containing NQTrp (dashed line), males (control, carrying the $A\beta_{1-42}$ transgene but not expressing it) grown on either regular medium (white) or on medium containing NQTrp (black), were analyzed using the climbing assay. Results show for each group the percent of flies climbing to the top of the vial after 18 seconds, during the course of 14 days.
doi:10.1371/journal.pone.0011101.g008

medium containing NQTrp displayed dramatic improvement, behaving almost identical to the control classes (males reared on medium lacking the compound) (Figure 8C). Importantly, no effect of NQTrp was observed on locomotion of the control flies. One tail ANOVA statistics showed $P<0.0005$ for all four classes.

To further assess the curative effect of NQTrp on AD flies, Aβ was extracted from fly brains over expressing the Arctic (Arc) (E22G) mutant form of Aβ, associated with increased aggregation and early-onset familial AD [50]. These flies displayed short life span and defective locomotion as reported [47] and both of these defects were ameliorated by NQTrp as described above for $A\beta_{1-42}$-expressing flies (data not shown). Aggregated forms of Aβ were readily detected in the soluble fraction of extracts from $A\beta_{arc1-42}$-expressing flies following immunoprecipitation with the 6E10 Aβ-specific antibody, followed by western blot. Using this procedure monomers of Aβ were detected in head extracts of both NQTrp-fed and in non treated $A\beta_{arc1-42}$-expressing flies. However, Aβ tetramers, which were evident in non treated $A\beta_{arc1-42}$ flies [51], were absent from extracts of flies fed with NQTrp (Figure 9A).

To evaluate the effect of NQTrp on Aβ accumulation in the brains of these flies, $A\beta_{arc1-42}$ expressing larvae and adult flies, fed or unfed with NQTrp, were immunostained with the 6E10 antibody. As reported [47,51], both the brains of untreated larvae and adult flies displayed robust staining (Figure 9 D, E, 10 A–D) representing accumulated Aβ assemblies, not seen at all in brains of control animals not expressing any Aβ (Figure 9 A, B). Importantly, brains of $A\beta_{arc1-42}$-expressing animals that were fed with NQTrp exhibited greatly reduced Aβ staining. (Figure 9 F, G, 10 E–H).

Taken together these results indicate that NQTrp reduced both Aβ oligomerization and accumulation in AD model flies.

Discussion

Our work provides a rational design route toward the development of novel amyloid aggregation inhibitors of high potency. The various levels of analysis indicate that indeed the hybrid linking of naphthoquinone and tryptophan moieties leads to a highly potent inhibitor of both the oligomerization and fibrillization of Aβ with a high affinity of 90 nM and an IC_{50} of 50 nM, which is markedly lower than that reported for other aromatic Aβ inhibitors (Table S6, Supp. references S1).

Our initial hypothesis that NQTrp should interact with the central diphenylalanine recognition motif has gained direct evidence by NMR spectroscopy and *in silico* analysis. The largest chemical shift deviation was observed with Phe20 (8 Hz). A large chemical shift deviation was also observed with Ala21 and Glu22, 5 and 3 Hz, respectively. These three sequential residues form a turn in the NMR-derived conformers. The electrostatic potential of the NMR conformers suggests that peptide association may be mediated by electrostatic interactions among the distinct positive and negative regions. Interactions between the Phe19-Phe20 aromatic side chains and NQTrp may interfere with peptide-association.

This observation is further supported by the results of molecular dynamics simulations which indicate that NQTrp is involved in stable hydrogen bonds most frequently with the Phe20, Ala21 and Glu22 backbone polar groups. Remarkably, both NMR spectroscopy and computer simulations provide evidence that NQTrp binds stronger to the backbone polar groups of Phe20 than Phe19, as shown by the cluster representatives reported in Figure 7. The van der Waals interaction analysis (Figure 6) revealed favourable interaction energies between NQTrp and both the Phe19 and Phe20 side chains. In fact, when NQTrp is involved in hydrogen bonds with the backbone of the Phe20-Glu22 region, the naphthoquinone and the indole ring are able to "clamp" the phenyl ring of either Phe19 or Phe20, as shown in three of the four most frequent binding modes (Figure 7). For geometrical reasons, NQTrp does not frequently bind to the Phe19 backbone. As revealed by visual inspection of the trajectories, in this conformation NQTrp "clamps" side chain of Val18 and the resulting interaction is not favourable enough to stabilize this binding mode.

In addition to NQTrp a series of twelve quinone derivatives were screened. The main result is that a hybrid between quinone and indole is needed for optimal inhibition of both oligomerization and fibril formation. As observed in the simulations, and in agreement with the experimental inhibition assays, the presence of an electron-deficient naphthoquinone moiety, together with the electron-dense indole ring leads to the formation of a stable complex with the side chains of Phe19 and Phe20. An essential element of the active compounds (IL, IID, and III) is the presence of a three or four rotatable bonds aliphatic linker between the two aromatic moieties.

Compounds with planar aromatic rings but devoid of the aliphatic linker (molecules IV–XIII, Figure S1, Table S1) are more rigid and for this structural reason their ability of inhibiting oligomer formation is reduced.

Nevertheless, several of the molecules inactive against the oligomers are still able to inhibit the fibril formation, probably because of their ability to intercalate between the exposed side-chains [52,53].

The main difference between IL, IID and III is the presence of a negatively charged group (only in IL, IID) which can influence the physical-chemical properties, e.g., the solubility and modify their ability of interacting with oligomers or fibrils. In addition, the most frequent hydrogen bonds with the peptide backbone of Aβ involve the quinonic carbonyls moieties, the anilinic nitrogen and the carboxyl group of NQTrp (Figure S4, Tables S4 and S5). Taken together these observations could explain the difference in activity of NQTrp and its decarboxylated analogue (molecule III, Figure S1, Table S1).

CD analysis shows a reduction in β-sheet conformation when increasing concentrations of NQTrp are titrated into the oligomeric "ordered" form of Aβ. *In silico* analysis is in accordance with these results (Figure 5). Molecular dynamics simulations revealed that NQTrp destabilizes the inter-chain backbone hydrogen bonds and increases considerably the structural disorder within the Aβ oligomer. Importantly, the inhibitory effects of the tryptophan-modified naphthoquinone on Aβ assembly *in vitro* correlate well with its effects *in vivo*. NQTrp reduced the toxicity of Aβ oligomers towards cultured cells and completely alleviated Aβ-engendered symptoms in a transgenic fly model of AD, which correlated with reduction of both Aβ oligomerization (Figure 9A) and accumulation of Aβ in the brains of these animals (Figure 9 B–G, 10 A–H).

Taken together, the results presented here for a tryptophan-modified naphthoquinone and our comparable results with D-tryptophan-Aib dipeptides [31] indicate that the targeting of the central recognition interface of Aβ by structural clamping and inhibition of further oligomerization is a promising approach for the inhibition of amyloid pathology *in vivo*. The unique properties of NQTrp and its remarkable activity *in vitro* and *in vivo* make it a promising lead for the development of small molecule inhibitors of oligomerization for the treatment of AD.

Materials and Methods

Compounds

1,4-naphthoquinon-2-yl-L-tryptophan (NQTrp) was synthesized from L-tryptophan and 1,4-naphthoquione by a one step synthesis according to the protocol by Shrestha-Dawadi *et al.* [39].

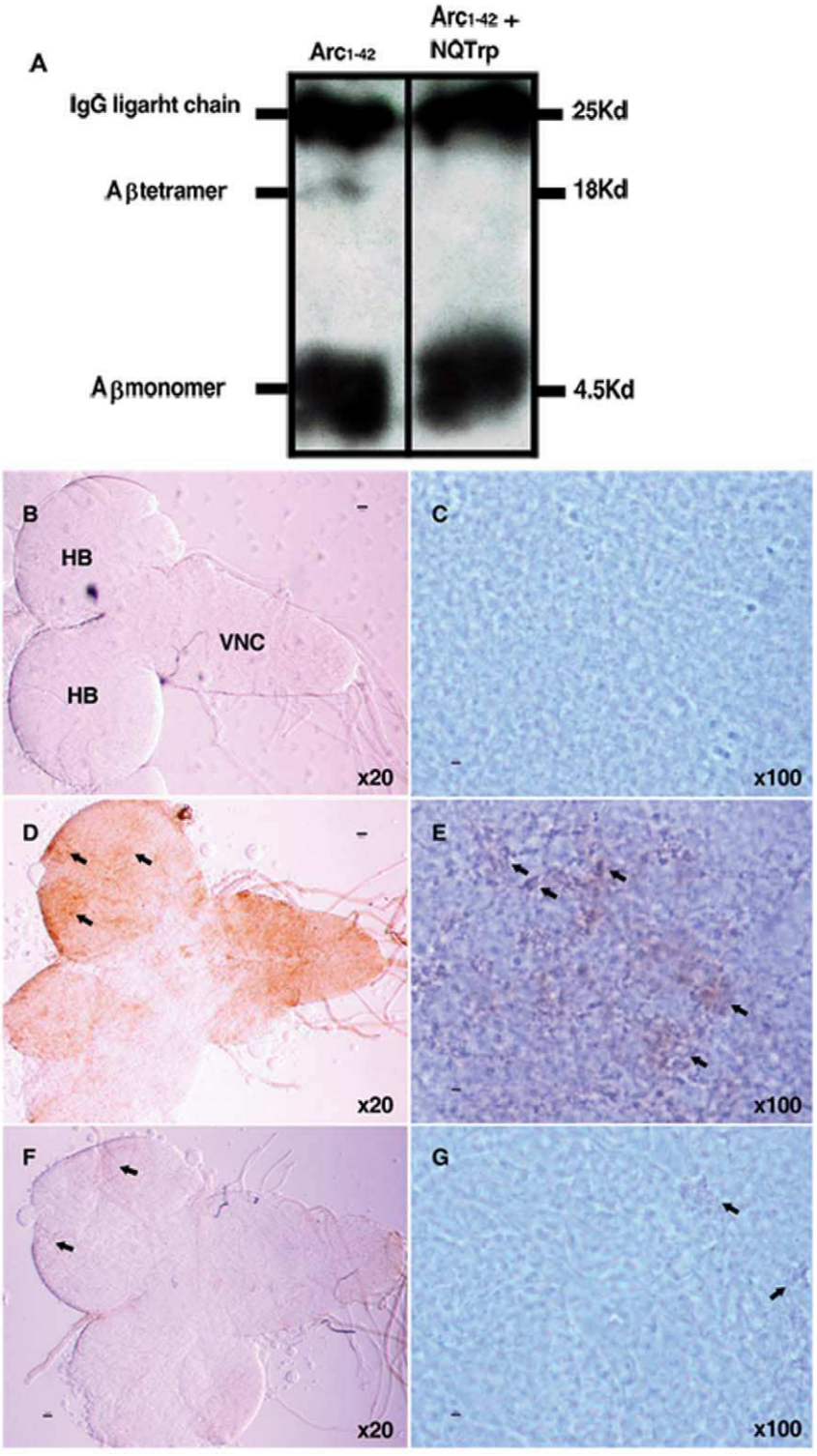

Figure 9. Effect of NQTrp on Aβ in larvae brains. A. Head extract from 6 days old $A\beta_{arc1-42}$-expressing flies unfed (left) and fed (right) with 0.75 mg/mL NQTrp (N = 25 in each group). Accumulation of Aβ tetramers is evident only in $A\beta_{arc1-42}$ flies which were not fed with NQTrp. (**B–G**) Immuno-staining of 3rd instar larval brains with specific Aβ antibody 6E10. (**B, C**) Control animals not expressing any Aβ (elav-GAL4/+; +/+). (**D, E**) $A\beta_{arc1-42}$-expressing animals fed with regular fly food. (**F, G**) $A\beta_{arc1-42}$-expressing animals fed with NQTrp (elav-GAL4/+; UAS-$A\beta_{arc1-42}$/+). N = 10 for each class examined. HB – hemi-brain; VNC – ventral nerve cord. Arrows indicate Aβ accumulation.
doi:10.1371/journal.pone.0011101.g009

^{1}H-NMR (DMSO-d_6): δ = 3.3 (m, CH_2), 3.9 (m, CH_2), 5.6 (s,1H), 6.8 (t, $\mathcal{J}$ = 3.3Hz, 1H), 6.8 (t, $\mathcal{J}$ = 7.4Hz,1H), 7.1 (s, 1H), 7.2 (br m, NH), 7.3 (d, $\mathcal{J}$ = 8.0 Hz, 1H), 7.4 (d, J = 7.5 Hz, 1H), 7.6–7.9 (m, 4H), 10.8 (NH). Reverse phase HPLC showed >95% purity. Synthetic $A\beta_{1-42}$, $A\beta_{1-40}$ and $A\beta_{12-28}$ were purchased from Bachem, (Bubendorf, Switzerland).

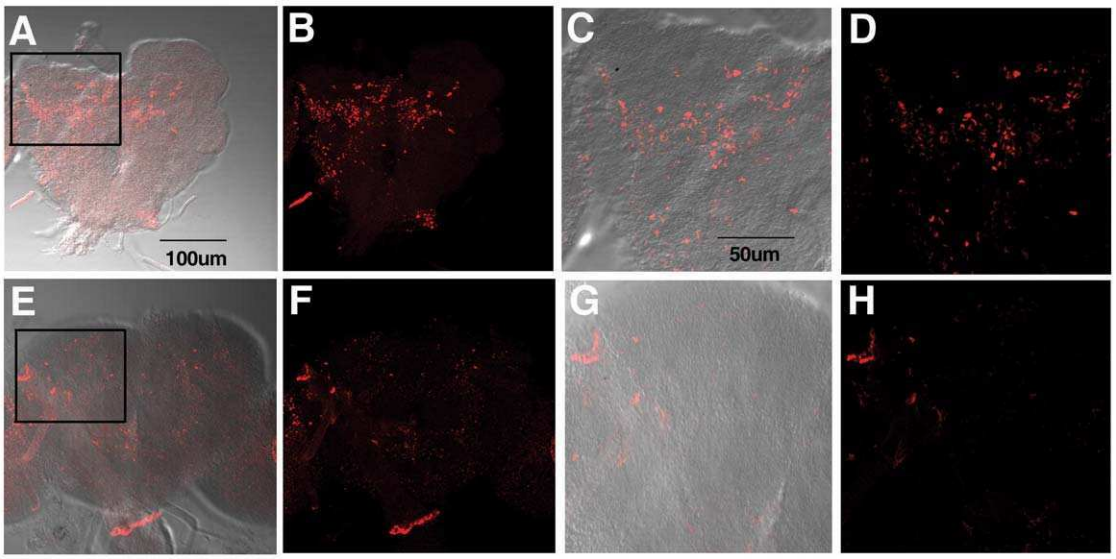

Figure 10. Effect of NQTrp on Aβ in drosophila brains. Immuno-staining of two-day old adult fly brains with specific Aβ antibody 6E10. (**A–D**) $A\beta_{arc1\text{-}42}$-expressing animals fed with regular fly food (elav-GAL4/+; UAS-$A\beta_{arc1\text{-}42}$/+). (**C, D**) Enlarged images of the boxed region. (**E–H**) $A\beta_{arc1\text{-}42}$-expressing animals fed with NQTrp (elav-GAL4/+; UAS-$A\beta_{arc1\text{-}42}$/+) (**G, H**) Enlarged images of the boxed region. N = 6 for each class examined.
doi:10.1371/journal.pone.0011101.g010

Determination of soluble oligomer formation

Aβ intermediates and toxic oligomers were produced according to Barghorn and coworkers [15]. To avoid pre-aggregation, synthetic lyophilized $A\beta_{1-42}$ was pretreated with HFIP. $A\beta_{1-42}$ was dissolved in 100% HFIP, sonicated for 20 seconds and incubated for 2 hours at 37°C under shaking at 100 RPM. NQTrp was dissolved in DMSO to a concentration of 30 mM, sonicated for 1 min and then diluted with DMSO to its final concentrations. After evaporation in a speedVac, $A\beta_{1-42}$ was resuspended in DMSO (with or without NQTrp) to 5 mM and diluted with 20 mM NaH_2PO_4, 140 mM NaCl, pH 7.4 to a final concentration of 400 μM and 1/10 volume 2% SDS (final concentration of 0.2%). The toxic Aβ oligomers were generated by further dilution with two volumes of H_2O and incubated for additional 18 hours or more (for the toxic oligomer stability assay). Aβ aggregation products were then separated using a 15% tris-tricine gel and stained using Imperial protein stain.

Fluorescence anisotropy studies

NQTrp was dissolved in DMSO to a concentration of 50 nM and sonicated for 5 min. The solution was immediately mixed with aliquots of an $A\beta_{1-42}$ intermediate (as described above) stock solution (20 μM) to varying final polypeptide concentrations. NQTrp polarization measurements were carried out using an ISS K2 fluorimeter. The solutions were excited at 280 nm and emission was monitored at 350 nm. For each single point, at least five measurements were collected and their average values were used for the calculation. All experiments were performed in phosphate-buffered saline, PBS [100 mM NaCl (pH 7.4)].

ThT kinetic binding fluorescence

Synthetic lyophilized $A\beta_{1-40}$ was dissolved in DMSO to a concentration of 100 μM and sonicated for 1 min to prevent pre-aggregation. Aβ solutions were prepared by immediate dilution with 10 mM PBS [100 mM NaCl and 0.5 mM EDTA (pH 7.4)] to a final concentration of 10 μM [containing 10% (v/v) DMSO]. The samples were diluted again to a final concentration of 5μM with the appropriate inhibitor concentration or with PBS for control samples. The samples were incubated at 37°C, and the rate of fibril formation was monitored using ThT fluorescence analysis over the course of 270 hours. The respective excitation and emission wavelengths were 450 nm (2.5 nm slit) and 480 nm (5 nm slit), respectively. A 10-fold diluted sample was taken and mixed with 900 mL of 0.4 μM ThT. The fluorescence of ThT was measured using a Jobin Yvon Horiba Fluoromax 3 fluorimeter. Each experiment was repeated in quadruplicates.

IC_{50} ThT measurements

Synthetic lyophilized $A\beta_{1-42}$ was dissolved in DMSO to a concentration of 100 μM and sonicated for 1 min to prevent pre-aggregation. Aβ solutions were prepared by immediate dilution with 10 mM PBS. The samples were again diluted to a final concentration of 5 μM with the appropriate inhibitor concentration or with PBS for control samples. ThT fluorescence was measured after 24 hours. The respective excitation and emission wavelengths were 450 nm (2.5 nm slit) and 480 nm (5 nm slit). A 10-fold diluted sample was taken and mixed with 900 mL of 0.4 μM ThT. The fluorescence of ThT was measured using a Jobin Yvon Horiba Fluoromax 3 fluorimeter. Each experiment was repeated in quadruplicates.

Transmission electron microscopy

Samples of Aβ were taken after 7 days and at the end of the ThT kinetic experiment and placed on a 400 mesh copper grid covered by carbon-stabilized Formvar film (SPI Supplies, West Chester, PA). The sample was allowed to stand for 1.5 min, excess fluid was removed and the grids were negatively stained for 2 min with 10 μL of a 2% uranyl acetate solution. Excess fluid was removed, and the samples were viewed using a JEOL 1200EX electron microscope operating at 80 kV.

NMR Analysis

Sample preparation. 1.06 mg of lyophilized $A\beta_{12-28}$ [was dissolved in d6-DMSO to which TDW with 0.02% w/v NaN3

was added to obtain a final sample of 1.13 mM peptide in 20% d6-DMSO solution. The order of dissolving the peptide is essential to achieve solubility.

NMR measurement. NQTrp was titrated into the $A\beta_{12-28}$ sample in 10 μL aliquots in the same solvent batch as the peptide samples to achieve increments of 0.11 mM of NQTrp concentration per aliquot. After each addition the ^{1}H-NMR spectrum was taken at 600 MHz with 16 scans at 21°C. Chemical shift assignment was taken from [31]; K16 and G25 were unresolved in the one-dimensional spectrum (designated by an asterisk in Fig 3A). The difference between each amide proton chemical shift and that of the peptide in the presence of with 0.1 mM NQTrp was determined for each subsequent aliquot. This value was chosen to see the effect of increasing NQTrp concentration.

Structural studies were done on the final sample from the above under the same conditions. NMR experiments were performed on a Bruker Avance 600 MHz DMX spectrometer operating at the proton frequency of 600.13 MHz, using a 5-mm selective probe equipped with a self-shielded xyz-gradient coil. The transmitter frequency was set on the hydrogen-deuterium exchange in water signal, which was calibrated at 4.811 ppm. Correlation spectroscopy (COSY) [54], total correlation spectroscopy (TOCSY), using the MLEV-17 pulse scheme for the spin lock [55], and nuclear Overhauser effect spectroscopy [56] experiments were acquired under identical conditions for all samples, using gradients for water saturation. The nuclear Overhauser effect spectroscopy experiments were acquired with a mixing time of 200 ms.

Spectra were processed and analyzed with the XWINNMR (Bruker Analytische Messtechnik GmbH) and SPARKY3 software. Resonance assignment followed the sequential assignment methodology developed by Wüthrich [57]. Stereospecificity was introduced according to the set which gave the lowest energies and RMSDs.

Electrostatic free energies were derived from finite difference solutions of the Poisson-Boltzman equation using the DelPhi program [58]. The AMBER forcefield [59] was employed and a full Coulombic calculation was performed. The positive and negative 2 kT/e isopotential surfaces were presented using [60].

CD analysis

To avoid pre-aggregation, synthetic lyophilized $A\beta_{1-42}$ was pretreated with HFIP. $A\beta_{1-42}$ was dissolved in 100% HFIP, sonicated for 20 seconds and incubated for 2 hours at 37°C under shaking at 100 RPM. NQTrp was dissolved in DMSO to a concentration of 30 mM, sonicated for 1 min and then diluted with H_20 to its final concentrations. After evaporation in a speedVac, $A\beta_{1-42}$ was resuspended in H_20 (with or without NQTrp) to 5 mM and diluted with 20 mM NaH_2PO_4, 140 mM NaCl, pH 7.4 to a final concentration of 400 μM and 1/10 volume 2% SDS (final concentration of 0.2%). The toxic Aβ oligomers were generated by further dilution with two volumes of H_2O and incubated for additional 18 hours or more (for the toxic oligomer stability assay). CD measurements were conducted using quartz cuvette 0.1 mm path length, at 25°C, using AVIV 202 CD spectrometer.

Simulation protocol and analysis

The molecular dynamics simulations were performed with the CHARMM program [61,62]. The peptides and compound were modeled using the united atoms CHARMM PARAM19 force field with its default truncation scheme for nonbonding interactions (cutoff of 7.5 Å). Hydration effects were accounted for by using SASA, a solvent-accessible surface based implicit model [63]. Partial charges for NQTrp were computed with the modified partial equalization of orbital electronegativity algorithm (MPEOE) [64,65]. The simulation box was prepared using the same protocol of Convertino *et al.* [39], having three monodispersed replicas of the same heptapeptide with or without the presence of a single NQTrp molecule. The concentration ratio peptide:compound was 3:1. Simulations were carried out with periodic boundary conditions at fixed peptide concentration of 5 mg/ml (the simulation box side was set to 98, 96 and 95 Å for $A\beta_{14-20}$, $A\beta_{16-22}$, and $A\beta_{18-24}$, respectively), using Langevin integrator at low friction constant (0.15 ps) and at a temperature of 330 K, which yields reversible aggregation within a reasonable computational time. For each system, ten indipendent MD runs out of 2.5 μs each were carried out using different random number generators for the assignment of the velocities. A 2.5 μs run takes three weeks on a single AMD Opteron 252 CPU at 2.6 GHz.

Order parameters are useful quantities to monitor the structural transition within peptide oligomers [46]. In particular, the nematic order parameter allows one to measure the amount of ordered β-structure in the system:

$$P_2 = \frac{1}{N}\sum_{i=1}^{N}\frac{3}{2}(\hat{z}_i\cdot\hat{d})^2 - \frac{1}{2}$$

The unit vector $\hat{d}$, that defines a preferential direction, is the eigenvector of the order matrix that corresponds to the largest positive eigenvalue. The N molecular unit vectors $\hat{z}_i$ are built joining the Cα atom of residue i to the Cα atom of residue i+2 ($N = 3\times7$). The values, ranging from zero to one, correspond to complete disorder and complete order respectively. The complete order is achieved when all the unit vectors are parallel or antiparallel, while the disorder is obtained when none of unit vectors is parallel to any of the others.

The threshold P_2^* is a value of the order parameter chosen such that it separates the ordered from the disordered phase, and was chosen as $P_2^* = 0.665$ [39]. Thus, the order-disorder ratio r is defined by the number of events where the system has a nematic order parameter lower than P_2^* (disorder) and greater that P_2^*(order):

$$r = \frac{n(P_2 > P_2)}{n(P_2 < P_2)} \quad (1)$$

Furthermore, the interference of NQTrp is measured by calculating the inter-peptide interaction energy, which is the CHARMM non-bond energy (van der Waals plus electrostatics) of a given peptide with the other two, without considering the interactions with NQTrp (Figure 5). The van der Waals interactions between NQTrp and individual Aβ residues (Figure 6) are estimated by averaging over all trajectories and neglecting the snapshots in which the interaction with all residues is zero. The criteria for hydrogen bond are the H-O distance smaller than 2.5 Å and a NH-O angle larger than 130 degrees.

Correlation between hydrogen bond pairs is calculated using the following formula:

$$C_{ij} = \frac{1}{T}\sum_t d_i(t)d_j(t)$$

where i and j are hydrogen bond indexes, T is the total number of frames in the simulation, and is one when the hydrogen bond i is formed at time t, and zero otherwise.

The binding modes depicted in Figure 6 were determined by selecting the simultaneous and most frequent hydrogen bonds between the peptide backbone and NQTrp (see Table S4). Single peptide conformations that interact with NQTrp through the selected hydrogen bonds were extracted. Resulting snapshots were clustered by using an algorithm from Dr. M. Schäfer (Michael Schäfer, Syngenta Crop Protection AG, unpublished work) with a cutoff of 1.5 Å and selecting peptide heavy atoms close to NQTrp and excluding symmetrical atoms.

Cell cytotoxicity assays

PC12 neuronal cells (2×10^5 cells/mL) were cultured in 96-well micro plates (100 µL/well) and incubated overnight at 37°C. To each well we added 100 µL of 5 µM Aβ toxic oligomers and inhibitors at various concentrations. Each experiment was repeated four times. Following incubation for 24 hours at 37°C, cell viability was evaluated using the MTT assay. Briefly, 20 µL of 5 mg/mL MTT dissolved in PBS were added to each well. After 4 hours of incubation at 37°C, 100 µL of extraction buffer [20% SDS dissolved in a solution of 50% dimethylformamide and 50% DDW (pH 4.7)] were added to each well, and the plates were incubated again overnight at 37°C. Finally, color intensity was measured using an ELISA reader at 570 nm.

Fly keeping

Flies were reared on standard corneal-molasses medium and were kept at 25°C. As Drosophila females can store sperm cells in their bodies, crosses were conducted using virgin females collected no longer than 8 hours after eclosion at 25°C or 18 hours after eclosion at 18°C. Adult offspring (F1) from the crosses were collected up to 9 days after the beginning of their eclosion at 25°C in order to avoid offspring from the next generation (F2).

Fly crossing

Male flies carrying the driver elav^{c155}-Gal4 (on their X chromosome) were crossed to females carrying the $A\beta_{1-42}$ transgene (located on an autosome) under the UAS promoter in a homozygous condition. This resulted in first generation (F1) female offspring expressing $A\beta_{1-42}$ in their nervous system. They served as our Alzheimer's Drosophila model. Male F1 offspring, which carried the $A\beta_{1-42}$ trasgene but did not express it (because they lacked the Gal4 driver) served as a control. Animals expressing $A\beta_{arc1-42}$ were generated in a similar way.

Fly feeding

NQTrp was added to standard corneal-molasses medium about 10 minutes after cooking (0.75 mg/mL). The compound was mixed thoroughly into the medium and the mixture was aliquoted into rearing vials. The vials were kept at 4°C until use. Crosses were performed either on regular Drosophila medium (control) or on medium supplemented with NQTrp. Animals fed on the appropriate medium from the beginning of the larval stage onwards. Animals expressing $A\beta_{arc1-42}$ were generated and assayed in a similar way.

Longetivity assay

Flies expressing one copy of $A\beta_{1-42}$ reared at 29°C on medium with and without NQTrp were classified into four classes: 1. Females expressing $A\beta_{1-42}$, on regular medium. 2. Females expressing $A\beta_{1-42}$, on medium supplemented with NQTrp. 3. Male controls (lacking the Gal4 driver), on regular medium. 4. Male controls (lacking the Gal4 driver), on medium supplemented with NQTrp. For each class, six vials each with 10 flies were collected and fresh food was provided every three days (whether with or without NQTrp). The number of viable Aβ-expressing and control flies treated with and without NQTrp was recorded daily post eclosion. Differences in survival rates were analyzed using the SPSS 11 Kaplan-Meir software package. Animals expressing $A\beta_{arc1-42}$ were generated and assayed in a similar way. The longetivity assay was repeated three times. All three analyses showed similar results.

Locomotive (climbing) assay

Test tubes of each of the four classes mentioned above, each containing 10 flies, were tapped gently on the table and were let stand for 18 seconds. The percent of flies which climbed to the top of the test tube was then calculated over time [50,51]. Each class had six independent vial-repeats. Statistical analysis was done using StatSoft Statistica 7, parametric ANOVA testing. The locomotive assay was repeated three times. All three analysis showed similar results.

Immuno-precipitation and western-blot of fly head extracts

Twenty five freshly decapitated heads from 6 day old $A\beta_{arc1-42}$ flies treated and non-treated with NQTrp were collected and homogenized in 30 µl PBS/protease inhibitor/ 1% SDS following [46]. Homogenates were then centrifuged at 13000 rpm for 25 seconds and the supernatant was further immuno-precipitated with specific 6E10 anti-Aβ antibody (1:10) over night at 4°C. Boiled samples were then western blotted and membranes were boiled in PBS for 10 minutes before antibodies were introduced. Total protein levels of the samples were quantified using Bradford analysis prior to gel loading. Since samples were loaded after IP with specific 6E10 anti-Aβ antibody, no marker protein levels could be measured.

Immuno-staining of larval brains

3rd instar larvae were dissected and stained using the following antibodies: primary 6E10 antibody (1:250) and secondary biotinylated anti-mouse antibody detected with Vecta-Stain-Elite ABC-HRP kit (Vector Laboratories). Stained larvae brains were mounted in 70% glycerol, 30% Tris pH 7.6 and viewed using bright-field microscopy (Nikon, Eclipse E600).

Immuno-staining of adult fly brains

Two-day old adult flies were dissected and their brains were removed. Whole brains were stained using the following antibodies: primary 6E10 antibody (1:250) and secondary anti-mouse Cy3 (1:100). Stained whole brains were imaged using confocal microscopy (LSM 510).

Supporting Information

Figure S1 Structure of naphthoquione-based molecules screened for inhibition of Aβ assembly. Compounds IL and IID are L and D isomers of NQTrp.
Found at: doi:10.1371/journal.pone.0011101.s001 (0.04 MB DOC)

Figure S2 1H-NMR spectra. Fingerprint regions of TOCSY (greens) spectrum overlaid on NOESY (reds) spectrum of Aβ12–28 with NQTrp (4:1 molar ratio) with assignment.
Found at: doi:10.1371/journal.pone.0011101.s002 (0.23 MB DOC)

Figure S3 1H-NMR derived structures. Ensemble of nine low energy structures generated for Aβ12–28 with NQTrp (4:1 molar ratio).

Found at: doi:10.1371/journal.pone.0011101.s003 (0.08 MB DOC)

Figure S4 Hydrogen bonds frequency between NQTrp and Aβ peptide backbone: For polar group labeling refer to the inset of Figure 5.
Found at: doi:10.1371/journal.pone.0011101.s004 (0.05 MB DOC)

Figure S5 Cytotoxicity analysis of NQTrp: PC12 cell line was incubated with different concentrations of NQTrp. The cytotoxic effect of NQTrp was determined using the MTT assay. Control - no NQTrp.
Found at: doi:10.1371/journal.pone.0011101.s005 (0.03 MB DOC)

Table S1 Summary of Aβ inhibition by all molecules examined: Twelve naphthoquione-based molecules were analyzed for inhibition of both oligomer and fibril formation. The relative degree of inhibition is indicated. No inhibition (−), low inhibition (+), moderate inhibition (++), significant inhibition (+++).
Found at: doi:10.1371/journal.pone.0011101.s006 (0.03 MB DOC)

Table S2 Neo constraints.
Found at: doi:10.1371/journal.pone.0011101.s007 (0.05 MB DOC)

Table S3 Average number of hydrogen bonds: [a]Average number of inter- and intra-peptide backbone-backbone hydrogen bonds, with (+) and without (−) NQTrp. The standard deviation is evaluated on ten independent simulations. [b]Ratio between order and disorder events sampled in the simulations.
Found at: doi:10.1371/journal.pone.0011101.s008 (0.05 MB DOC)

Table S4 Hydrogen bond correlations: Correlation among pair of hydrogen bonds between individual polar groups of NQTrp and the peptide backbone. The pairs occurring more frequently are reported in bold. The naming convention of the polar groups of NQTrp is as Fig. 6.
Found at: doi:10.1371/journal.pone.0011101.s009 (0.11 MB DOC)

Table S5 Highest probability hydrogen bonds: Pairs of hydrogen bonds with the highest probability (>0.01) to be simultaneously formed. The naming convention of the polar groups of NQTrp is as Fig. 2 bottom.
Found at: doi:10.1371/journal.pone.0011101.s010 (0.06 MB DOC)

Table S6 IC50 of aromatic inhibitors of Aβ.
Found at: doi:10.1371/journal.pone.0011101.s011 (0.03 MB DOC)

References S1 References for table S6.
Found at: doi:10.1371/journal.pone.0011101.s012 (0.02 MB DOC)

Acknowledgments

We thank Yaacov Delarea for help with electron microscopy experiments and Prof. David Gubb for fly stocks. We are indebted to Prof. Shmuel Bittner and his research group for help with chemical synthesis. We are grateful to Anna Shusterovich for help with graphic work. We thank Dr. Ludmila Buzhansky and the rest of the Gazit research group for fruitful discussions.

Author Contributions

Conceived and designed the experiments: RSA AFM MLS AC EG DS. Performed the experiments: RSA RP MC NEM SP DES. Analyzed the data: RSA RP MC AFM NEM SP DES AC EG DS. Contributed reagents/materials/analysis tools: RSA RP MC DES AC. Wrote the paper: RSA. Did all *in silico* work: RP MC. In charge of NMR work: DES.

References

1. Blennow K, de Leon MJ, Zetterberg H (2006) Alzheimer's disease. The Lancet 9533: 387–403.
2. Ferri CP, Prince M, Brayne C, Brodaty H, Fratiglioni L, et al. (2005) Global prevalence of dementia: a Delphi consensus study. The Lancet 9503: 2112–2117.
3. Selkoe DJ (1991) The molecular pathology of Alzheimer's disease. Neuron 6: 487–498.
4. Terry R (1994) Neuropathological changes in Alzheimer disease. Prog Brain Res 101: 383–390.
5. Hardy J, Allsop D (1991) Amyloid deposition as the central event in the aetiology of Alzheimer's disease. Trends Phamac 12: 383–388.
6. Mann D (1989) Cerebral amyloidosis aging and Alzheimer's disease; a contribution from studies on Down's syndrome. Neurobiol Aging 10: 397–399.
7. Price D, Tanzi R, Borchelt D, Sisodia S (1998) Alzheimer's disease: genetic studies and transgenic models. Annu Rev Genet 32: 461–493.
8. Van Leuven F (2000) Single and multiple transgenic mice as models for Alzheimer's disease. Prog Neurobiol 61: 305–312.
9. Fraser P, Yang D, Yu G, Levesque L, Nishimura M, et al. (2000) Presenilin structure, function and role in Alzheimer disease. Biochem Biophys Acta 1502: 1–15.
10. Cleary JP, Walsh DM, Hofmeister JJ, Shankar GM, Kuskowski MA, et al. (2005) Natural oligomers of the amyloid-β protein specifically disrupt cognitive function. Nat Neuroscience 1: 79–84.
11. Kirkitadze MD, Bitan G, Teplow DB (2002) Paradigm shifts in Alzheimer's disease and other neurodegenerative disorders: the emerging role of oligomeric assemblies. J Neurosci Res 69: 567–577.
12. Lashuel HA, Hartley D, Petre BM, Walz T, Lansbury PTJ (2002) Neurodegenerative disease: amyloid pores from pathogenic mutations. Nature 418: 291.
13. Kayed R, Head E, Thompson JI, McIntire TM, Milton SC, et al. (2003) Common structure of soluble amyloid oligomers implies common mechanism of pathogenesis. Science 300: 486–489.
14. Gazit E (2004) The role of prefibrillar assemblies in the pathogenesis of amyloid diseases. Drugs Fut 29: 613–619.
15. Barghorn S, Nimmrich V, Striebinger A, Krantz C, Keller P, et al. (2005) Globular amyloid beta-peptide oligomer - a homogenous and stable neuropathological protein in Alzheimer's disease. J Neurochemistry 3: 834–847.
16. Azriel R, Gazit E (2001) Analysis of the minimal amyloid-forming fragment of the islet amyloid polypeptide. An experimental support for the key role of the phenylalanine residue in amyloid formation. J Biol Chem 276: 34156–34161.
17. Gazit E (2002) A possible role for π-stacking in self-assembly of amyloid fibrils. FASEB J 16: 77–83.
18. Gazit E (2003) Global Analysis of Tandem Aromatic Octapeptide Repeats: The Significance of Aromatic-Glycine Motif. Bioinformatics 18: 880–883 (2002).
19. Reches M, Gazit E (2003) Casting metal nanowires within discrete self-assembled peptide nanotubes. Science 300: 625–627.
20. Makin OS, Atkins E, Sikorski P, Johansson J, Serpell LCM (2005) Molecular basis for amyloid fibril formation and stability. Proc Natl Acad Sci U S A 102: 315–320.
21. Inouye H, Sharma D, Goux WJ, Kirschner DA (2006) Structure of core domain of fibril-forming PHF/Tau fragments. Biophys J 90: 1774–1789.
22. Colombo G, Daidone I, Gazit E, Amadei A, Di Nola A (2005) Molecular dynamic simulation of the aggregation of the core-recognition of the Islet amyloid polypeptide in explicit water. Proteins 59: 519–527.
23. Wu C, Lei HX, Duan Y (2005) The role of Phe in the formation of well-ordered oligomers of amyloidogenic hexapeptide (NFGAIL) observed in molecular dynamic simulation with explicit solvent. Biophys J 88: 2897–2906.
24. Tartaglia GG, Cavalli A, Pellarin R, Caflisch A (2004) The role of aromaticity, exposed surfaces and dipole moment in determining protein aggregation rates. Prot Sci 13: 1939–1941.
25. Zanuy D, Porat Y, Gazit E, Nussinov R (2004) Peptide sequence and amyloid formation: molecular simulation and experimental study of a human Islet amyloid polypeptide fragment and its analogs. Structure 12: 439–455.
26. Pawar AP, Dubay KF, Zurdo J, Chiti F, Vendruscolo M, et al. (2005) Prediction of "aggregation-prone" and "aggregation susceptible" regions in proteins associated with neurodegenerative diseases. J Mol Biol 350: 379–392.
27. Porat Y, Mazor Y, Efrat S, Gazit E (2004) Inhibition of Islet amyloid polypeptide fibril formation: a potential role for heteroaromatic interactions. Biochemistry 43: 14454–14462.
28. Porat Y, Abramowitz A, Gazit E (2006) Inhibition of amyloid fibril formation by polyphenols: structural similarity and aromatic interactions as a common. Chem Biol Drug Des 67: 27–37.

29. Bastianetto S, Krantic S, Quirion R (2008) Polyphenols as potential inhibitors of amyloid aggregation and toxicity: possible significance to Alzheimer's disease. Mini Rev Med Chem 5: 429–435.
30. Rivièrea C, Richarda T, Quentina L, Krisab S, Mérillonb JM, et al. (2007) Inhibitory activity of stilbenes on Alzheimer's β-amyloid fibrils in vitro. Bioorg & Med Chem 15: 1160–1167.
31. Frydman-Marom A, Rechter M, Shefler I, Bram Y, Shalev DE, et al. (2009) Cognitive-Performance Recovery of Alzheimer's Disease Model Mice by Modulation of Early Soluble Amyloidal Assemblies. Angew Chem Int Ed 48: 1981–1986.
32. Cohen T, Frydman-Marom A, Rechter M, Gazit E (2006) Inhibition of amyloid fibril formation and cytotoxicity by hydroxyindole derivatives. Biochemistry 45: 4727–4735.
33. Frew T, Powis G, Berggren M, Berggren M, Abraham RT, et al. (1995) Novel quinone antiproliferative inhibitors of phosphatidylinositol-3-kinase. Anticancer Drug Des 4: 347–359.
34. Gulielmo BJ, MacDougall C (2004) Pharmacokinetics of valaciclovir. J Antimicrob Chemother 6: 899–901.
35. Tomiyama T, Kaneko H, Kataoka, Asano S, Endo N (1997) Rifampicin inhibits the toxicity of pre-aggregated amyloid peptides by binding to peptide fibrils and preventing amyloid-cell interaction. Biochem J 322: 859–865.
36. Lieu VH, Wu JW, Wang SS, Wu CH (2007) Inhibition of amyloid fibrillization of hen egg-white lysozymes by rifampicin and p-benzoquinone. Biotechnol Prog 23: 698–706.
37. Pickhardt M, Gazova Z, von Bergen M, Khlistunova I, Wang Y, et al. (2005) Anthraquinones inhibit tau aggregation and dissolve Alzheimer's paired helical filaments in vitro and in cells. J Biol Chem 280: 3628–3635.
38. Necula M, Kayed R, Milton S, Glabe CG (2007) Small Molecule Inhibitors of Aggregation Indicate That Amyloid β Oligomerization and Fibrillization Pathways Are Independent and Distinct. J Biol Chem 282: 10311–10324.
39. Convertino M, Pellarin R, Catto M, Carotti A, Caflisch A (2009) 9,10-Anthraquinone hinders β-aggregation: How does a small molecule interfere with Aβ-peptide amyloid fibrillation? Prot Sci 18: 792–800.
40. Shrestha-Dawadi PB, Prativa B, Bittner S, Fridkin M, Rahimipour S (1996) On the Synthesis of Naphthoquinonyl Heterocyclic Amino Acids. Synthesis 12: 1468–1472.
41. Roychaudhuri R, Yang M, Hoshi MM, Teplow DB (2009) Amyloid beta-protein assembly and Alzheimer disease. J Biol Chem 284: 4749–4753.
42. Balbach JJ, Ishii Y, Antzutkin ON, Leapman RD, Rizzo NW, et al. (2000) Amyloid Fibril Formation by Aβ16–22, a Seven-Residue Fragment of the Alzheimer's β-Amyloid Peptide, and Structural Characterization by Solid State NMR. Biochemistry 39: 13748–13759.
43. Jarvet J, Damberg P, Bodell K, Eriksson LEG, Graslund A (2000) Reversible Random Coil to β-Sheet Transition and the Early Stage of Aggregation of the Aβ(12–28) Fragment from the Alzheimer Peptide. J Am Chem Soc 122: 4261–4268.
44. Xu-Rong Q, Hiroshi A, Hiroshi N (2002) NMR and CD studies on the interaction of Alzheimer beta-amyloid peptide (12–28) with beta-cyclodextrin. Biochem Biophys Res Commun 297: 1011–1015.
45. Gazit E (2005) Arrest of amyloid fibril formation associated to type II diabetes: structural and functional links to the mechanism of Alzheimer's β-amyloid fibrillization. Drug Des Rev 2: 115–119.
46. Cecchini M, Curcio R, Pappalardo M, Melki R, Caflisch A (2006) A Molecular Dynamics Approach to the Structural Characterization of Amyloid Aggregation. JMB 357: 1306–1321.
47. Crowther DC, KIinghorn KJ, Miranda E, Page R, Curry JA, et al. (2005) Intraneuronal Aβ, non-amyloid aggregates and neurodegeneration in a drosophila model of Alzheimer's disease. Neuroscience 132: 123–135.
48. Feany MB, Bender WW (2000) A Drosophila model of Parkinson's disease. Nature 404: 394–398.
49. Ganetzky B, Flanagan JR (1978) On the relationship between senescence and age-related changes in two wild-type strains of Drosophila melanogaster. Exp Gerontol 13: 189–196.
50. Nilsberth C, Westlind-Danielsson A, Eckman CB, Condron MM, Axelman K, et al. (2001) The 'Arctic' APP mutation (E693G) causes Alzheimer's disease by enhanced Abeta protofibril formation. Nat Neurosci 4: 887–893.
51. Iijima K, Chiang H, Hearn SA, Hakker I, Gatt A, et al. (2008) Aβ42 mutants with different aggregation profiles induce distinct pathologies in Drosophila. PloS one 3(2): e1703.
52. Wu C, Biancalana M, Shea JE (2009) Binding modes of thioflavin-T to the single-layer ß-sheet of the peptide self-assembly mimics. J Mol Biol 394: 627–633.
53. Wu C, Wang Z, Lei H, Zang W, Duan Y (2007) Dual binding modes of Congo red to amyloid protofibril surface observed in molecular dynamics simulations. J Am Chem Soc 129: 1225–1242.
54. Aue WP, Bartholdi E, Ernst RR (1976) Two-dimensional spectroscopy. Application to nuclear magnetic resonance. J Chem Phys 64: 2229.
55. Piotto M, Saudek V, Sklenár V (1992) Gradient-tailored excitation for single-quantum NMR spectroscopy of aqueous solutions. J Biomol NMR 2: 661–665.
56. Wagner R, Berger S (1996) Gradient-Selected NOESY—A Fourfold Reduction of the Measurement Time for the NOESY Experiment. J Magn Reson A 123: 119–121.
57. Wüthrich K (1986) NMR of Proteins and Nucleic Acids. John Wiley & Sons, New York.
58. Honig B, Sharp K, Yang AS (1993) Macroscopic Models of Aqueous Solutions: Biological and Chemical Applications. J Phys Chem 97: 1101–1109.
59. Pearlmen DA, Case DA, Caldwell JW, Ross WS, Cheatham ITE, et al. (1995) AMBER, a package of computer programs for applying molecular mechanics, normal mode analysis, molecular dynamics and free energy calculations to simulate the structural and energetic properties of molecules. Comp Phys 91: 6.
60. Pettersen EF, Goddard TD, Huang CC, Couch GS, Greenblatt DM, et al. (2004) UCSF Chimera - A Visualization System for Exploratory Research and Analysis. J Comput Chem 25: 1605–1612.
61. Brooks BR, Bruccoleri RE, Olafson BD, States DJ, Swaminathan S (1983) CHARMM: A program for macromolecular energy, minimization, and dynamics calculations. J Comp Chem 4: 187–217.
62. Brooks BR, Brooks CL, Mackerell AD, Nilsson L, Petrella RJ, et al. (2009) CHARMM: the biomolecular simulation program. J Comput Chem 30(10): 1545–614.
63. Ferrara P, Apostolakis J, Caflisch A (2002) Evaluation of a fast implicit solvent model for molecular dynamics simulations. Proteins: Structure, Function, and Bioinformatics 46: 24–33.
64. No K, Grant J, Jhon M, Scheraga H (1990a) Determination of net atomic charges using a modified partial equalization of orbital electronegativity method. 2. Application to ionic and aromatic molecules as models for polypeptides. J Phys Chem 94: 4740–4746.
65. No K, Grant J, Scheraga H (1990b) Determination of net atomic charges using a modified partial equalization of orbital electronegativity method. 1. Application to neutral molecules as models for polypeptides. J Phys Chem 94: 4732–4739.

Chapter 4

$A\beta_{12-28}$ conformational change induced by small molecules

The present project was defined in follow-up to the results of the fruitful collaborations with the labs of Prof. E. Gazit and Prof. A. Carotti presented herein in previous chapters. Implicit solvent MD simulations were employed to further investigate the interactions between two small-molecules, which were identified as Aβ aggregation inhibitors (1,4-naphtoquinon-2-yl-L-tryptophan and 9,10-anthraquinone, here reported as NQTrp[48] and AQ[49], respectively) during our previous studies, and the central amino acid sequence of the β-amyloid peptide ($A\beta_{12-28}$). MD results suggest that both NQTrp and AQ play an important role in promoting a conformational change in $A\beta_{12-28}$, inducing the formation of a collapsed loop, thus creating a binding pocket with which NQTrp and AQ can interact via hydrogen bonds, electrostatic and van der Waals interactions.

4.1 Simulations setup

Langevin MD simulations of the highly aggregation-prone capped $A\beta_{12-28}$ segment were undertaken both alone and in presence of a single NQTrp or AQ molecule (molecular structures are represented in Figure 2 of the Introduction), at a temperature of 300 K, with an inhibitor concentration of 5 mg/ml and under periodic boundary conditions. Multi-microseconds (3x5μs) simulations were performed using the united atom (param19) CHARMM[78,79] force field and FACTS[89] implicit solvent model.
The cut-based Free Energy Profile (cFEP) approach[101] (see Introduction for further details) was used to study the free-energy landscape of $A\beta_{12-28}$, and thus, to isolate energetic basins of kinetically closed conformational states, as well to identify potential NQTrp and AQ binding modes.

4.2 Variation of $A\beta_{12\text{-}28}$ secondary structure propensity

Among numerous analyses of the simulated systems, the present project issued from calculations of the secondary structure propensity (computed using the sstruct module in WORDOM[107]) of $A\beta_{12\text{-}28}$ alone and in presence of inhibitor molecules in equimolar concentration. Both NQTrp or AQ induce a variation in the secondary structure propensity along the amino acid sequence of $A\beta_{12\text{-}28}$. These inhibitors reduce the helical propensity of this peptide, particularly along the V_{12}-D_{23} segment.

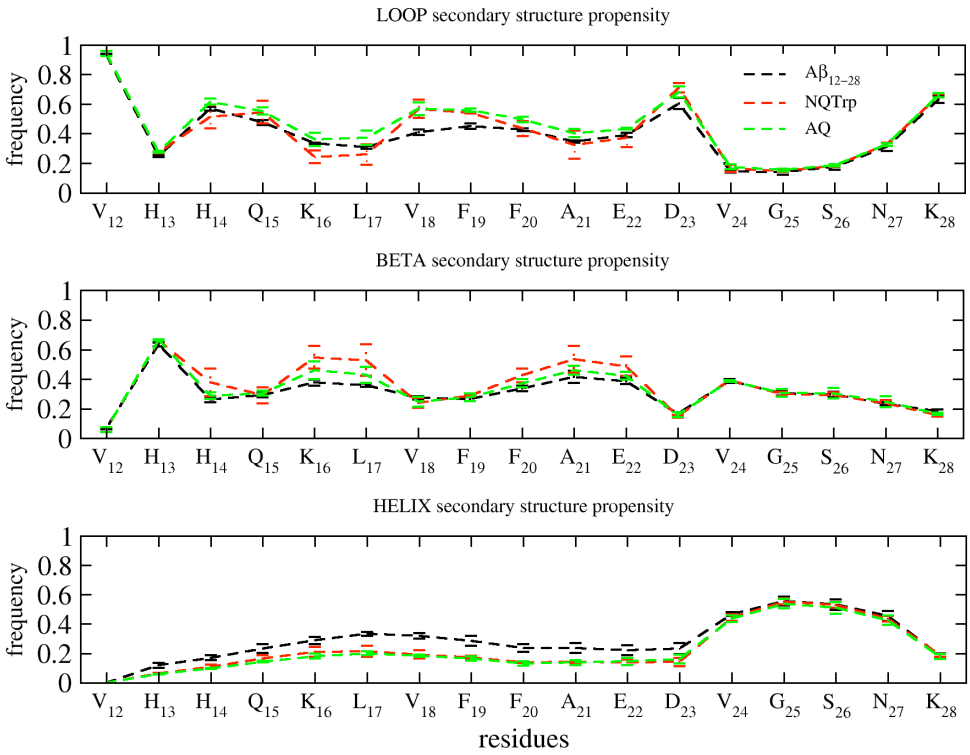

Figure 1. Variation of $A\beta_{12\text{-}28}$ secondary structure propensity in presence of NQTrp or AQ.

4.3 Isolation of conformational basins

Based on the results of the above described analysis, a more in-depth investigation of the conformational changes induced by the presence of NQTrp and AQ was undertaken using the cFEP approach[101] to study the free-energy landscape of $A\beta_{12-28}$, and thus, to isolate energetic basins of kinetically closed conformational states of $A\beta_{12-28}$ alone and in presence of NQTrp or AQ.

4.3.1 cFEP analysis of the MD trajectory of $A\beta_{12-28}$

The set of network nodes of the MD-generated conformations, derived by clustering the simulation snapshots according to user-defined metrics, serves as input for cFEP profile determinations. In the present study, a cluster analysis based on $C\alpha(H_{14}\text{-}S_{26})$-RMSD was performed over the entire 15μs trajectory using the LEADER algorithm as implemented in WORDOM[107].
As the first and last two residues forming the N- and C-terminus, respectively, were highly mobile throughout the simulations, these residues were discarded in order to reduce excessive noise in the data.
Three cFEP curves were derived starting from different initial clusters (obtained using 1.5 Å, 1.8 Å, 2.0 Å cutoff values, Figure 2a). All three cFEP profiles clearly indicate the presence of an energetic basin accounting for about 10% of the full conformational space.
In order to identify the representative conformations of the isolated energetic basins, the MD time-series was rearranged according to the Z_A/Z progress coordinate into a new time-independent trajectory; $A\beta_{12-28}$ secondary structure (Figure 2b) and radius of gyration (Figure 2c), as well as Cα-RMSD with respect to the representive of the most populated node of $A\beta_{12-28}$ alone (Figure 2d) and in presence of NQTrp (Figure 2e) were calculated. As shown in Figure 2 (b-e), the first basin is characterized by the presence of $A\beta_{12-28}$ in helical conformation (Figure 5, left). This basin is separated from a basin corresponding to a collapsed loop conformation, which accounts for about 2% of the full conformational space ($0.94 \leq Z_A/Z \leq 0.96$), by a large entropic basin of extended random-coil structures.

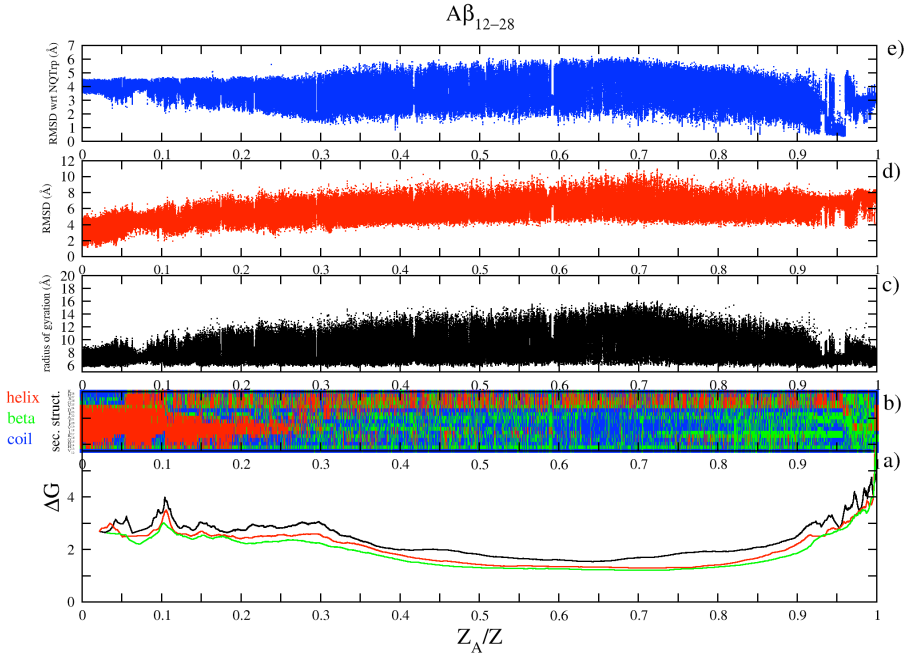

Figure 2. cFEP analysis of $A\beta_{12\text{-}28}$ alone. **a)** cFEP curves obtained using the $C\alpha(H_{14}\text{-}S_{26})$-RMSD clustering with 1.5Å (black), 1.8 Å (red) and 2.0 Å (green) cutoff starting from the most populated node; nodes are ranked according to their mfpt values. **b)** Secondary structure analysis for the full time-series rearranged according to the Z_A/Z progress coordinate. **c)** Radius of gyration along the Z_A/Z-rearranged trajectory. **d)** Cα-RMSD computed along the Z_A/Z-rearranged trajectory with respect to the representative of the most populated node of $A\beta_{12\text{-}28}$ alone and **e)** in presence of NQTrp. Diffusivity test plots can be found in the Appendix sections.

4.3.2 cFEP analysis of $A\beta_{12\text{-}28}$ trajectories in presence of NQTrp or AQ

The same set of analyses was performed for $A\beta_{12\text{-}28}$ in presence of a single molecule of NQTrp or AQ, using the already cited settings for the $A\beta_{12\text{-}28}$ system. As expected, the cFEP curves show a different profile with respect to the one retrieved for $A\beta_{12\text{-}28}$ alone.

In the two 'inhibited' systems (i.e., Aβ simulated in presence of an inhibitor molecule), the first basin corresponds to a collapsed loop conformation (Figure 5, right) covering about 22% and 10% of the conformational space for NQTrp and AQ, respectively. In both the $A\beta_{12\text{-}28}$/NQTrp and $A\beta_{12\text{-}28}$/AQ systems, this basin is separated from a second one, corresponding to a helical conformational state, by a large entropic basin of extend random coil conformations (Figures 3 and 4).

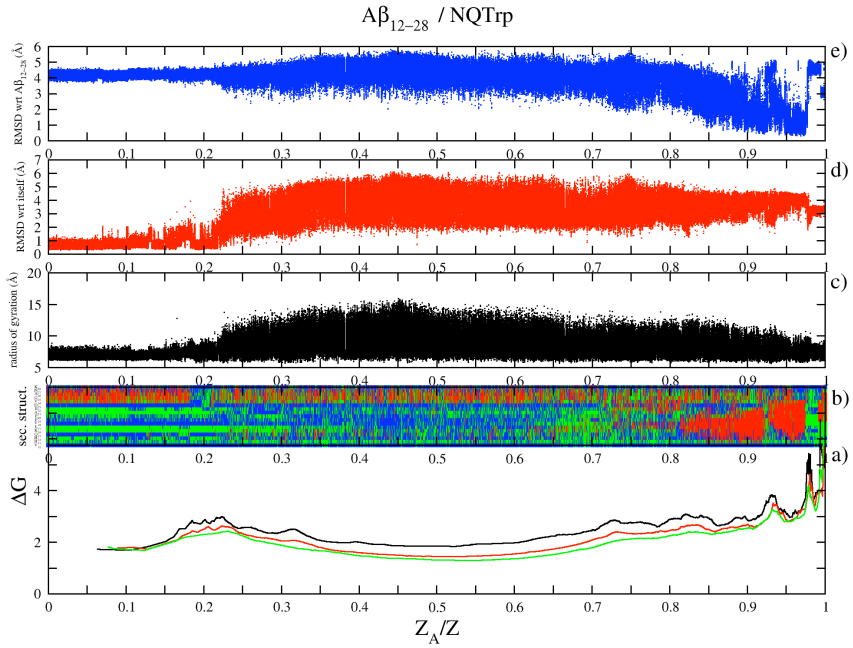

Figure 3. cFEP analysis of $A\beta_{12\text{-}28}$ in presence of NQTrp. **a-c)** Same as Figure 2 for NQTrp. **d)** Cα-RMSD computed along the Z_A/Z-rearranged trajectory with respect to the representative of the most populated node of $A\beta_{12\text{-}28}$ in presence of NQTrp and **e)** alone. Diffusivity test plots in the Appendix.

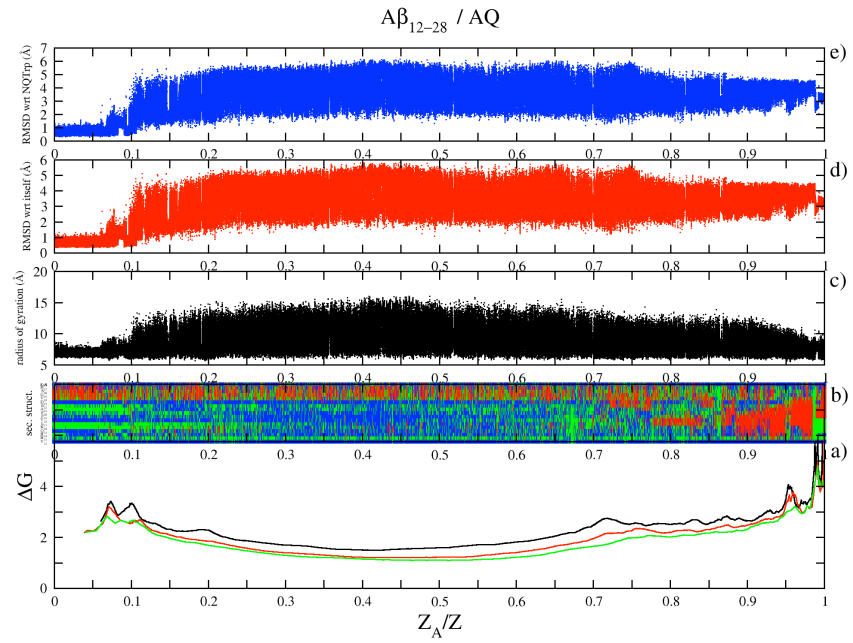

Figure 4. cFEP analysis for $A\beta_{12\text{-}28}$ in presence of AQ. **a-c)** Same as Figure 2 for AQ. **d)** Cα-RMSD computed along the Z_A/Z-rearranged trajectory with respect to the representative of the most populated node of $A\beta_{12\text{-}28}$ in presence of AQ or **e)** NQTrp.

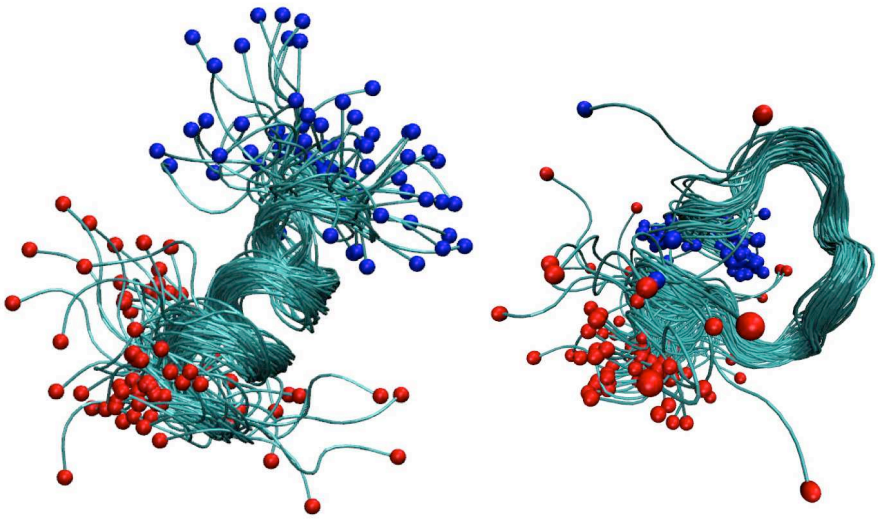

Figure 5. (Left) Representative conformations of the 1st basin indentified by the cFEP for the $A\beta_{12-28}$ monomer alone (statistical weight 10% of the conformational space). **(Right)** Conformations of the 1st basin indentified by cFEP in presence of NQTrp or AQ (statistical weight 22% and 10% of the conformational space for NQTrp and AQ, respectively). Representative structures are plotted skipping each 1000 conformations and fitting over the sequence Q_{15}-F_{20} Cα; the blue and red spheres indicate the N- and C-terminus, respectively.

4.4 Potential $A\beta_{12-28}$ binding modes of NQTrp and AQ

The generated cFEP profiles revealed that the formation of a collapsed loop conformation of amyloid peptide is increased from about 2% in the case of $A\beta_{12-28}$ alone to about 22% or 10% in presence of NQTrp or AQ, respectively.

The analyses of the intermolecular distances between $A\beta_{12-28}$ and NQTrp or AQ pointed out that the former inhibitor is more tightly bound to $A\beta_{12-28}$ than the latter; in particular, for both NQTrp and AQ, the statistical weight of the bound state is about 10% higher in the first cFEP basin (see Table 1 in Appendix and figure 6) from which the $A\beta_{12-28}$ collapsed loop conformations were identified.

All snapshots belonging to the first basin of $A\beta_{12-28}$/NQTrp and $A\beta_{12-28}$/AQ were isolated and a second cFEP analysis was performed, clustering the snapshots according to the (H_{14}-Q_{15}-K_{15})/NQTrp or to the (H_{14}-Q_{15}-K_{16})-AQ DRMS with a cutoff of 1.0 Å (see Figures A3-A6 in the Appendix).

These three Aβ amino acids were selected as their interaction energies were the most favourable as computed by CHARMM and as they formed a high number of hydrogen bonds with NQTrp and AQ over the full trajectory (see

Figures A7 and A8 in the Appendix). All of the snapshots of the first basin obtained with the second cFEP analysis (covering about 7% and 4% of the selected conformational space of $A\beta_{12\text{-}28}$/NQTrp and $A\beta_{12\text{-}28}$/AQ, respectively) were isolated and one of the possible NQTrp and AQ binding modes was identified.

The NQTrp and AQ atomic distributions around $A\beta_{12\text{-}28}$ within the first basin of the DRMS-based-cFEP profile, as well as the representatives of the most populated nodes (about 2% and 1% of the selected conformational space for NQTrp and AQ, respectively) are represented in Figure 7.

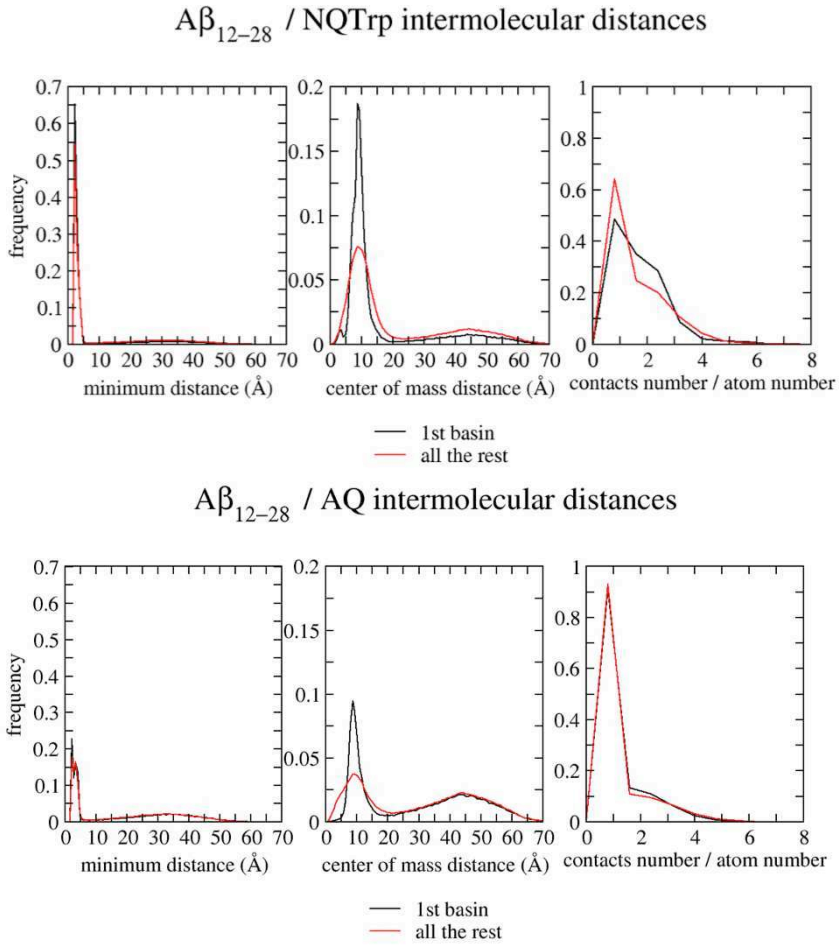

Figure 6. Intermolecular distances between $A\beta_{12\text{-}28}$ and NQTrp **(top)** or AQ **(bottom)**. For each of the two systems all snapshots belonging to the 1st cFEP basin were isolated from the other snapshots of the simulations; for the resulting two subsets, the minimum all-atom distance between the inhibitor and $A\beta_{12\text{-}28}$, the distance of their centers of mass, and the contact efficiency (number of contacts/number of heavy atoms in the inhibitor, distance-cutoff set at 4.0 Å) were computed.

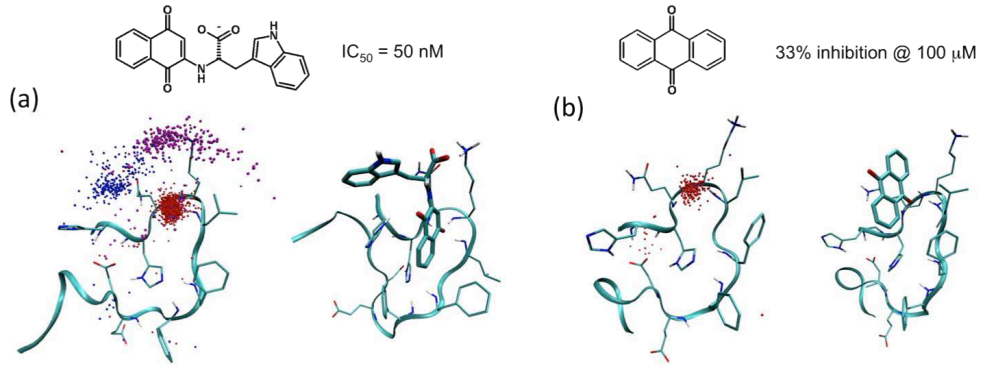

Figure 7. (a, left) NQTrp quinonic oxigens (red), carboxylic carbon (magenta) and indolic nitrose (blue) distributions within 3.5 Å from $A\beta_{12-28}$ are symbolized as spheres (DRMS-based-cFEP 1st basin, denser clouds indicate a higher coordination); **(a, right)** representative structure of the most populated node indicating one of the possible NQTrp binding mode. **(b, left)** AQ quinonic oxigen (red) distribution within 3.5 Å from $A\beta_{12-28}$ is symbolized as spheres (DRMS-based-cFEP 1st basin, denser clouds indicate a higher coordination); **(b, right)** representative structure of the most populated node indicating one of the possible AQ binding mode.

4.5 Comparison between NMR- and MD-derived NOE

The NOE distance r(*t*) (i.e., the inter-proton distance at simulation time *t*) was calculated along 15 μs of MD sampling of a 1:1 system of $A\beta_{12-28}$ and NQTrp. The NOE upper distance limits were derived from MD simulations using the formula $\langle r(t)^{-6} \rangle^{-1/6}$ as suggested by Tropp[108] for small peptides or molecules for which the timescale of internal fluctuations is longer than the overall tumbling time. The plot in Figure 8 shows that intramolecular NOE upper distance limits were only marginally violated (seven statistically significant violations over twentyfive).

4.6 Conclusions

A detailed description of the interactions between selected aggregation inhibitors and the $A\beta_{12-28}$ monomer was obtained using implicit solvent MD simulations.

The presence of NQTrp or AQ was found to induce a conformational change over the $A\beta_{12-28}$ sequence, from a helix to a collapsed loop, that creates a binding pocket with which inhibitors molecules can interact.

In silico results are supported by NMR data; indeed, NOE long-range intermolecular upper distance limits were only marginally violated.

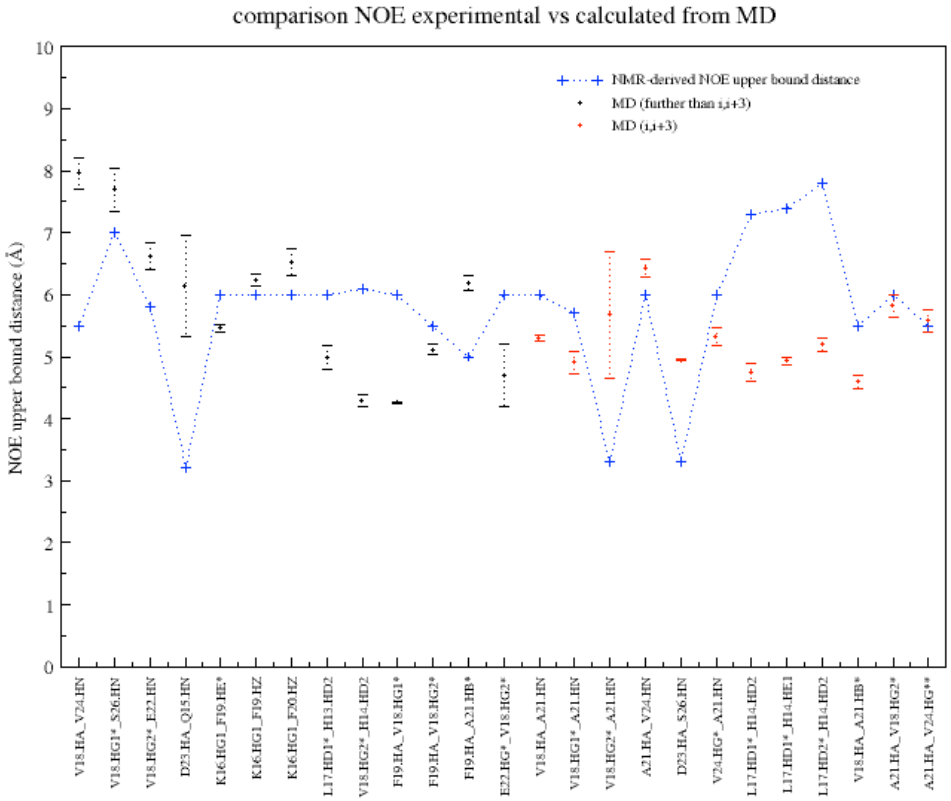

Figure 8. NMR NOE upper distance constraints (blue empty diamonds) and calculated from the MD runs (filled circles with dashed bars for standard deviations). The colors indicate *further than i, i+3* (black), and *i, i+3* (red) NOE signals, respectively. The blue dashed line at the bottom indicates van der Waals distance values as they were obtained from the NMR experiment.

Appendix to Chapter 4

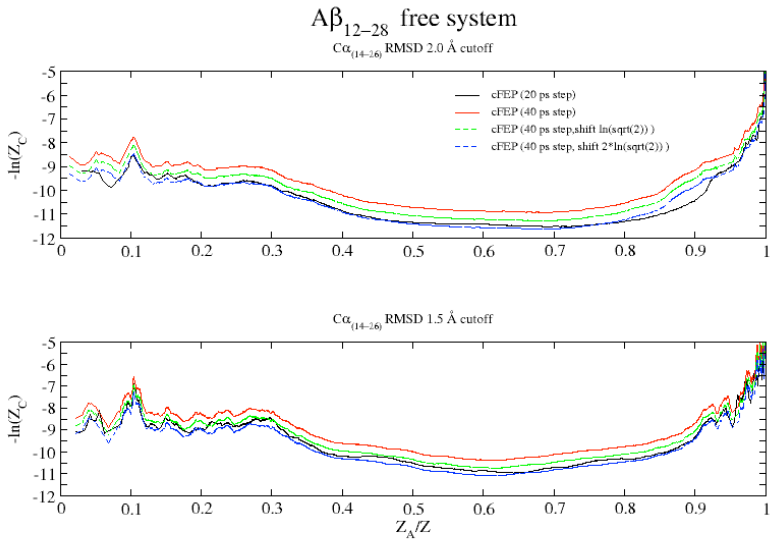

Figure A1. Diffusivity test of the cFEP analysis on $A\beta_{12-28}$ as reccomended by Krivov and Karplus[109].

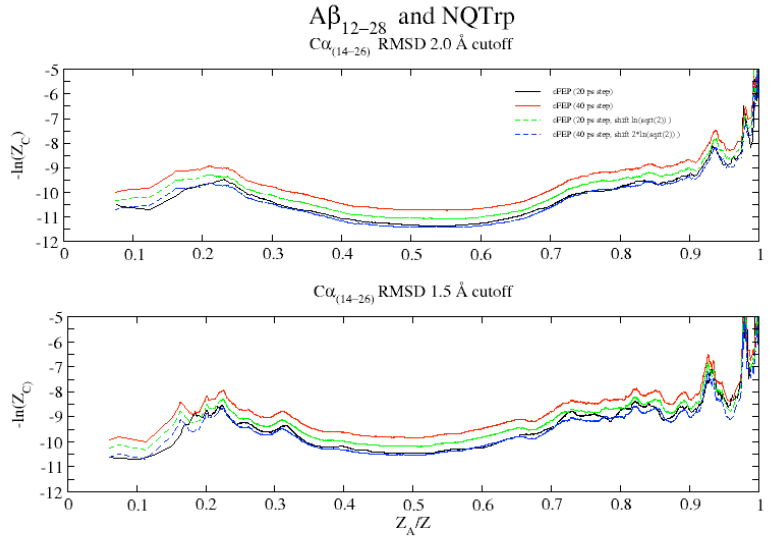

Figure A2. Diffusivity test of the cFEP analysis on $A\beta_{12-28}$ in presence of NQTrp (as in Figure A1).

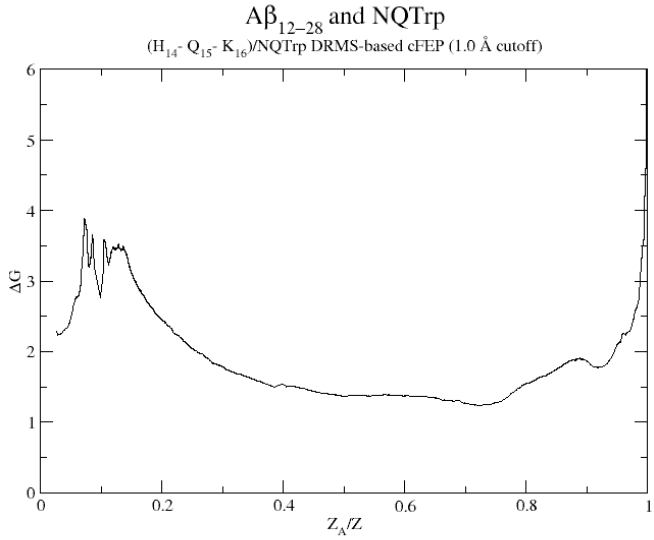

Figure A3. cFEP profile for $A\beta_{12\text{-}28}$ in presence of NQTrp. The cluster analysis was performed using (H_{14}-Q_{15}-K_{16})/NQTrp DRMS with 1.0 Å cutoff. The first basin covers about 7% of the selected conformational space.

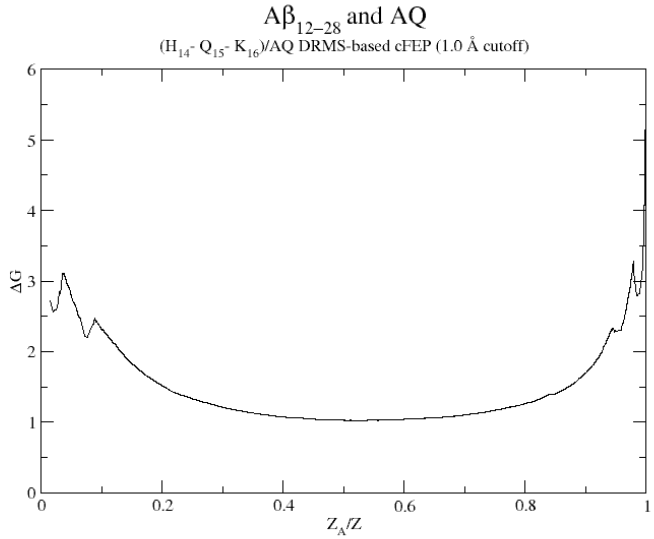

Figure A4. cFEP profile for Aβ1228 in presence of NQTrp. The cluster analysis was performer using (H_{14}-Q_{15}-K_{16})/NQTrp DRMS with 1.0 Å cutoff. The first basin covers about 4% of the selected conformational space.

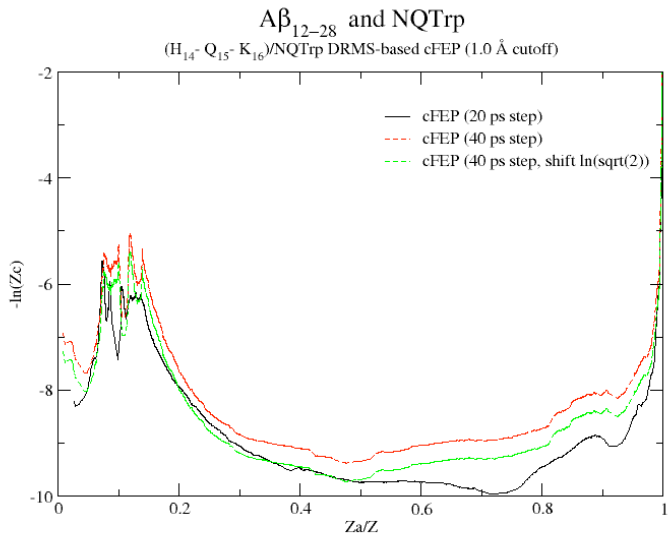

Figure A5. Diffusivity test of the DRMS-based cFEP analysis on $A\beta_{12\text{-}28}$ in presence of NQTrp (as in Figure A1).

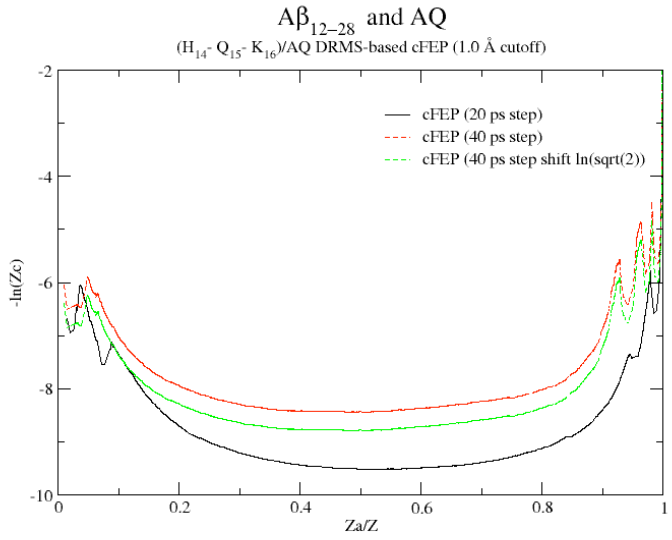

Figure A6. Diffusivity test of the DRMS-based cFEP analysis on $A\beta_{12\text{-}28}$ in presence of AQ (as in Figure A1).

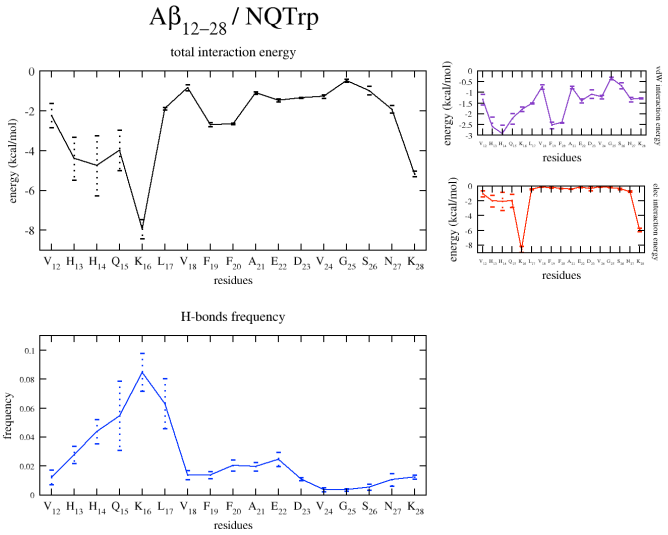

Figure A7. CHARMM interaction energies and hydrogen bond frequency between $A\beta_{12\text{-}28}$ and NQTrp computed over the full trajectory.

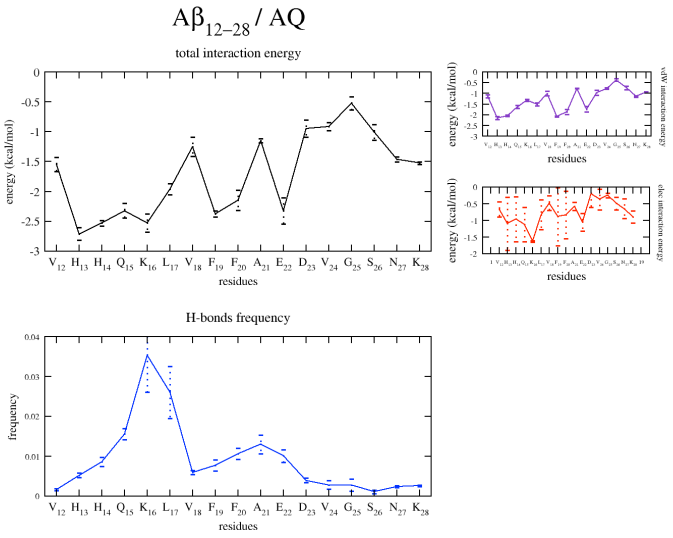

Figure A8. CHARMM interaction energies and hydrogen bond frequency between $A\beta_{12\text{-}28}$ and AQ computed over the full trajectory.

Table A1. Statistical weight of the bound state of NQTrp and AQ.

conformational space	cutoff (Å)	NQTrp (%)	AQ (%)
full trajectory	5	70	38
	6	70	38
	8	71	39
1st basin of RMSD-based cFEP profile	5	79	41
	6	80	41
	8	80	42
all RMSD-based cFEP profile excluding the1st basin	5	67	37
	6	68	38
	8	68	39

Chapter 5

Conclusions and outlooks

"E scoperse cosi, non senza umiliazione,
che un piccolo ippopotamo è sempre
un po' più grosso di un grossissimo moscone."
G. Rodari

Three research projects are presented hereabove in which molecular dynamics (MD) simulations provide an atomistic level description of the mechanisms of interference of selected low molecular weight compounds in β-amyloid peptide (Aβ) aggregation.
First, the influence of 9,10-anthraquinone (AQ) and antracene (AC) on $A\beta_{14\text{-}20}$ aggregation was studied, using the nematic order parameter P_2 to monitor the extent of β-aggregation perturbation. Through favorable polar interactions with the peptide backbone, AQ was found to destabilize the interstrand hydrogen bond pattern of $A\beta_{14\text{-}20}$ aggregates to a greater degree than AC. Specifically, the AQ quinonic moiety tightly binds the peptide backbone through hydrogen bonds and exa-/octupolar (herein named $\pi^{+}\delta^{-}$) interactions[47].
The property of the quinonic structure as an amyloid aggregation inhibitor, together with tryptophan's amyloid recognition propensity, provided a rational design route leading to the definition of a new hybrid molecule, 1,4-napthoquinon-2-yl-L-tryptophan (NQTrp), whose evaluation formed the basis of the second project. NQTrp was found to be a highly potent inhibitor of Aβ oligomerization and fibrillization in silico; this was confirmed using a variety of experimental techniques, including Thioflavin T (ThT) binding assays, Circular Dicrohism (CD) and Transmission Electron Microscopy (TEM). NQTrp notably reduced the neurotoxicity due to Aβ oligomerization in the in vivo transgenic *Drosophyla Melanogaster* model (AlzhaFly)[46].
A more detailed description of the interactions between selected aggregation inhibitors and $A\beta_{12\text{-}28}$ monomers resulted from the third project. Using the cut-based free-energy profile (cFEP) method[101], an inhibitor-induced conformational change in the form of a collapsed loop in $A\beta_{12\text{-}28}$ was identified. This conformational change creates a binding pocket with which

inhibitor molecules can preferentially interact.
Using the cut-based free-energy profile (cFEP) method[101], an inhibitor-induced conformational change in the form of a collapsed loop in $A\beta_{12-28}$ was identified. This conformational change creates a binding pocket with which inhibitor molecules can preferentially interact.
The presence of collapsed-loop Aβ conformations induced by quinonic moieties was confirmed by NMR spectroscopic techniques. Nonetheless, the ease of transition over the first conformational barrier (of about 1 kcal/mol) of the two 'inhibited' and the inhibitor-free systems, suggests that the $A\beta_{12-28}$ conformational change in presence of quinonic moieties plays only a secondary role in aggregation inhibition. Indeed, an increase in the aggregation lag-phase was not detected by *in vitro* ThT binding assays, though the influence of differing experimental and *in silico* conditions cannot be excluded. Rather, the proposed inhibition mechanism referring to the hindering of inter-peptide hydrogen bond formation between Aβ monomers is likely to be of primary relevance.
In conclusion, the atomistic descriptions resulting from the MD simulations in these three studies provide a reliable starting point for the screening and design of small-molecule inhibitors of amyloid aggregation having therapeutic potential for the treatment of Alzheimer's disease.
Future studies could include structure-based virtual screening (docking on the $A\beta_{12-28}$ collapsed conformation) of appropriately selected chemical libraries in order to identify improved Aβ aggregation inhibitors.
Moreover, computational and experimental evaluations of putative chimeric inhibitors (such as quinonic derivatives of nicotine or cotinine, or chimeric molecules based on the results of the proposed virtual screening) could be performed. Such new chemical entities might present advantageously high inhibitory activity towards Aβ aggregation, thus allowing a reduction in the needed dose relative to current lead compounds, thereby potentially limiting the risk of side-effects.

Bibliography

[1] Alois Alzheimer Bibliography, International Brain Research Organization.

[2] Möller H.J., Gräber M.B. The case described by Alois Alzheimer in 1911. Historical and conceptual perspectives based on the clinical record and neurohistological sections. *Eur Arch Psychiatry Clin Neurosci* **1998**, *248*:111-122.

[3] Blennow K., de Leon M.J., Zetterberg H. Alzheimer's Disease. *Lancet* **2006**, *368*:387-403.

[4] Ferri C.P., Prince M., Brayne C. et al. Global prevalence of dementia: a Delphi consensus study. *Lancet* **2005**, *366*:2112-2117.

[5] Selkoe D.J. The molecular pathology of Alzheimer's disease. *Neuron* **1991**; *6*:487-498.

[6] Terry R. Neuropathological changes in Alzheimer's disease. *Prog Brain Res* **1994**, *101*:383-390.

[7] Selkoe D.J. Folding proteins in fatal ways. *Nature* **2003**, *426*:900-904.

[8] Lansbury P.T. and Lashuel H.A. A century-old debate on protein aggregation and neurodegeneration enters the clinic. *Nature* **2006**, *443*:774-779.

[9] Goate A. et al. Segregation of a missense mutation in the amyloid precursor protein gene with familial Alzheimer's disease. *Nature* **1991**, *349*:704-406.

[10] Zhen H. and Koo E. The amyloid precursor protein: beyond amyloid. *Molecular Neurodegeneration* **2006**, *1*:5.

[11] Masters C.L. et al. Amyloid plaque core protein in Alzheimer's disease and Down syndrome. *Proc Natl Acad Sci* **1985**, *82*:4245-4249.

[12] Hardy J. and Selkoe D.J. The amyloid hypothesis of Alzheimer's disease: progress and problems on the road to therapeutics. *Science* **2002**, *297*:353-356.

[13] Sunde M. and Blake C. The structure of amyloid fibrils by electron microscopi and x-ray diffraction. *Adv Protein Chem* **1997**, *50*:123-159.

[14] Petkova A.T., Ishii Y., Balbach J.J., Antzutkin O.N., Leapman R.D., Delaglio F., Tycko R. A structural model for Alzheimer's β-amyloid fibrils based on experimental constraints from solid state NRM. *Proc Natl Acad Sci* **2002**, *99*:16742-16747.

[15] Rochet J.C., and Lansbury P.T. Amyloid fibrillogenesis: themes and variations. *Curr Opin Struct Biol* **2000**, *10*:60-68.

[16] Kodali R. and Wetzel R. Polymorphism in the intermediates and products of amyloid assembly. *Curr Opin Struct Biol* **2007**, *17*:48-57.

[17] Chiti F. et al. Designing conditions for in vitro formation of amyloid protofilaments and fibrils. *Prot Natl Acad Sci* **1999**, *96*:3590-3594.

[18] Guijarro J.I., Sunde M., Jones J.A. Campbell, I.D. and Dobson C.M. Amyloid fibril formation by an sh3 domain. *Proc Natl Acad Sci* **1998**, *95*:4224-4228.

[19] Litvinovich S.V. at al. Formation of amyloid-like fibrils by self-association of a partially unfolded fibronectin type III module. *J Mol Biol* **1998**, *280*:245-258.

[20] Fändrich M. et al. Myoglobin forms amyloid fibrils by association of unfolded polipeptide segments. *Proc Natl Acad Sci* **2003**, *100*:15463-15468.

[21] Chiti F. et al. Mutational analysis of the propensity for amyloid formation by a globular protein. *EMBO J* **2000**, *19*:1441-1449.

[22] Dobson C.M. Protein misfolding, evolution and diseas. *Trends Biochem Sci* **1999**, *24*:329-332.

[23] Naiki H., Hashimoto N., Suzuki S., Kimura H., Nakakuki K. Geijo F. Estabilishment of a kinetic model of dialisi-related amyloid fibril extension in vitro. *Amyloid* **1997**, *4*:223-232.

[24] Serio T.R., Cashikar A.G., Kowal A.S., Sawicki G.J., Moslehi J.J. et al. Nucleated conformational conversion and the replication of conformational information by a prion determinant. *Science* **2000**, *289*:1317-1321.

[25] Uversky V.N., Li J., Souillac P., Millet I.S., Doniach S. et al. Evidence for a partially folded intermediate in α-synuclein fibril formation. *J Mol Biol* **2004**, *341*:575-588.

[26] Harper J.D., Lieber C.M., Lansbury P.T. Atomic force microscopy imaging of seeded fibril formation and fibril branching by the Alzheimer's disease amyloid-β-protein. *Chem Biol* **1997**, *4*:951-959.

[27] Harper J.D., Wong S.S., Lieber C.M., Lansbury P.T. Observation of metastable Aβ amyloid protofibrils by atomic force microscopy. *Chem Biol* **1997**,*4*:119-125.

[28] Walsh D.M., Lomakin A., Benedek G.B., Condron M.M., Teplow D.B. Amyloid β-protein fibrillogenesis. Detection of a protofibrillar intermediate. *J Biol Chem* **1997**, *272*:22364-22372.

[29] Walsh D.M., Hartley D.M., Kusomoto Y., Fezoui Y., Condron M.M., Lomakin A., Benedek G.B., Selkoe D.J, Teplow D.B. Amyloid β-protein fibrillogenesis. Structure and biological activity of proto fibrillar intermediates. *J Biol Chem* **1999**, *274*:25945-25952.

[30] Bitan G., Lomakin A., Teplow B.D. Amyloid β-protein oligomerization. Prenucleation interactions revealed by photo-induced cross-linking of unmodified proteins. *J Biol Chem* **2001**, *276*:35176-35184.

[31] Bitan G., Kirkitadze M.D., Lomakin A., Vollers S.S., Benedek G.B., Teplow D.B. Amyloid β-protein (Aβ) assembly: $A\beta_{40}$ and $A\beta_{42}$ oligomerize through distinct pathways. *Proc Natl Acad Sci* **2003**, *100*:330-335.

[32] Roher A.E., Chaney M.O., Kuo Y.M., Webster S.D., Stine W.B. et al. Morphology and toxicity of Aβ-(1-42) dimer derived from neuritic and vascular amyloid deposits of Alzheimer's disease. *J Biol Chem* **1996**, *271*:20631-20635.

[33] Podlisny M.B., Ostszewski B.L, Squazzo S.L., Koo E.H., Rydell R.E. et al. Aggregation of secreted β-protein into SDS-stable oligomers in cell culture. *J Biol Chem* **1995**, *270*:9564-9570.

[34] Walsh D.M., Tseng B.P., Rydell R.E., Podlisny M.B., Selkoe D.J. The oligomerization of amyloid β-protein begins intracellularly in cells derived from human brain. *Biochemistry* **2000**, *39*:10831-10839.

[35] Yankner B.A., Duffy L.K., Kirschner D.A. Neurotrophic and neurotoxic effects of amyloid beta protein: reversal by tachykinin neuropeptides. *Science* **1990**, *250*: 279–82.

[36] Iijima K., Liu H.P., Chiang A.S., Hearn S.A., Konsolaki M., Zhong Y. Dissecting the pathological effects of human Abeta40 and Abeta42 in Drosophila: a potential model for Alzheimer's disease. *Proc Natl Acad Sci* **2004**, *101*: 6623–8.

[37] Abramov A.Y., Canevari L., Duchen M.R. Calcium signals induced by amyloid beta peptide and their consequences in neurons and astrocytes in culture. *Biochim. Biophys. Acta* **2004**, *1742*:81–87.

[38] Cecchini M., Curcio R., Pappalardo M., Melki M. and Caflisch A. A molecular dynamics approach to the structural characterization of amyloid aggregation. *J Mol Biol* **2006**, *357*:1306-1321.

[39] Porat Y., Mazor Y., Efrat S., Gazit E. Inhibition of islet amyloid polipeptide fibril formation: a potential role for heteroaromatic interactions. *Biochemistry* **2004**, *43*:14454-14462.

[40] Cardone M. Prospects for gene therapy in inherited neurodegenerative diseases. *Curr Opin Neurol* **2007**; *20*:151-158.

[41] Boudreau R.L., Davidson B.L., RNAi terapy for neurodegenerative diseases. *Curr Top Dev Biol* **2006**, *75*:73-92.

[42] Koutsilieri E., Rethwilm A., Scheller C. The therapeutic potential of siRNA in gene therapy of neurodegenerative disorders. *J Neural Transm Suppl* **2007**, *27*:43-49.

[43] Kan I., Melamed E., Offen D. Autotransplantation of bone marrow-derived stem cells as a therapy for neurodegenerative diseases. *Handb Exp Pharmacol* **2007**, *180*:219-242.

[44] Sonntag K.C., Sanchez-Pernaute R., Tailoring human embryonic stem cells for neurodegenerative disease therapy. *Curr Opin Investig Drugs* **2006**, *7*:614-618.

[45] Cohen F.E., Kelly J.W. Therapeutich approaches to protein-misfolding diseases. *Nature* **2003**, *426*:905-909.

[46] Salomon A.R., Marcinowski K.J., Friedland R.P., Zagorski M.G. Nicotine inhibits amyloid formation by the beta peptide. *Biochemistry* **1996**, *35*:13568-13578.

[47] Ono K., Hasegawa K., Yamada M., Naiki H. Nicotine breaks down preformed Alzheimer's beta-amyloid fibrils in vitro. *Biological Psychiatry* **2002**, *52*:880-806.

[48] Scherzer-Attali R., Pellarin R., Convertino M., Frydman-Marom A., Egoz-Matia N., Peled A., Levy-Sakin M., Shalev D. E., Caflisch A., Gazit E., Segal D. Complete phenotypic recovery o fan Alzheimer's diseas model by a quinone-tryptophan hybrid aggregation inhibitor. *PLoS ONE* **2010**, *5(6)*:e11101.

[49] Convertino M., Pellarin R., Catto M., Carotti A., Caflisch A. 9,10-anthraquinone hinders β-aggregation: how does a small molecule interfere with Aβ-peptide amyloid fibrillation? *Protein Sci.* **2009**, *18*:792-800.

[50] Villegas V., Zurdo J., Filimonov V.V. et al. Protein engineering as a strategy to avoid formation of amyloid fibrils. *Protein Sci.* **2000**, *9*:1700-1708.

[51] Schenk D., Barbour R., Dunn W., et al. Immunization with amyloid-beta attenutates Alzheimer-disease-like pathology in PDAPP mouse. *Nature* **1999**, *400*:173-177.

[52] Solomon B., Koppel R., Hanan E., Katzav T., Monoclonal antibodies inhibit in vitro fibrillar aggregation of the Alzheimer bet-amyloid peptide. *Proc Natl Acad Sci* **1996**, *93*:452-455.

[53] Solomon B., Koppel R., Frankel D., Hanan-Aharon E. Disaggregation of Alzheimer beta-amyloid by site-directed mAb. *Proc Natl Acad Sci* **1997**, *94*:4109-4112.

[54] Morgand D., Diamond D.M., Gottschall P.E., et al. Abeta peptide vaccination prevents memory loss in an animal model of Alzheimer's disease. *Nature* **2000**, *408*:982-985.

[55] Janus C., Pearson J., McLaurin J., et al. Abeta peptide immunization reduces behavioural impairments and plaques in a model of Alzheimer's disease. *Nature* **2000**, *408*: 979-982.

[56] McGavern D.B. Immunotherapeutics relief from persistent infections and amyoid disorders. *Neurology* **2006**, *66*:S59-64.

[57] McGeer E.G., McGeer P.L. Abeta immunotherapy and other means to remove amyloid. *Curr Drug Targets CNS Neurol Disord* **2005**, *4*:569-573.

[58] Gandy S., Heppner F.L., Alzheimer's amyloid immunotherapy: quo vadis? *Lancet Neurol* **2005**, *4*:452-453.

[59] Schenk D. Amyloid-beta immunotherapy for Alzheimer's disease: the end of the beginning. *Nat Rev Neurosci* **2002**, *3*:824-828.

[60] Findeis M.A., Musso G.M., Arico-Muendel C.C., et al. Modified-peptide inhibitors of amyloid beta-peptide polymerization. *Biochemistry* **1999**, *38*:6791-67800.

[61] Gilead S., Gazit E. Inhibition of amyloid fibril formation by peptide analogues modified with alpha-aminoisobutyric acid. *Angew Chem Int Ed Engl* **2004**, *43*:4041-4044.

[62] Gordon D.J., Sciarretta K.L., Meredith S.C., Inhibition of beta-amyloid40; fibrillogenesis and disassembly of beta-amyloid40; fibrils by short beta-amyloid

congeners containing N-methyl amino acids at alternate residues. *Biochemistry* **2001**, *40*:8237-8245.

[63] Hughes E., Burke R.M., Doig A.J., Inhibition of toxicity in the beta-amyloid peptide fragment beta-(25-35) using N-methylated derivatives: a general strategy to prevent amyloid formation. *J Biol Chem* **2000**, *275*:25109-2015.

[64] Kapurniotu A., Schmauder A., Tenedis K., Structure-based design and study of non-amyloidogenic, double N-methylated IAPP amyloid core sequenze as inhibitors of IAPP amyloid formation and cytotoxicity. *J Mol Biol* **2002**; *315*:339-350.

[65] Soto C., Sigurdsson E.M., Morelli L. et al. Beta-sheet breaker peptides inhibit fibrillogenesis in a rat brain model of amyloidosis: implication for Alzheimer's therapy. *Nat Med* **1998**, *4*:822-826.

[66] Soto C., Kindy M.S., Baumann M., Frangione B., Inhibition of Alzheimer's amyloidosis by peptides that prevent beta-sheet conformation. *Biochem Biophys Res Commun* **1996**, *226*:672-680.

[67] Ghanta J., Shen C.L., Kiessling L.L, Murphy R.M. A strategy for designing inhibitors of beta-amyloid toxicity. *J Biol Chem* **1996**, *271*:8545-8548.

[68] Adessi C., Soto C., Converting a peptide into a drug: strategies to improve stability and bioavailability. *Curr Med Chem* **2002**, *9*:963-978.

[69] Kanapathipillai M., Lentzen G., Sierks M., Park C.B. Ectoine and hydroxyectoine inhibit aggregation and neurotoxicity of of Alzheimer's β-amyloid. *FEBS Lett* **2005**, *579*:4775-4780.

[70] Gervais F., Pasquette J., Morisette C., Krzywkowski P., Yu M., Azzi M., Lacombe D., Kong X., Aman A., Laurin., Szarek W.A., Tremblay P. Targeting soluble Aβ peptide with tramiprosate for the treatment of brain amyloidosis. *Neurobiol Aging* **2007**, *28*:537-547.

[71] Mishra R., Bulic B, Sellin D., Jha S., Waldmann H., Winter R. Small-molecule inhibitors of islet amyloid polipeptide fibril formation. *Angew Chem Int Ed Engl* **2008**, *47*:4679-4682.

[72] Cohen T., Frydman-Marom A., Rechter M., Gazit E. Inhibition of amyloid fibril formation and cytotoxicity by hydroxyindole derivatives. *Biochemistry* **2006**, *45*:4727-4735.

[73] Ono K., Hasegawa K., Naiki H., Yamada M. Curcumin has potent anti-amyloidogenic effects for Alzheimer's β-amyloid fibrils in vitro. *J Neurosci Res* **2004**, *75*:742-750.

[74] Ehrnhoefer D.E., Bieschke J., Boeddrich A., Herbst M., Masino L., Lurz R., Engemann S., Pastore A. and Wanker E. EGCG redirects amyloidogenic polypeptides into unstructured, off-pathway oligomer. *Nat Struct Mol Biol* **2008**, *15*:558-566.

[75] McCammon J.A., Gelin B.R. and Karplus M. Dynamics of folded proteins. *Nature* **1977**, *267*: 585-590.

[76] Karplus M. and McCammon J.A. Molecular dynamics simulation of biomolecules. *Nat Struct Biol* **2002**, *9*:646-652.

[77] van Gunsteren W.F. and Berendsen H.J.C. Computer simulation of molecular dynamics: methodology, applications and perspectives in chemistry. *Angew Chem Int Ed Engl* **1990**, *29*:992-1023

[78] Brooks B.R., Bruccolieri, R.E., Olafson B.D., States D.J., Swaminathan S. and Karplus M. CHARMM: A program for macromolecular Energy, minimization and dynamics calculations. *J Comput Chem* **1983**, *4*:187-217.

[79] Brooks B.R., Brooks C.L., McKerell A.D., Nilsson L., Petrella R.J., Roux B., Won Y., Archontis G., Bartels C., Boresch S., Caflisch A., Caves L., Cui Q., Dinner A.R., Feig M., Fischer S., Gao J., Hodoscek M., Im W., Kuczera K., Lazaridis T., Ma J., Ovchinnikov V., Paci E., Pastor R.W., Post C.B., Pu J.Z., Schaefer M., Tidor B., Venable R.M., Woodcock H.L., Wu X., Yang W., York D.M. and Karplus M. CHARMM: the biomolecular simulation program. *J Comput Chem* **2009**, *30*:1545-1614.

[80] McKerell A.D., Bashford D., Ballot M., Dunbrack R.L., Evanseek J., Field M.J., Fischer S., Gao J., Ha S., Joseph D., Kuchnir L., Kuczera K., Lau F.T.K., Mattos C., Michnick S., Ngo T., Nguyen D.T., Prodrom B., Reiher W.E., Roux B., Schlenkrich M., Smith J., Stote R., Straub J., Watanabe M., Wiorkiewcz-Kuczera J., Yin D. and Karplus M. All-atom empirical potential for molecular modeling and dynamics studies of protein. *J Phys Chem B* **1998**, *102*:3568-3616.

[81] Guvench O., Greene S.N., Kamath G., Brady J.W., Venable R.M., Pastor R.W. and McKerell A.D. Additive empirical force field for hexopyranose monosaccharides. *J Comput Chem* **2008**, *29*:2543-2564.

[82] Cornell W.D. et al. A second generation force field for the simulation of proteins, nucleic acids and organic molecules. *J Am Chem Soc* **1995**, *117*:5170-5197.

[83] Schuler L.D., Daura X. and van Gunsteren W.F. An improved Gromos96 force field for aliphatic hydrocarbons in the condensed phase. *J Comput Chem* **2001**, *22*:1205-1218.

[84] Jorgensen W.L., Maxwell D.S. and Tirado-Rives J. Development and testing of the OPLS all-atom force field on conformational energetics and properties of organic liquids. *J Am Chem Soc* **1996**, *118*:11225-11236

[85] Jorgensen W.L. and Tirado-Rives J. Potential energy functions for atomic-level simulations of water and organic and biomolecular systems. *Prot Natl Acad Sci* **2005**, *102*:6665-6670.

[86] Roux B. and Simonson T. Implicit Solvent Models. *Biophys Chem* **1999**, *78*:1-20.

[87] Nina M., Im W., and Roux B. Optimized atomic radii for protein continuum electrostatics solvation forces. *Biophys Chem* **1999**, *78*:89-96.

[88] Still W.C., Tempczyk A. and Hendrickson T. Semianalitycal treatment of solvation for molecular mechanics and dynamics. *J Am Chem Soc* **1990**, *112*:6127-6129.

[89] Habertür U. and Caflisch A., FACTS: Fast Analytical Continuum Treatment of Solvation. J Comput Chem 2007, 29(5): 701-715.

[90] Wesson L. and Eisemberg D. Atomic solvation parameters applied to molecular dynamics of proteins in solution. *Protein Sci* **1992**, *1*:227-235.

[91] Ferrara P., Apostolakis J. and Caflisch A. Evaluation of a fast implicit solvent model for molecular dynamics simulations. *Proteins* **2002**, *46*:24-33.

[92] Fraternali F. and van Gunsteren W.F. An efficient mean solvation force model for use in molecular dynamics simulations of proteins in aqueous solution. *J Mol Biol* **1996**, *256*:939-948.

[93] Kabsch W., Sander C. Dictionary of protein secondary structure: pattern recognition of hydrogen-bonded and geometrical features. *Biopolymers* **1983**, *22(12)*: 2577–637.

[94] Chandrasekhar S. Liquid Crystals, *Cambridge University Press*, *Cambridge*, *England*, **1992**.

[95] de Gennes P.G. and Prost J. The Physics of Liquid Crystals 2nd edit., *Oxford University Press*, *Oxford*, *England*, **1993**.

[96] Zannoni, C. Molecular design and computer simulations of novel mesophases. *J Mater Chem* **2001**, *11*:2637–2646.

[97] Cecchini M., Rao F. Seeber M. and Caflisch A. Replica exchange molecular dynamics simulations of amyloid peptide aggregation. *J Chem Phys* **2004**, *121*:10748–10756.

[98] Frauenfelder H., Sligar S.G., Wolynes P.G., *Science* **1991**, *254*:1598-1603.

[99] Chan H.S., Dill K.A. Protein folding in the landscape perspective: chevron plots and non–arrhenius kinetics. *Proteins: Struct, Funct, Bioinf* **1998**, *30*:2-33.

[100] Rao F. and Caflisch A. The protein folding network. *J Mol Biol* **2004**, *432*:299-306.

[101] Krivov S.V., Karplus M. One-dimensional free-energy profiles of complex systems: Progress variables that preserve the barriers *J Phys Chem B* **2006**, *110*:12689-12698.

[102] Caflisch A. Network and graph analyses of folding free energy surfaces. *Curr Opin Struct Biol* **2006**, *16(1)*:71-78.

[103] Krivov S.V., Muff S., Caflisch A., Karplus M. One-dimensional barrier-preserving free-energy projections of a beta-sheet miniprotein: new insights into the folding process. *J Phys Chem B* **2008**, *112(29)*:8701-8714.

[104] Paoli B., Pellarin R. and Caflisch A. Slow folding of cross-linked α-helical peptides due to steric hindrance. *J Phys Chem B* **2010**, *114(5)*:2023-2027.

[105] Pellarin R., Guarnera E. and Caflisch A. Pathways and intermediates of amyloid fibril formation. *J Mol Biol* **2007**, *374*:917-924.

[106] Pellar R., Schütz P., Guarnera E., Caflisch A. Amyloid fibril polymorphism is under kinetic control. *J Am Chem Soc* **2010**, *132*:14960-14970.

[107] Seeber M., Cecchini M., Rao A., Settanni G. and Caflisch A. Wordom: a program for efficient analysis of molecular dynamics simulations. *Bioinformatics* **2007**, *23*:2625-2627.

[108] Tropp J. Dipolar relaxation and nuclear Overhauser effects in nonrigid molecole: the effect of fluctuating internuclear distances. J Chem Phys **1980**, *72*:6035-6043.

[109] Krivov S.V. and Karplus M. Diffusive reaction dynamcis on invariant free energy profiles. *Prot Natl Acad Sci* **2008**, *105*:13841-13846.

Acknowledgments

"Datemi il tempo di salutare, di riverire, di ringraziare
tutti gli artefici del girotondo."
F. De Andrè

As I sit back and reflect on the last four years of my life, I can't believe the time has flown by. It's now the moment to stop, sit down, take time, mention who was important and to thank.
To begin, I offer my many thanks to Prof. Amedeo Caflisch for trusting, encouraging and having faith in me, even during difficult situations. Our 'disagreements' were challenging at times, but the one constant was Amedeo's unending support. I hope I never failed to meet his expectations and I will take his 'can do' attitude with me when facing new challenges.
I'd also like to thank Prof. Angelo Carotti, whose vision and outlook on new experiences and collaborations allowed me to receive not one, but two doctorates. Not bad, wouldn't you say?
I don't know how to express my gratitude to Riccardo Pellarin; an excellent scientist, a master, a shoulder to cry on during the difficult times and a true friend in and outside of the lab. He taught me how to think critically, which is necessary in our job, and for that I owe him an immense debt of gratitude.
I cannot seem to find the right words to express my thanks to Beatrice Paoli and her husband Andrea Sacchetti. During my time in Zurich, they were like family and their friendship is a precious gift.
Is there any way to thank Pietro? If yes, please advise. Pietro Alfarano has been a pillar of strength during these last four years. At work and during good and some tough times of daily life, Pietro has always been - and still is - a reference point. His advice, suggestions, gaffes, sudden fits of rage, his non-senses and our common emotional upheavals have kept me company.
I am proud to call myself one of his (good?) friends.
Thank you to Andrea Prunotto and Enrico Guarnera: our endless and never-ending discussions about politics, economics, sociology, science, music, religion, history and women have been invaluable to my learning (un)experience.
I must also thank Orazio Nicolotti and his co-workers of MDMl@b; their presence over these years has been a very good school of research and life.
I have learned to never give up. Ever.
I am grateful to all of the PhD students of the Caflisch Group in Zurich and

of the Dipartimento Farmaco Chimico in Bari; I learned something from everyone and I owe something to everyone.
Especially, I am also indebted to François Marchand, Riccardo Scalco, Sandra Steiner, Andrea Magno, Sandra Rennebaum and Emilie Frugier for their feedback in reviewing my dissertation.
I am grateful to Prof. Saverio Cellamare for every, always inspiring exchange. Thank you to Rossana Pascale for everything that she already knows and you don't; it's your problem!
I am also thankful to Silvia Ravera, Svava Wetzel, Danzhi Huang, Marco Catto, Antonio Salomone, Paola Vitale, Valentina Cocco, Nathalie Caretta Cartozo, Claudio Bruno, Peter Kolb, Michela Lavagnini, Angelo Lovece, Fabian Dey, Ran and Esthi Friedman, Roni Scherzer-Attali, Anat Frydman-Marom, Philipp Schütz, Emanuele Spadaro and Sofie Kimmig.
Speaking of my stay in Switzerland, what shall I say about 'pasta&cozze di mia madre' (pasta with mussels cooked by my mother)? Thank you, really, so much. Because it's not like you just need pasta and mussels to make 'pasta&cozze di madre'. If you take away my mother from 'pasta&cozze di madre', then it remains just a generic, simple and trite pasta&cozze. Instead if you take away just pasta&cozze from 'pasta&cozze di mia madre', there remains my mother, who can always prepare another one. It's pointless, she is unbeatable. Thank you to my father, the official supplier of mussels, for some good pieces of advice and uncalled for criticism.
My thanks goes out to Marina Galvagni for her eccentric imagination and for her way of speaking of concepts and poetry and because, as far as it seems, the Convertino-Galvagni method works.
I would like to express my sincere gratitude to Astrid Armili for looking over every single word of mine and for helping me finding better ones in English, German and, often, in Italian.
I am grateful to all of you for having been there, supported me during my little discouragements, as well as in my moments of great distrust and for not ever having had the slightest doubt.
Che al fin della licenza…

Curriculum Vitae

Personal Data

Name	Marino CONVERTINO
Date of Birth	March 9, 1981
Nationality	Italian

Education

2007-present	Double PhD in Biochemistry and Pharmaceutical Science University of Zurich and University of Bari
2005	MSc in Pharmacy University of Bari

Working Experience

2007-present	Teaching Assistant University of Zurich
2006	Research Assistant University of Bari

Publications

- M. Convertino, R. Pellarin, M. Catto, A. Carotti and A. Caflisch. *Protein Sci.* **2009**, *18*:792-800 (DOI: 10.1002/pro.87).
- O. Nicolotti, I. Giangreco, T. F. Miscioscia, M. Convertino, F. Leonetti, L. Pisani and A. Carotti. *J. Comput. Aided Mol. Des.* **2010**, *24*:117-129 (DOI: 10.1007/s10822-010-9320-1).
- R. Scherzer-Attali, R. Pellarin, M. Convertino, A. Frydman-Marom, N. Egoz-Matia, S. Peled, M. Levy-Sakin, D. E. Shalev, A. Caflisch, E. Gazit and D. Segal. *PLoS ONE*, **2010**, *5(6)*:e11101 (DOI: 10.1371/journal.pone.0011101).
- A. Frydman-Marom, M. Convertino, R. Pellarin, A. Lampel, R. Shaltiel-Kario, A. Caflisch, D. E. Shalev, E. Gazit. *Submitted manuscript*, **2010**.
- M. Convertino and A. Caflisch. $A\beta_{12\text{-}28}$ conformational change induced by small molecules. *Manuscript in preparation*, **2010**.

Congress Attendance

- Molecular Modelling for Life and Materials Sciences; Melbourne, Australia; **2010**.
- European School of Medicinal Chemistry, XXVIII Advanced Course in Medicinal Chemistry; Urbino, Italy; **2010**.
- Benzon Symposium No. 56. Functional and Pathogenic Protein Aggregation; Copenhagen, Denmark; **2009**.
- IV Meeting on the Molecular Mechanism of Neurodegeneration; Milan, Italy; **2009**.
- Conference Jacques Monod. Protein Misfolding and Aggregation in Ageing Disease; Roscoff, France; **2007**.